



score

D6.1 - Risk characterisation report for all CCLs

DATE OF DELIVERY – 30/06/2023

AUTHOR(S):

Rui Figueiredo (RED)

Raymundo Rangel (RED)

Gianbattista Bussi (RED)

Paola Ceresa (RED)

Gabriele Coccia (RED)





DOCUMENT TRACKS DETAILS

Project acronym	SCORE
Project title	Smart Control of the Climate Resilience in European Coastal Cities
Starting date	01.07.2021
Duration	48 months
Call identifier	H2020-LC-CLA-2020-2
Grant Agreement No	101003534

Deliverable Information	
Deliverable number	D6.1
Work package number	WP6
Deliverable title	Risk characterisation report for all CCLLs
Lead beneficiary	RED
Author(s)	Rui Figueiredo (RED), Raymundo Rangel (RED), Gianbattista Bussi (RED), Paola Ceresa (RED), Gabriele Coccia (RED)
Due date	30/06/2023
Actual submission date	30/06/2023
Type of deliverable	Report
Dissemination level	Public

VERSION MANAGEMENT

Revision table			
Version	Name	Date	Description
V 0.1	Rui Figueiredo (RED), Raymundo Rangel (RED), Gianbattista Bussi (RED)	07/06/2023	First draft
V 0.2	Paola Ceresa, Gabriele Coccia (RED)	09/06/2023	Updated draft internally reviewed
V 0.3	Rui Figueiredo (RED), Gianbattista Bussi (RED)	23/06/2023	Updated draft after peer review from Elena Marie Ensenado (IHS) and Gregorio Iglesias (UCC)
V 1.0	Iulia Anton (ATU), Salem Gharbia (ATU)	30/06/2023	Final version

All information in this document only reflects the author's view. The European Commission is not responsible for any use that may be made of the information it contains.





LIST OF ACRONYMS AND ABBREVIATIONS

Acronym / Abbreviation	Meaning / Full text
CCLL	Coastal City Living Lab
CLC	Corine Land Cover
CORINE	Coordination of information on the environment
DEM	Digital Elevation Model
DSM	Digital surface model
EBA	Ecosystem-Based Approach
ECMWF	European Centre for Medium-Range Weather Forecasts
EFAS	European Flood Awareness System
ELSUS	European Landslide Susceptibility Map
ERA5-HEAT	European Environment Agency - Human thermal comfort
ESRM20	European Seismic Risk Model
Eurostat	European statistics
GDP	Gross domestic product
GIS	Geographic information system
GPEX	Global Precipitation Extremes
GTSM	Global Tide and Surge Model
GTSR	Global Tide and Surge Reanalysis
GVA	Gross value added
JRC	European Commission's Joint Research Centre
LHASA	Landslide Hazard Assessment for Situational Awareness
NACE	Nomenclature générale des Activités économiques dans les Communautés Européennes
NASA	National Aeronautics and Space Administration
NUTS	Nomenclature of territorial units for statistics
OSM	OpenStreetMap
RISE	Real-time Earthquake Risk Reduction for a Resilient Europe
SERA	Seismology and Earthquake Engineering Research Infrastructure Alliance for Europe
UTCI	Universal Thermal Climate Index





BACKGROUND: ABOUT THE SCORE PROJECT

SCORE is a four-year EU-funded project aiming to increase climate resilience in European coastal cities.

The intensification of extreme weather events, coastal erosion and sea-level rise are major challenges to be urgently addressed by European coastal cities. The science behind these disruptive phenomena is complex, and advancing climate resilience requires progress in data acquisition, forecasting, and understanding of the potential risks and impacts for real-scenario interventions. The Ecosystem-Based Approach (EBA) supported by smart technologies has potential to increase climate resilience of European coastal cities; however, it is not yet adequately understood and coordinated at European level.

SCORE outlines a co-creation strategy, developed via a network of 10 coastal city 'living labs' (CCLs), to rapidly, equitably and sustainably enhance coastal city climate resilience through EBAs and sophisticated digital technologies.

The 10 coastal city living labs involved in the project are: Sligo and Dublin, Ireland; Barcelona/Vilanova i la Geltrú, Benidorm and Basque Country, Spain; Oeiras, Portugal; Massa, Italy; Piran, Slovenia; Gdansk, Poland; Samsun, Turkey.

SCORE will establish an integrated coastal zone management framework for strengthening EBA and smart coastal city policies, creating European leadership in coastal city climate change adaptation in line with The Paris Agreement. It will provide innovative platforms to empower stakeholders' deployment of EBAs to increase climate resilience, business opportunities and financial sustainability of coastal cities.

The SCORE interdisciplinary team consists of 28 world-leading organisations from academia, local authorities, RPOs, and SMEs encompassing a wide range of skills including environmental science and policy, climate modelling, citizen and social science, data management, coastal management and engineering, security and technological aspects of smart sensing research.





EXECUTIVE SUMMARY

This document is a deliverable of the SCORE project, funded under the European Union's Horizon 2020 research and innovation programme under grant agreement No 101003534. In this document, the activities carried out within the Task 6.1 of the Work Package 6 are described and their results are shown. WP6 (Strategies to increase the financial resilience of coastal cities) aims at assessing natural risks of coastal cities, quantifying the benefits of ecosystem-based interventions as risk reduction measures, and defining financial strategies to increase the resilience of coastal cities to natural disasters. Task 6.1 (Coastal city risk characterisation), in particular, aims at providing a semi-quantitative risk assessment for all 10 CCLLs of the SCORE project (Benidorm – Spain, Dublin – Ireland, Gdańsk – Poland, Massa – Italy, Oarsoaldea – Spain, Oeiras – Portugal, Piran – Slovenia, Samsun – Turkey, Sligo – Ireland, Vilanova i la Geltrú – Spain) for fluvial flooding, coastal flooding, extreme precipitation, landslide, heat wave, and coastal erosion. The objectives are twofold: to define a screening methodology based on open data to be used for a quick assessment of the impacts of natural phenomena in coastal cities and to provide a classification of the SCORE CCLLs in terms of their exposure to natural risks.

The document shows a novel semi-quantitative risk assessment approach, based on scoring, which can be easily extended to other coastal cities in Europe, since it is based on large-scale open datasets which cover all or most of Europe. The methodology is relatively quick and straightforward, thus being suitable for a light, non-data-intensive risk assessment whose purposes are to define priorities and identify critical situations worth of a deeper, more detailed assessment. The document provides risk scores for all the six perils and 10 CCLLs, showing which perils are most impactful across cities and which ones are specific of certain areas. For example, results suggest that both heavy precipitation (which causes pluvial/urban floods) and heat waves can cause significant impacts in more than half of the CCLLs, while other perils such as fluvial flooding and coastal erosion cause impacts to a more limited number of CCLLs (although their impacts can be extreme, such as the case of fluvial flood in Gdańsk or coastal erosion in Piran). Furthermore, a financial categorisation of the CCLLs was also carried out to identify which risk transfer strategies might be more suitable to protect CCLLs from coastal and fluvial floods, showing that not all the CCLLs should face natural phenomena with the same financial strategy: some of them are characterised by low-frequency, high-intensity events, others by high-frequency, low-intensity events. The methodology described in this report helps understanding whether a coastal city should focus their risk management towards risk transfer or towards risk retention.

LINKS WITH OTHER PROJECT ACTIVITIES

In terms of links with other project activities, the main purpose of Task 6.1 is to provide a basis for other tasks in WP6, in particular Task 6.3 (Residual coastal risk assessment) and Task 6.4 (Financial resilience strategies). In Task 6.1, data and knowledge were collected about the risk exposure of CCLLs. Some of these data will be used in Task 6.3 to develop a flood risk assessment model for three cities: Massa, Vilanova i la Geltrú and Oarsoaldea. Furthermore, the results of this task highlighted the issues these cities are subject to in terms of natural risks: extreme precipitation risk appears to be relatively high in all three cities and deserves a more detailed assessment, also because of the uncertainty of the semi-quantitative approach used in Task 6.1, which uses extreme precipitation as a proxy for urban flood risk. Additionally, results suggest that for these three CCLLs fluvial and coastal flood risks are low, either because the hazard level is low (for example, no major river crosses any of these three cities) or because





the exposure is located in areas with low hazard levels (most of the urbanised areas in these three cities are located at elevations above the sea level that make them almost completely protected from sea storms).

Apart from contributing to other tasks in WP6, this task serves to the whole project as a screening and prioritisation tool for CCLs. Other WPs can use the risk assessment presented here to define priorities in terms of focusing on certain natural hazards or on certain cities rather than others and can learn whether certain risks are relevant or not for the CCLs, and what level of impacts are to be expected. In this sense, it is worth highlighting the complementarity of the results of this task with the results of Task 1.4 (Baseline risk analysis and mapping of extreme climate impacts and sea level rise). Both tasks look at the same problem (risk caused by natural phenomena) but have a different focus, use different tools, and their results speak to different audiences. The outcomes of Task 6.1 use modelling concepts that are closer to traditional risk modelling and focus on financial resilience of coastal cities, thus looking at natural risks from the point of view of risk managers, decision makers and administrators. However, in the context of semi-quantitative/qualitative risk assessments there is not a single correct answer or a single suitable approach, and the complementarity of approaches allows obtaining a more comprehensive picture of risks at city level.





TABLE OF CONTENT

1. Introduction	12
1.1. Study areas	12
2. Data	13
2.1. Exposure	14
2.1.1. Population	14
2.1.1.1. Number	14
2.1.1.2. Age distribution	15
2.1.2. Residential buildings	16
2.1.3. Land cover	17
2.1.4. Economic activities	18
2.1.5. Road and railway networks	19
2.2. Hazard	20
2.2.1. Fluvial flooding	20
2.2.2. Coastal flooding	21
2.2.3. Extreme precipitation	22
2.2.4. Landslide	23
2.2.4.1. European Landslide Susceptibility Map	24
2.2.4.2. Landslide Hazard Assessment for Situational Awareness Model	24
2.2.5. Heat wave	25
2.2.6. Coastal erosion	26
3. Methodology	28
3.1. Risk scores	29
3.1.1. Fluvial and coastal flooding	29
3.1.1.1. Population	30
3.1.1.2. Residential buildings	31
3.1.1.3. Economic activities	32
3.1.1.4. Road and railway networks	33
3.1.2. Extreme precipitation	34
3.1.3. Landslide	35
3.1.3.1. Population	35
3.1.3.2. Residential buildings	36
3.1.3.3. Economic activities	36
3.1.3.4. Road and railway networks	37
3.1.4. Heat wave	37
3.1.5. Coastal erosion	38
3.1.5.1. Population	39
3.1.5.2. Residential buildings	40
3.1.5.3. Economic activities	40
3.1.5.1. Road and railway networks	40
3.2. Financial categorization of risk	40
4. Results	41
4.1. Risk scores	41





4.1.1.	Fluvial flooding.....	42
4.1.1.1.	Disaggregated by exposure type.....	43
4.1.2.	Coastal flooding.....	48
4.1.2.1.	Disaggregated by exposure type.....	49
4.1.3.	Extreme precipitation.....	53
4.1.4.	Landslide.....	54
4.1.4.1.	Disaggregated by exposure type.....	54
4.1.5.	Heat wave.....	59
4.1.6.	Coastal erosion.....	59
4.1.6.1.	Disaggregated by exposure type.....	60
4.2.	Financial categorization of risk.....	63
5.	Conclusion.....	65
6.	References.....	66





INDEX OF FIGURES

Figure 1: Geographical location of SCORE's ten CCLLs.....	13
Figure 2: WorldPop top-down methods comparison: unconstrained (left) and constrained (right) (WorldPop, 2023).....	15
Figure 3: Example of the WorldPop datasets for the cities of Benidorm (left) and Vilanova i la Geltrú (right). Coordinate Reference System (CRS) – EPSG:3035 (note that all maps in the document follow this CRS).....	15
Figure 4: CORINE Land Cover version 2018. For the legend, please refer to https://land.copernicus.eu/pan-european/corine-land-cover/clc2018	18
Figure 5: Road and railways network for the CCLLs of Oeiras (left) and Oarsoaldea (right).	20
Figure 6: JRC fluvial flood hazard map for a 100-year return period.	21
Figure 7: Aqueduct coastal flood hazard map for a 100-year return period.	22
Figure 8: GPEX precipitation map for a 5-year return period and duration of 24 hours.	23
Figure 9: ELSUS v2 landslide susceptibility map	24
Figure 10: LHASA landslide susceptibility map	25
Figure 11: UTCI daily maxima: 99 th percentile for each grid cell over a spatial domain covering SCORE's ten CCLLs.....	26
Figure 12: EUROSION coastal erosion dataset with coast segments classified according to their evolutionary trend.....	28
Figure 13: Methodological framework.....	28
Figure 14: Schematic representation of the suitability of risk transfer mechanisms to different layers of risk.....	41
Figure 15: Fluvial flooding potential impact indices $i_{pop,g}$ at grid cell level for population in the Gdańsk CCLL.....	43
Figure 16: Fluvial flooding potential impact indices $i_{resbldg,g}$ at grid cell level for residential buildings in the Gdańsk CCLL.....	44
Figure 17: Fluvial flooding potential impact indices $i_{agr,g}$ at grid cell level for agriculture in the Gdańsk CCLL.....	45
Figure 18: Fluvial flooding potential impact indices $i_{ind,g}$ at grid cell level for industry in the Gdańsk CCLL.	45
Figure 19: Fluvial flooding potential impact indices $i_{tou,g}$ at grid cell level for tourism in the Gdańsk CCLL.	46
Figure 20: Fluvial flooding potential impact indices for the road network in the Gdańsk CCLL.	47
Figure 21: Fluvial flooding potential impact indices for the railway network in the Gdańsk CCLL.....	47
Figure 22: Coastal flooding potential impact indices $i_{pop,g}$ at grid cell level for population in the Piran CCLL.....	49
Figure 23: Coastal flooding potential impact indices $i_{resbldg,g}$ at grid cell level for residential buildings in the Piran CCLL.	50
Figure 24: Coastal flooding potential impact indices $i_{agr,g}$ at grid cell level for agriculture in the Piran CCLL.	51
Figure 25: Coastal flooding potential impact indices $i_{tou,g}$ at grid cell level for tourism in the Piran CCLL.	51
Figure 26: Coastal flooding potential impact indices for the road network in the Piran CCLL.	52
Figure 27: Landslide susceptibility indices at grid cell level for population and residential buildings in the Oeiras CCLL.	54
Figure 28: Landslide susceptibility indices $u_{agr,g}$ at grid cell level for agriculture in the Oeiras CCLL.....	55
Figure 29: Landslide susceptibility indices $u_{ind,g}$ at grid cell level for industry in the Oeiras CCLL.	56
Figure 30: Landslide susceptibility indices $u_{tou,g}$ at grid cell level for tourism in the Oeiras CCLL.	56
Figure 31: Landslide susceptibility indices for the road network in the Oeiras CCLL.....	57





Figure 32: Landslide susceptibility indices for the railway network in the Oeiras CCLL.	58
Figure 33: Coastal erosion susceptibility indices at grid cell level for population and residential buildings in the Sligo CCLL.	60
Figure 34: Coastal erosion susceptibility indices $u_{agr,g}$ at grid cell level for agriculture in the Sligo CCLL...61	61
Figure 35: Coastal erosion susceptibility indices $u_{ind,g}$ at grid cell level for industry in the Sligo CCLL.	61
Figure 36: Coastal erosion susceptibility indices $u_{tou,g}$ at grid cell level for tourism in the Sligo CCLL.	62
Figure 37: Coastal erosion susceptibility indices for the road network in the Sligo CCLL.....	63

INDEX OF TABLES

Table 1: Overview of the datasets adopted in this study.....	14
Table 2: Population age distribution for the ten CCLLs, based on Eurostat data.	16
Table 3: Distribution of building height classes for the ten CCLLs, based on SERA data.	17
Table 4: Distribution of building construction materials for the ten CCLLs, based on SERA data.	17
Table 5: Estimated economic activity GVA fractions for the ten CCLLs, based on Eurostat data.....	19
Table 6: Adopted reclassification of OSM classes.	20
Table 7: Erosion evolutionary trend code descriptions in the EUROSION dataset.....	27
Table 8: hazard properties (variable adopted for hazard quantification and spatial variability of the hazard at the scale of a CCLL).	29
Table 9: Vulnerability indices considered for different age ranges.....	31
Table 10: Vulnerability indices considered for different classes of building properties.	32
Table 11: Correspondence between economic activities and CLC classes.	33
Table 12: Flood potential impact indices for road and railway network elements.	34
Table 13: Correspondence between qualitative landslide susceptibility classes and semi-quantitative susceptibility indices.....	36
Table 14: Correspondence between qualitative coastal erosion susceptibility classes and semi-quantitative susceptibility indices.	39
Table 15: Risk scores S for each hazard and CCLL.	42
Table 16: Fluvial flooding risk scores both for each type of exposed element and combined into a single risk score for each CCLL.	42
Table 17: Fluvial flooding potential impact sub-scores I_{pop} and risk scores S_{pop} for population.....	43
Table 18: Fluvial flooding potential impact sub-scores $I_{resbldg}$ and risk scores $S_{resbldg}$ for residential buildings.....	44
Table 19: Fluvial flooding potential impact sub-scores I'_j and risk scores S_{econ} for economic activities.....	46
Table 20: Fluvial flooding potential impact sub-scores I'_j and risk scores S_{transp} for road and railway networks.	48
Table 21: Coastal flooding risk scores both for each type of exposed element and combined into a single risk score for each CCLL.	48
Table 22: Coastal flooding potential impact sub-scores I_{pop} and risk scores S_{pop} for population.	49
Table 23: Coastal flooding potential impact sub-scores $I_{resbldg}$ and risk scores $S_{resbldg}$ for residential buildings.....	50
Table 24: Coastal flooding potential impact sub-scores I'_j and risk scores S_{econ} for economic activities. ..	52
Table 25: Coastal flooding potential impact sub-scores I'_j and risk scores S_{transp} for road and railway networks.	53
Table 26: Extreme precipitation intensities and risk scores.....	53
Table 27: Landslide risk scores both for each type of exposed element and combined into a single risk score for each CCLL.....	54





Table 28: Landslide susceptibility sub-scores and risk scores S_{pop} and $S_{resbldg}$ for population and residential buildings, respectively.	55
Table 29: Landslide susceptibility sub-scores U'_j and risk scores S_{econ} for economic activities.	57
Table 30: Landslide susceptibility sub-scores U'_j and risk scores S_{transp} for road and railway networks. ...	58
Table 31: Heat wave sub-scores and risk scores.	59
Table 32: Coastal erosion risk scores both for each type of exposed element and combined into a single risk score for each CCLL.	59
Table 33: Coastal erosion susceptibility sub-scores and risk scores for population and residential buildings.....	60
Table 34: Coastal erosion susceptibility sub-scores U'_j and risk scores S_{econ} for economic activities.....	62
Table 35: Coastal erosion susceptibility sub-scores U'_j and risk scores S_{transp} for road and railway networks.	63
Table 36: Comparison of fluvial flooding risk scores with 20- and 500-year return periods for residential buildings, agriculture, and industry.....	64
Table 37: Comparison of coastal flooding risk scores with 20- and 500-year return periods for residential buildings, agriculture, and industry.....	64





1. INTRODUCTION

Coastal cities are particularly exposed to hydro-meteorological and climate-related natural hazards and their consequences. The SCORE project, within its various activities, aims to provide a better understanding of the risks associated with such hazards, based on which more effective risk management and mitigations actions can be implemented in European coastal cities.

Within the SCORE project, different CCLLs act as frontrunners for each WP, calling for targeted, CCLL-specific activities to be carried out. Notwithstanding, the scope of the project also calls for a large-scale characterisation of the different risks that each of the ten CCLLs is subject to. This was the overarching objective of WP6's Task 6.1, which the present document describes.

The characterization of the risks associated with multiple natural hazards with significantly different characteristics in terms of intensity, frequency, and duration, and which affect exposed population and assets in different manners, is a challenging task from a technical and scientific viewpoint, particularly when the risk assessment is to be performed for several distinct locations. In this case, location-specific hazard and/or exposure data are often incomplete or not readily available. Moreover, existing data for different locations are often developed following different methodological approaches that can result in inconsistencies among them, rendering them unsuitable for obtaining comparable estimates of risk. Lastly, a suitable methodological framework for the consistent estimation of multiple risks is required.

In this context, the main objective of Task 6.1 was to perform a semi-quantitative characterisation of risks associated with six hydro-meteorological and climate-related hazards in SCORE's ten CCLLs: fluvial flooding, coastal flooding, extreme precipitation, landslide, heat wave, and coastal erosion. To achieve this, a comprehensive data collection effort was first undertaken in order to identify, compare and obtain state-of-the-art datasets characterizing the different components of risk, particularly hazard and exposure, over a spatial domain covering SCORE's ten CCLLs in a consistent manner. A novel methodological framework for the semi-quantitative, score-based assessment of risk was then developed. This framework is based on state-of-the-art modelling concepts and approaches for the risk assessment of different types of perils, which in this case were adapted to the specificities of the study areas, hazards of interest, and available data. Despite the semi-quantitative, large-scale nature of this study, a simple framework for the preliminary categorization of the risk profile of the CCLLs in terms of potential risk transfer strategies is also provided.

The outputs of this task provide a high-level identification and characterization of the most pressing risks for each CCLL, which can serve as a basis for subsequent, more detailed CCLL- and/or hazard-specific quantitative risk assessments such as those developed in subsequent WP6 tasks.

1.1. Study areas

The geographical locations of SCORE's ten CCLLs are shown in Figure 1. The study areas considered for each CCLL correspond to the respective municipality administrative boundaries, with the exceptions of Oarsoaldea, which is *subcomarca* (a type of Spanish administrative entity) comprising four municipalities (i.e, Errenteria, Lezo, Oiartzun and Pasaia), and Sligo, which refers to the Sligo county.





Figure 1: Geographical location of SCORE's ten CCLLs.



2. DATA

This section briefly describes the datasets adopted for the development of the risk assessments carried out within Task 6.1. Risk is generally modelled as a function of three components: hazard, exposure, and vulnerability. The hazard component characterizes the different perils in terms of spatial extent, intensity and/or probability of occurrence. The exposure component characterizes the population and elements at risks in terms of their spatial distribution and relevant features for the assessment of risk. The vulnerability component defines the propensity of exposed population and elements to be adversely affected by a hazard, based on physically- and/or expert-based models and/or assumptions. Therefore, in this section, the collected data refer to the hazard and exposure components, i.e., they characterize the perils and exposed population and elements. The vulnerability component, instead, is reflected in various steps of the semi-quantitative risk assessment methodology where that information is used in the calculation of the risk scores, as described in Section 3. The datasets used to characterize exposure are presented in Section 2.1, while the hazard datasets are presented in Section 2.2. In each subsection, a large-scale map with a spatial domain covering SCORE's ten CCLLs is presented. CCLL-specific maps are included in Appendix 1 and 2.

Table 1 provides an overview of all the datasets, including references to the variables that they define, sources, and spatial resolutions. All datasets used in this study have open formats and open licenses, and their use/reuse is free of charge, in line with the EU's Open Data Directive.





Table 1: Overview of the datasets adopted in this study.

Risk component	Data	Variable	Source	Spatial resolution
Exposure	Population	Number	WorldPop	3" (\approx 90 m)
		Age distribution	Eurostat	NUTS 3 region
	Residential buildings	Building type distribution	ESRM20	Administrative units
	Land cover	Land cover class	CORINE Land Cover	100 m
	Economic activities	Gross value added (EUR)	Eurostat	NUTS 3 region
	Road and railway networks	Road and railway length, road type	OpenStreetMap	Object
Hazard	Fluvial flooding	Water depth (m)	JRC/EFAS	100 m
	Coastal flooding	Water depth (m)	Aqueduct	30" (\approx 900 m),
				downscaled to 25 m
	Extreme precipitation	Precipitation intensity (mm)	GPEX	0.1° (\approx 11 km)
	Landslide	Susceptibility index	ELSUS	200 m
			LHASA	30" (\approx 900 m)
	Heatwave	Universal Thermal Climate Index (°C)	ERA5-HEAT	0.25° (\approx 28 km)
Coastal erosion	Susceptibility index	EUROSION	Coastline segments	

2.1. Exposure

2.1.1. Population

2.1.1.1. Number

In order to estimate the spatial distribution of population within the CCLs, and subsequently the population exposed to the assessed hazards, WorldPop data were adopted (WorldPop, 2023). High-resolution contemporary data of human population distributions, their characteristics and changes over time are a prerequisite for the accurate measurement of the impacts of population growth, for monitoring changes and for planning interventions. WorldPop aims to meet these needs by providing detailed and open access spatial demographic datasets built using transparent approaches (Tatem, 2017).

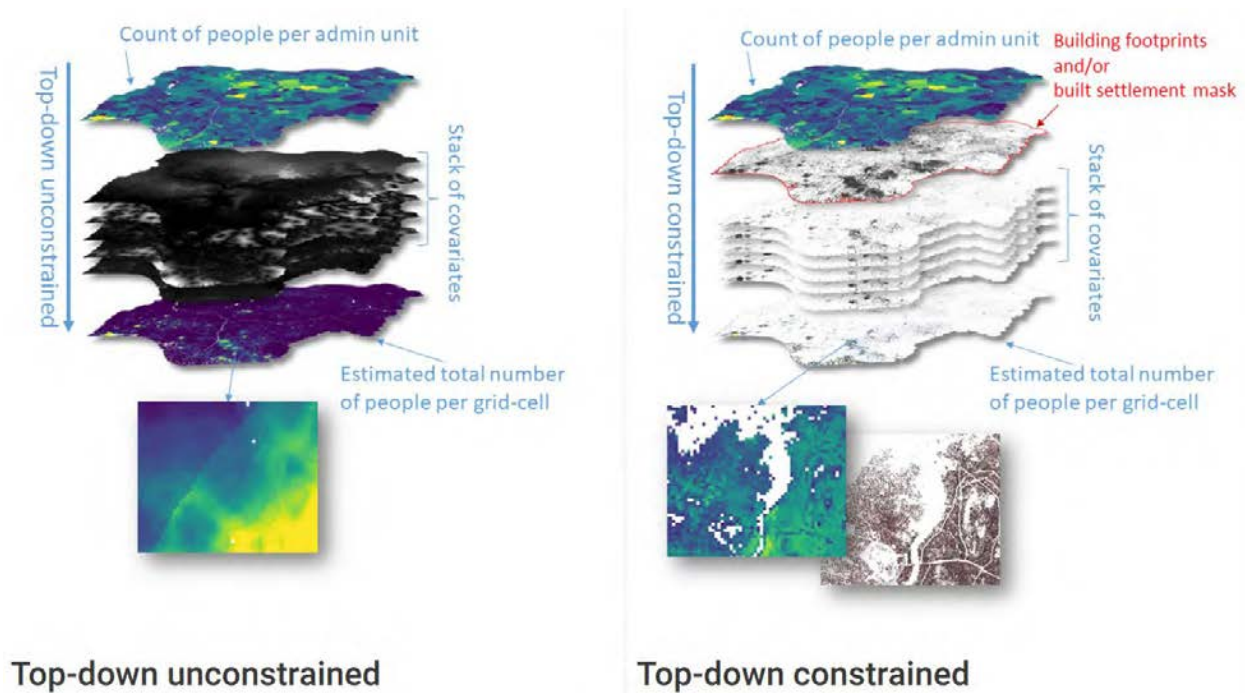
Population and housing censuses remain the most important resource for production of accurate population data at national and subnational scales. However, these are typically only made available as counts per administrative unit, which is suboptimal for modelling exposure in the context of natural hazard risk assessment, due to the high spatial variability of physical phenomena (e.g., flooding) within an administrative unit. WorldPop addresses this through top-down modelling methods which take a global database of administrative unit-based census counts and utilise a set of detailed geospatial data to disaggregate them to grid cell-based counts. Two methods are used to produce the datasets over multiple countries using Random Forest machine learning methods (Stevens et al., 2015): 1) estimation over all land grid squares globally (i.e., unconstrained), and 2) estimation only within areas mapped as containing





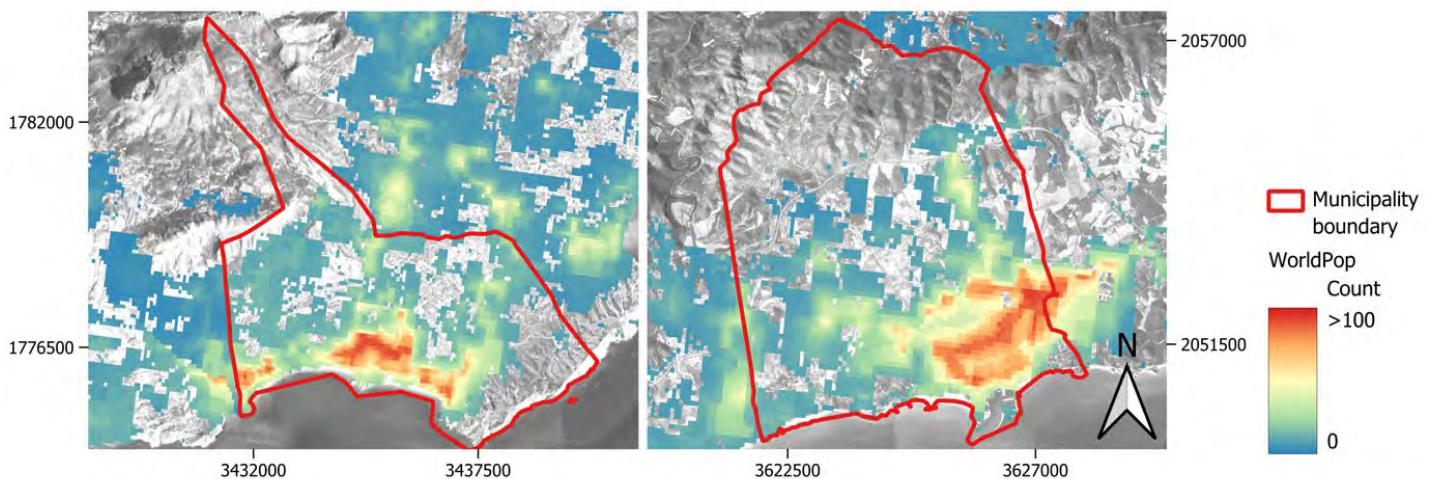
built settlements (i.e., constrained) (WorldPop, 2023). The two methods are illustrated in Figure 2, which shows how the constrained method includes a geospatial layer of building footprints and/or built settlements to constrain the population count to their spatial locations, generating results that are generally more realistic than considering spatially continuous values throughout the grid, even where there are no buildings and/or settlements.

Figure 2: WorldPop top-down methods comparison: unconstrained (left) and constrained (right) (WorldPop, 2023).



In this study, the population distribution within each CCLL was based on the WorldPop top-down constrained datasets for 2020; residential building count fractions at grid cell level were assumed to follow the same distributions. Figure 3 shows an example of the dataset for the CCLLs of Benidorm and Vilanova i la Geltrú, with a grid resolution of 100 m. The data are available at <https://hub.worldpop.org/geodata/listing?id=78>.

Figure 3: Example of the WorldPop datasets for the cities of Benidorm (left) and Vilanova i la Geltrú (right). Coordinate Reference System (CRS) – EPSG:3035 (note that all maps in the document follow this CRS).



2.1.1.2. Age distribution

Population age data were obtained from Eurostat, the statistical office of the European Union, which is responsible for publishing Europe-wide statistics and indicators that enable comparisons among countries and regions. Eurostat





data describing the fractions of population belonging to different age intervals are available at the level of different territorial units up to NUTS 3 region level. Accordingly, the population age distribution in each CCLL was assumed to be similar to that of the NUTS 3 region where the CCLL is located. Data for the year of 2021 were used.

Table 2 shows the age distributions considered for each CCLL, where the age intervals were selected to allow for a meaningful characterization of the vulnerability of the population in the CCLLs based on the population structure, as further described in Section 3. The Eurostat data are available at https://ec.europa.eu/eurostat/databrowser/view/DEMO_R_PJANIND3/default.

Table 2: Population age distribution for the ten CCLLs, based on Eurostat data.

CCLL	Age interval fractions (0-1)				
	0 – 4	5 – 14	15 – 64	65 – 74	>= 75
Benidorm	0.04	0.102	0.654	0.108	0.097
Dublin	0.061	0.124	0.684	0.074	0.058
Gdańsk	0.067	0.132	0.666	0.09	0.045
Massa	0.029	0.079	0.616	0.132	0.144
Oarsoaldea	0.039	0.101	0.631	0.115	0.115
Oeiras	0.051	0.106	0.619	0.116	0.107
Piran	0.043	0.099	0.638	0.13	0.091
Samsun	0.06	0.138	0.68	0.078	0.044
Sligo	0.061	0.145	0.629	0.095	0.072
Vilanova i la Geltrú	0.043	0.106	0.656	0.097	0.096

2.1.2. Residential buildings

For characterizing residential buildings, the ESRM20 building exposure model version 1.0 was adopted. This model, which was developed as part of the Horizon 2020 projects SERA (Seismology and Earthquake Engineering Research Infrastructure Alliance for Europe) and RISE (Real-time Earthquake Risk Reduction for a Resilient Europe), describes the distribution of buildings of different occupancy types according to classes that are relevant to characterize their seismic performance in a consistent manner. The building attributes included in the model are the main construction material, the lateral load resisting system, the number of storeys, the seismic design code level, and the lateral force coefficient used in the seismic design (Crowley et al., 2020). Although certain seismic-specific attributes in the ESRM20 model are not relevant for perils other than earthquakes, information on construction materials and number of storeys (expressed in terms of height classes) are informative for characterizing the vulnerability of buildings to the hazards considered in the present task.

The ESRM20 exposure data for residential buildings are available in different administrative-level resolutions depending on the country, as described in the model documentation (e.g., municipality-level for Italy, province-level for Spain). Therefore, for the two building properties adopted herein – construction material and height class – the estimated distributions of building fractions belonging to different classes in each CCLL were assumed to correspond to the SERA distributions of the administrative unit where the CCLL is located. The data can be accessed at <https://zenodo.org/record/5730071>.





Table 3: Distribution of building height classes for the ten CCLs, based on SERA data.

CCLL	Building fractions by height class (0-1)		
	Low rise	Mid rise	High rise
Benidorm	0.896	0.092	0.012
Dublin	0.747	0.253	0
Gdańsk	0.408	0.592	0
Massa	0.945	0.055	0
Oarsoaldea	0.640	0.331	0.029
Oeiras	0.701	0.227	0.073
Piran	0.655	0.345	0
Samsun	0.726	0.274	0
Sligo	0.747	0.253	0
Vilanova i la Geltrú	0.815	0.159	0.026

Table 4: Distribution of building construction materials for the ten CCLs, based on SERA data.

CCLL	Building fractions by construction material (0-1)		
	Reinforced concrete	Masonry	Wood
Benidorm	0.162	0.838	0
Dublin	0.253	0.671	0.076
Gdańsk	0.592	0.384	0.023
Massa	0.442	0.558	0
Oarsoaldea	0.256	0.744	0
Oeiras	0.816	0.172	0
Piran	0.228	0.766	0.006
Samsun	0.502	0.47	0.028
Sligo	0.253	0.671	0.076
Vilanova i la Geltrú	0.213	0.787	0

2.1.3. Land cover

In order to map different classes of land cover within the CCLs, which are then used to define the spatial location of economic activity types therein (as described in Section 3), the Corine Land Cover (CLC) dataset was adopted. CLC is the oldest and most sought-after database of Copernicus Land Monitoring Service, providing geographical information on land cover and its changes, land use, vegetation state, water cycle and earth surface energy variables to a broad range of users in Europe and across the world in the field of environmental terrestrial applications (Büttner et al., 2021). It was specified to standardize data collection related to land in Europe to support environmental policy development. The reference year of the first CLC inventory was 1990 (CLC1990), and the first update was created in 2000 covering a total area of nearly 6 Mkm². Further inventories followed with an update cycle of 6 years, with the last available update for 2018, which is used herein.

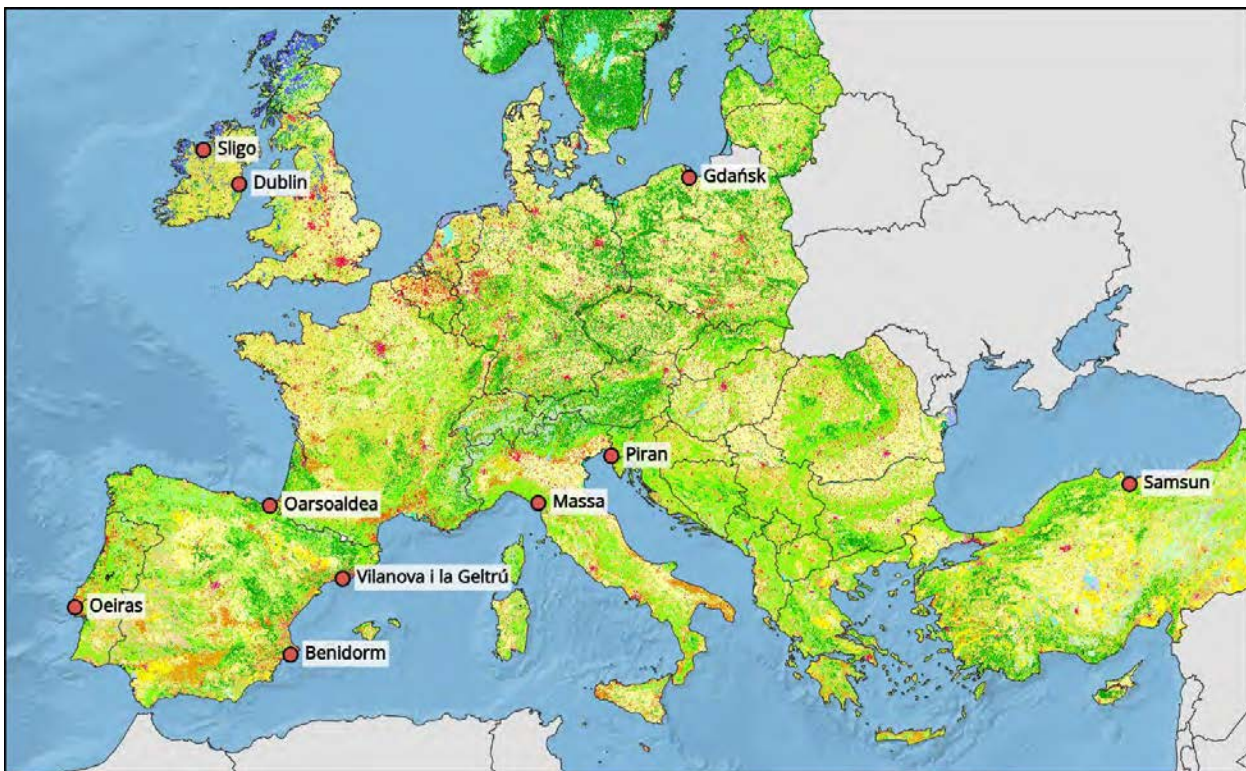




The CLC mapping is performed using high spatial resolution satellite imagery supported by in-situ ancillary data including topographic maps, ortho-photos and ground survey data. The basic technical parameters of CLC have not changed since its inception, namely: 1) the nomenclature including 44 classes in five main land cover/use groups (Artificial surfaces, Agriculture, Forests and seminatural areas, Wetlands and Water); 2) the geometric detail (25-hectare minimum mapping unit and 100-meter minimum mapping width). European validation studies have shown that the achieved thematic accuracy is above the specified minimum of 85% (Büttner et al., 2021).

Figure 4 shows the CLC 2018 data over a spatial domain covering SCORE's ten CCLLs, with each colour corresponding to one of the 44 classes mentioned in the above paragraph. For additional details on the CORINE nomenclature, see Büttner et al. (2021). The dataset is available at <https://land.copernicus.eu/pan-european/corine-land-cover/clc2018>.

Figure 4: CORINE Land Cover version 2018. For the legend, please refer to <https://land.copernicus.eu/pan-european/corine-land-cover/clc2018>



2.1.4. Economic activities

In order to characterize the importance of different types of economic activities for each CCLL, gross value added (GVA) data from Eurostat were adopted. GVA is a measure of productivity calculated as the value of output of goods and services less the value of intermediate consumption of goods and services. It is the basis for estimating the contribution of industries, sectors and/or regions to the gross domestic product (GDP) through the output approach.

Eurostat contains GVA data by economic sector using different aggregation levels of NACE (Nomenclature générale des Activités économiques dans les Communautés Européennes) Rev. 2, which is a widely used classification system for economic activities (Eurostat, 2008). For the purpose of establishing a breakdown of economic activities for SCORE's ten CCLLs and subsequently computing risk scores (as described in Section 3), three broad sectors were adopted: agriculture, industry, and tourism. Although these do not cover all economic sector (such as activities in the tertiary sector other than tourism), they can be considered representative of the economies of the ten CCLLs. Here, agriculture was defined as corresponding to NACE class "Crop and animal production, hunting and related





service activities”, industry to NACE class “Industry (except construction)”, and tourism to NACE class “Accommodation and food service activities”. The fractions of GVA corresponding to these activities for each CCLL were estimated by combining NUTS 3 data, available at a high-level aggregation (i.e., breakdown into less sectors), with national GVA data, which are aggregated at a lower level (i.e., more sectors). The former is available at https://ec.europa.eu/eurostat/databrowser/view/NAMA_10R_3GVA/default and the latter at https://ec.europa.eu/eurostat/databrowser/view/NAMA_10_A64/default. The elaborated data are shown in Table 5.

Table 5: Estimated economic activity GVA fractions for the ten CCLLs, based on Eurostat data.

CCLL	Economic activity GVA fractions (0-1)		
	Agriculture	Industry	Tourism
Benidorm	0.088	0.531	0.382
Dublin	0.004	0.862	0.135
Gdańsk	0.082	0.873	0.046
Massa	0.031	0.792	0.177
Oarsoaldea	0.017	0.813	0.17
Oeiras	0.017	0.583	0.401
Piran	0.047	0.700	0.253
Samsun	0.345	0.547	0.107
Sligo	0.139	0.804	0.057
Vilanova i la Geltrú	0.020	0.729	0.251

2.1.5. Road and railway networks

Exposure data for roads and railways was obtained from OpenStreetMap (OSM). OSM is an open, editable geographic dataset of the world licensed under the Open Data Commons Open Database License by the OpenStreetMap Foundation. This initiative is dedicated to fostering the growth, development and distribution of free geospatial data and to providing geospatial data for anyone to use and share. The development of OSM is a global mapping effort involving more than two million volunteers around the world. OSM data is widely used by individuals, governments and commercial companies for a wide range of applications, and in many countries, OpenStreetMap is a viable alternative to other map providers (OSM, 2023b).

OSM incorporates openly-licensed data from, among other sources, national mapping agencies from all over the world, some of which from countries where SCORE CCLLs are located (OSM, 2023a), such as:

- Italy: Regional Administration of Tuscany;
- Poland: UMP pcPL project (UMP is a map project for the whole of Poland);
- Portugal: Lisbon City Council and Porto City Council;
- Slovenia: Republic of Slovenia, Ministry of Agriculture, Forestry and Food;
- Spain: National Mapping Agency and National Cartographic System for Spain.

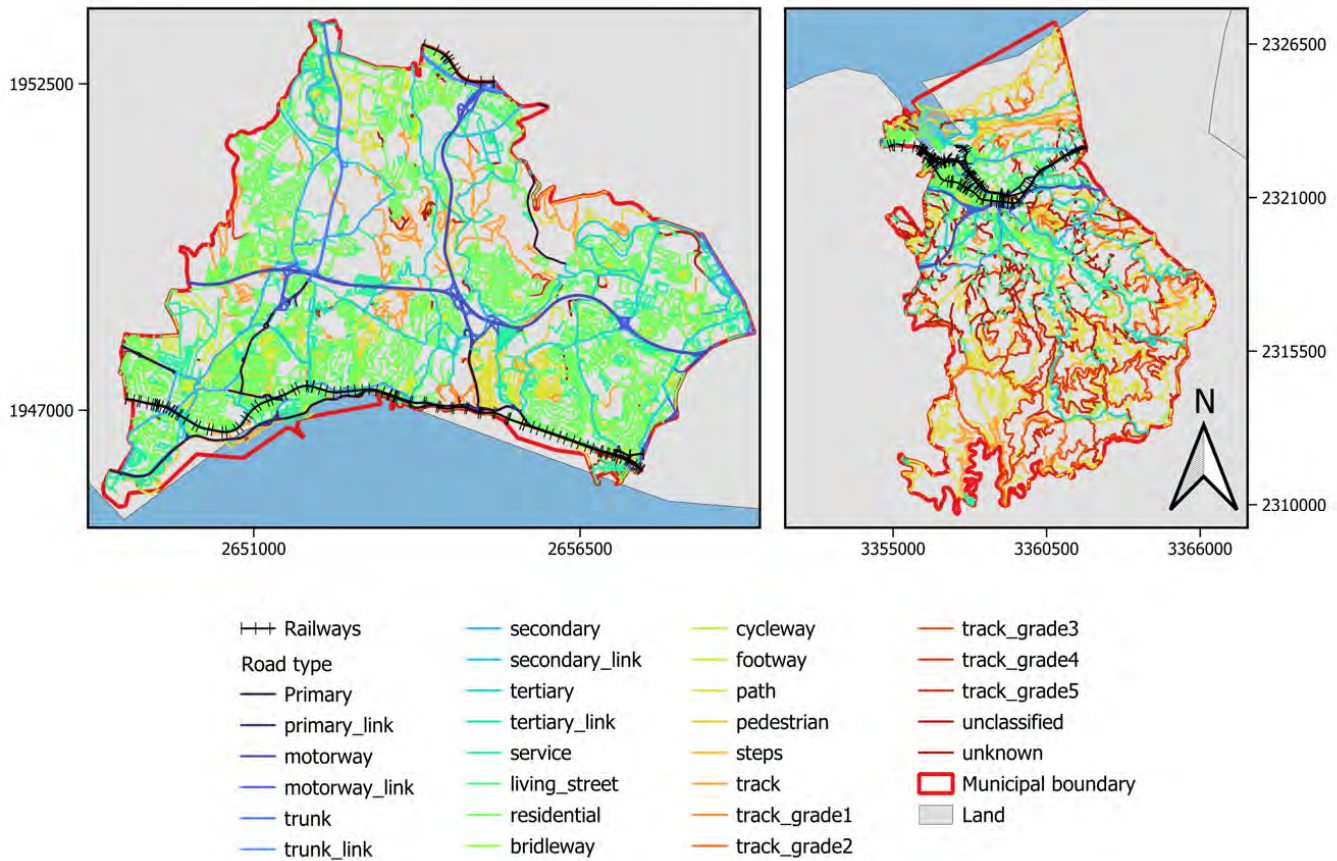
The OSM dataset uses a categorisation that differentiates the type and/or complexity of land transportation network elements. This categorisation divides roads into primary, secondary, tertiary, motorways, interchanges, residential,





pedestrian, cycle paths, footpaths, among others. Regarding railways, the categorisation includes rail, metro, tram, light rail, among others. For illustration, Figure 5 shows the roads and railways in the municipalities of Oeiras (on the left) and Oarsoaldea (on the right) with their original OSM road classification.

Figure 5: Road and railways network for the CCLLs of Oeiras (left) and Oarsoaldea (right).



For this study, a reclassification of the road and railways categories considered to be more relevant for risk assessment purposes was performed, as shown in Table 6. The OSM maps were obtained from the Geofabrik website at <https://download.geofabrik.de/europe.html>.

Table 6: Adopted reclassification of OSM classes.

Primary road	primary, primary_link, motorway, motorway_link, trunk, trunk_link
Secondary road	secondary, secondary_link, tertiary_link, service, tertiary, residential, living_street
Railway	funicular, light_rail, tram, monorail, rail, narrow_gauge
Reclassification	Original OSM classification

2.2. Hazard

2.2.1. Fluvial flooding

For fluvial flooding, the JRC hazard maps for Europe and the Mediterranean Basin produced by Dottori et al. (2021, 2022) were adopted. The maps were developed as a component of EFAS using a physically-based model chain, which includes hydrological modelling with long-term meteorological data, derivation of flood hydrographs based on statistical methods, and flood propagation simulation through hydrodynamic modelling. This recently published,



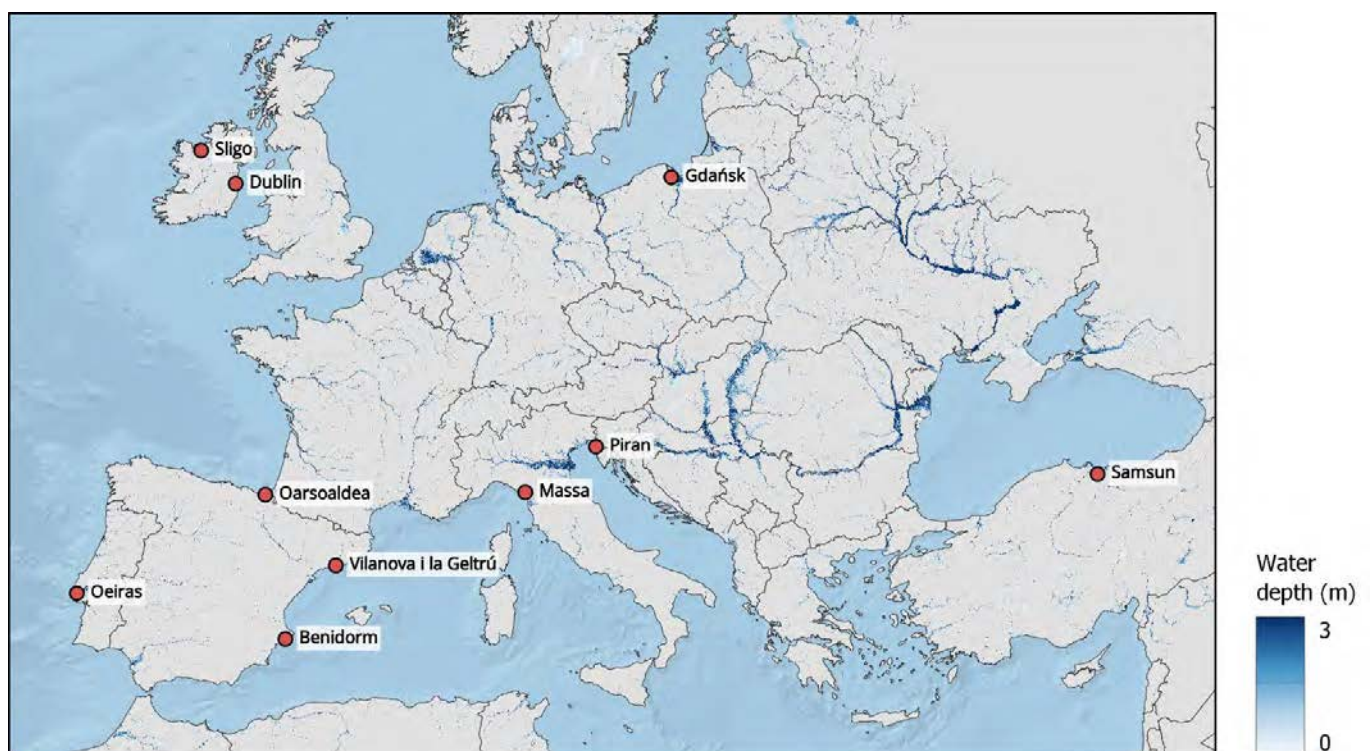


state-of-the-art dataset features various improvements over its first version (Alfieri et al., 2014; Dottori et al., 2016a), including an expanded geographical domain that includes, among other areas, the country of Turkey. This is an important feature in the context of SCORE due to the presence of the Turkish CCLL of Samsun.

The JRC fluvial flood hazard maps contain information on flood extents and water depths associated with return periods of 10, 20, 50, 100, 200 and 500 years, and have a spatial resolution of 100 m, which is considered high for a continental-scale flood hazard dataset. A drawback of this large-scale model is that it does not cover catchments with less than 500 km², where flooding is typically caused by short and intense rainfall events. In the context of Task 6.1, extreme precipitation estimates (see Section 2.2.3) are used to compute risk scores associated with such events.

A continental-level view of the JRC flood hazard map for a 100-year return period is shown in Figure 6. The dataset is available at the JRC Data Catalogue website (<https://data.jrc.ec.europa.eu/dataset/1d128b6c-a4ee-4858-9e34-6210707f3c81>). For additional details, the reader is referred to Dottori et al. (2022).

Figure 6: JRC fluvial flood hazard map for a 100-year return period.



2.2.2. Coastal flooding

Coastal flooding hazard assessment was based on Aqueduct Floods, which uses the Global Tide and Surge Reanalysis (GTSR) dataset (Muis et al., 2016). GTSR is a global dataset of daily sea levels (due to tide and storm surge) for 1979–2014, based on the hydrodynamic Global Tide and Surge Model (GTSM). Surge is simulated using wind and pressure fields from the European Centre for Medium-Range Weather Forecasts (ECMWF) Re-analysis-Interim (ERA-Interim) dataset (Dee et al., 2011). Tide is simulated using a separate model, the Finite Element Solution 2012 (FES 2012) model (Carrere et al., 2015). Extreme sea level values 2, 5, 10, 25, 50, 100, 250, 500, and 1,000-year return periods were obtained by fitting a Gumbel distribution at all locations. To translate near-shore tide and surge levels to overland inundation, a geographic information system (GIS)-based inundation routine was used.

Given the relatively coarse resolution of the GTSR product within the scope of a city-scale analysis such as the one being presented here, a simple downscaling methodology was applied. The 25m resolution EU-DEM Digital Elevation





Model (Bashfield and Keim, 2011), a digital surface model (DSM) of the European Environment Agency member and cooperating countries, was used to determine the extent of the inland penetration of coastal flood, assuming a local “bathtub” behaviour, i.e., assuming that the water depth provided by GTSR right off the shore propagates homogeneously towards inland, and therefore the inland water depths are the difference between the off-shore water depth and the local elevation. In this way, a 25m map of the water depth caused by coastal flood was obtained for all the cities, covering also inland areas if exposed to coastal flood (i.e., if their elevation is lower than the water depth provided by GTSR).

A continental-level view of the GTSR flood hazard map for a 100-year return period is shown in Figure 7. The dataset is available on the World Resources Institute website <https://www.wri.org/data/aqueduct-floods-hazard-maps>. For additional details, the reader is referred to Ward et al. (2020).

Figure 7: Aqueduct coastal flood hazard map for a 100-year return period.



2.2.3. Extreme precipitation

The GPEX dataset (Gründemann et al., 2021, 2023) was adopted to characterize extreme precipitation. This state-of-art dataset aims to overcome several issues associated with global extreme precipitation models, particularly by using a precipitation dataset that merges gauge, reanalysis and satellite data, estimating extremes for several event durations (including sub-daily), and using hydrological years in the analyses. In addition, precipitation is estimated using different extreme value distributions, allowing the authors to perform a comparative analysis among them. Based on this, in the present study, extreme precipitation data based on the recently developed metastatistical extreme value distribution was adopted, as it is found to have a higher spatial coherence.

GPEX provides global estimates of extreme precipitation for ten return periods and eight durations ranging from 3 hours to 10 days, and has a spatial resolution of 0.1° , which corresponds to approximately 11 km at the equator. This is a relatively standard resolution for a global-scale precipitation dataset and provides information that is considered sufficient for the purpose of Task 6.1.

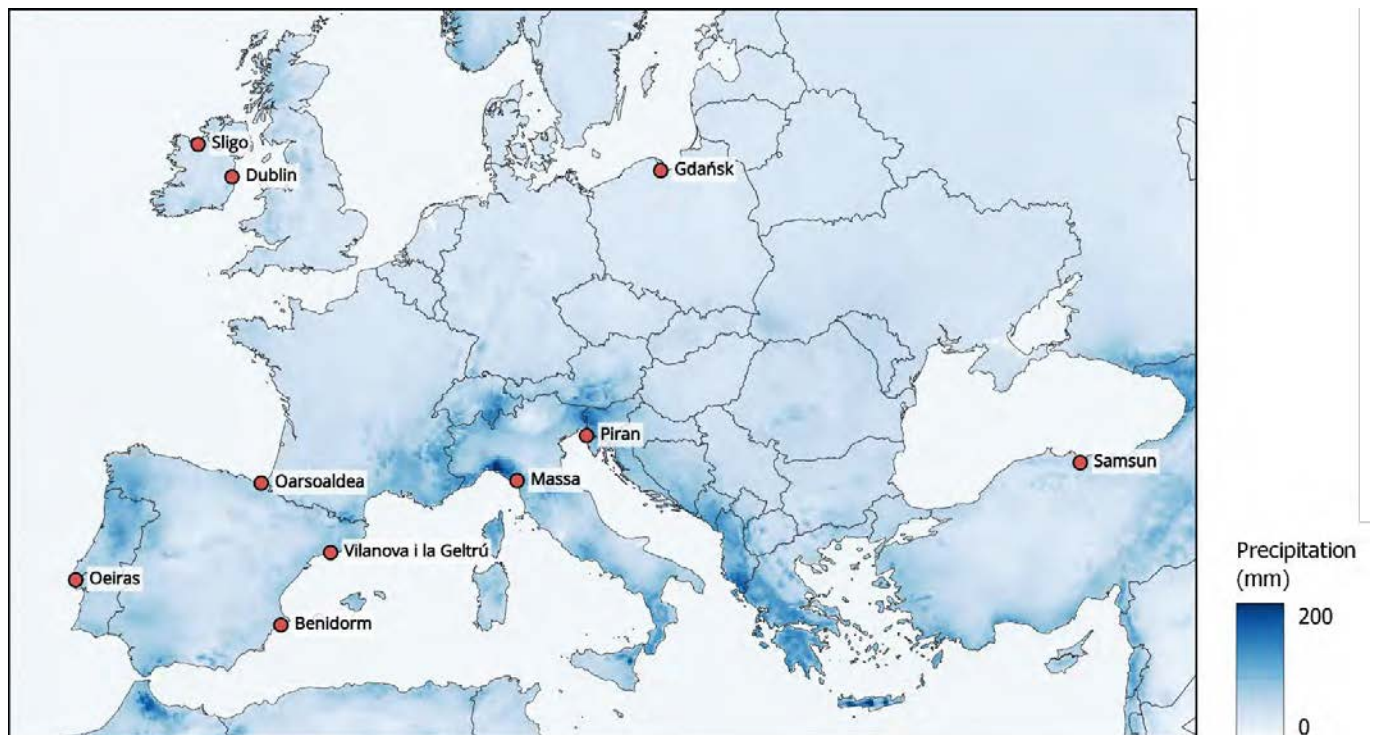




Extreme precipitation can have different types of consequences depending on its intensity and duration. In the context of this task, given that fluvial flood and landslide perils – caused by precipitation – are explicitly considered using specific hazard models, interest lies mainly on capturing short and intense rainfall events than can cause, apart from direct damage, urban pluvial floods. For this reason, extreme precipitation with a duration of 24 hours was adopted. It should be noted that accurately modelling pluvial flooding requires highly detailed, location-specific flood propagation modelling that includes the surface drainage network (Palla et al., 2018), which is outside the scope of the present task. However, considering the overall objective of performing a semi-quantitative score-based comparative assessment of different risks in the ten CCLLs, extreme precipitation is considered an adequate proxy for the occurrence of pluvial flood events.

Figure 8 shows GPEX extreme precipitation estimate with a return period of 5 years and a duration of 24 hours over a spatial domain that includes SCORE's ten CCLLs. The dataset is available at the 4TU.ResearchData repository (<https://data.4tu.nl/datasets/9c547b34-f9d0-410c-be38-f0bdb46318cf/4>). For additional details, the reader is referred to Gründemann et al. (2023).

Figure 8: GPEX precipitation map for a 5-year return period and duration of 24 hours.



2.2.4. Landslide

For the characterization of the landslide hazard, two datasets were used. The main dataset is the European Landslide Susceptibility Map version 2 (ELSUS v2), developed specifically for Europe, which has a spatial resolution of 200 m. However, because its spatial domain does not include Samsun, it was complemented with the Landslide Hazard Assessment for Situational Awareness (LHASA) susceptibility map for that CCLL. LHASA has global coverage and a lower but acceptable spatial resolution of 1000 m. Moreover, its susceptibility scale is compatible with the one used in ELSUS v2.



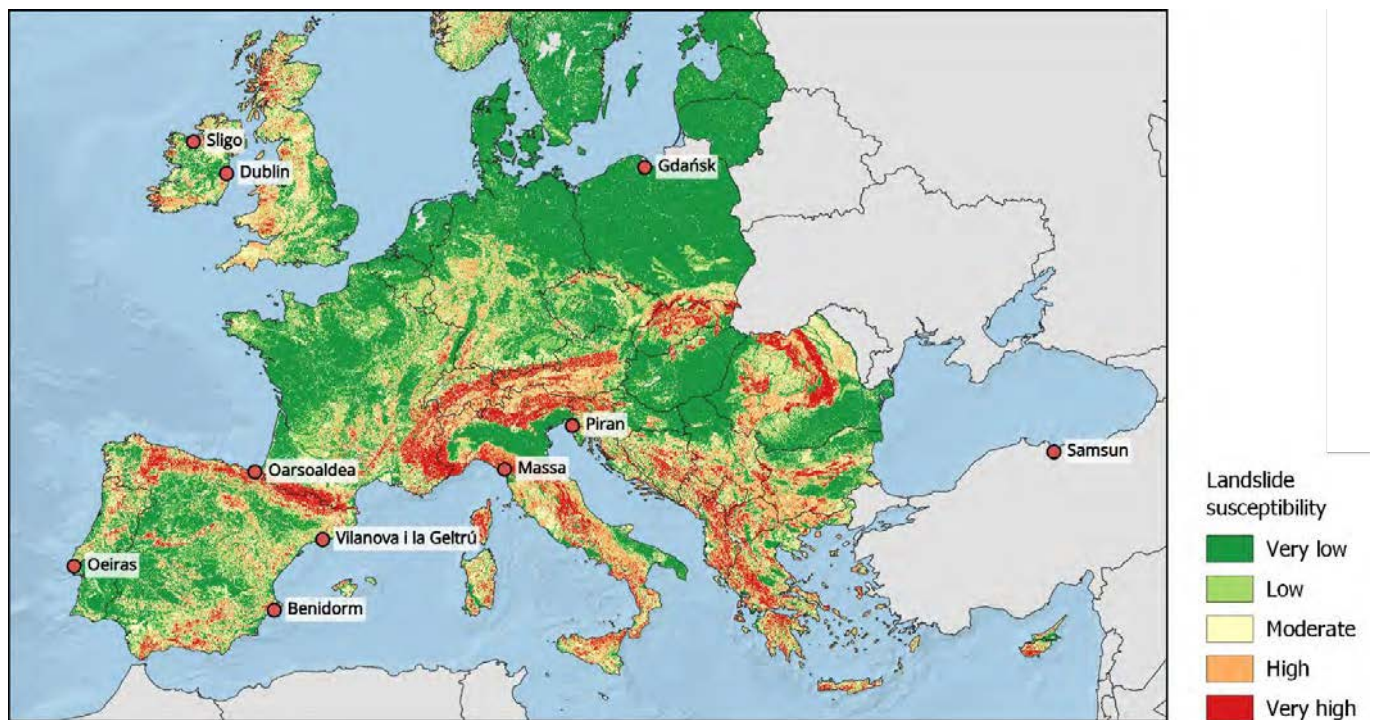


2.2.4.1. European Landslide Susceptibility Map

The ELSUS v2 geospatial dataset provides levels of probability of generic landslide occurrence at continental scale. It covers all European Union member states except Malta, and several neighbouring countries. The map has been produced by regionalizing the study area based on elevation and climatic conditions, followed by spatial multi-criteria evaluation modelling using pan-European slope angle, shallow sub-surface lithology, and land cover spatial datasets as the main landslide conditioning factors. In addition, the location of over 149,000 landslides across Europe, provided by various national organizations or collected by the authors, has been used for model calibration and map validation. ELSUS v2 describes landslide susceptibility according to five classes: very low, low, moderate, high, and very high.

The ELSUS v2 susceptibility dataset is shown in Figure 9. It is available on request at <https://esdac.jrc.ec.europa.eu/content/european-landslide-susceptibility-map-elsus-v2>, where additional information is provided. For more details, the reader is referred to Wilde et al. (2018)

Figure 9: ELSUS v2 landslide susceptibility map



2.2.4.2. Landslide Hazard Assessment for Situational Awareness Model

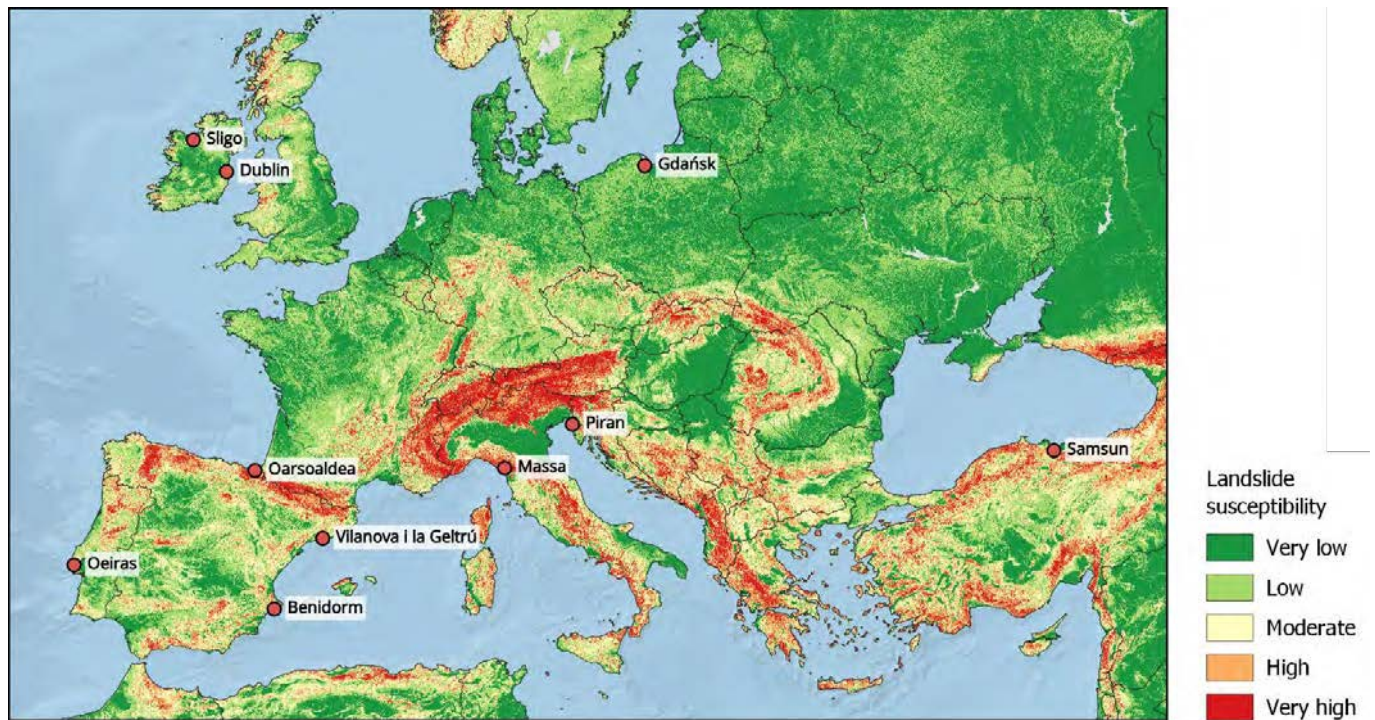
The LHASA susceptibility map was developed building on prior research efforts to map the geographic distribution of landslide activity at continental and global scales, taking into account both existing and previously unavailable data. It combines data on slope, faults, geology, forest loss, and road networks using a heuristic fuzzy approach. The map was evaluated with a Global Landslide Catalog developed at NASA, as well as several local landslide inventories. The LHASA landslide susceptibility map is intended for use in disaster planning, situational awareness, and for incorporation into global decision support systems. Here, the recent 2023 update of the LHASA susceptibility map was adopted, which includes improvements such as the inclusion of forest loss as well as updated road density information (Emberson et al., 2020; Stanley and Kirschbaum, 2017).





The LHASA map over the spatial domain of SCORE is shown in Figure 10. The dataset can be obtained at <https://gpm.nasa.gov/landslides/projects.html#LHASA>. Additional information may be found at this website and on the provided references.

Figure 10: LHASA landslide susceptibility map



2.2.5. Heat wave

A heat wave is an extended period of abnormally hot weather, usually defined as having a duration of at least two days (IPCC, 2022). Although heat waves can cause impacts on different sectors, their most severe consequences typically occur on populations (Schär and Jendritzky, 2004). Therefore, even if heat waves are meteorological events, their analysis necessarily involves understanding and assessing their human impacts (Robinson, 2001). Accordingly, in this study, the development of a heat wave risk score is based on the universal thermal climate index (UTCI), which is a state-of-the-art bioclimatic index that estimates the thermal stress that the human body undergoes when exposed to outdoor conditions (Jendritzky et al., 2012). The UTCI is a widely used variable that has been evaluated and validated in multiple climate regions and across different spatial scales.

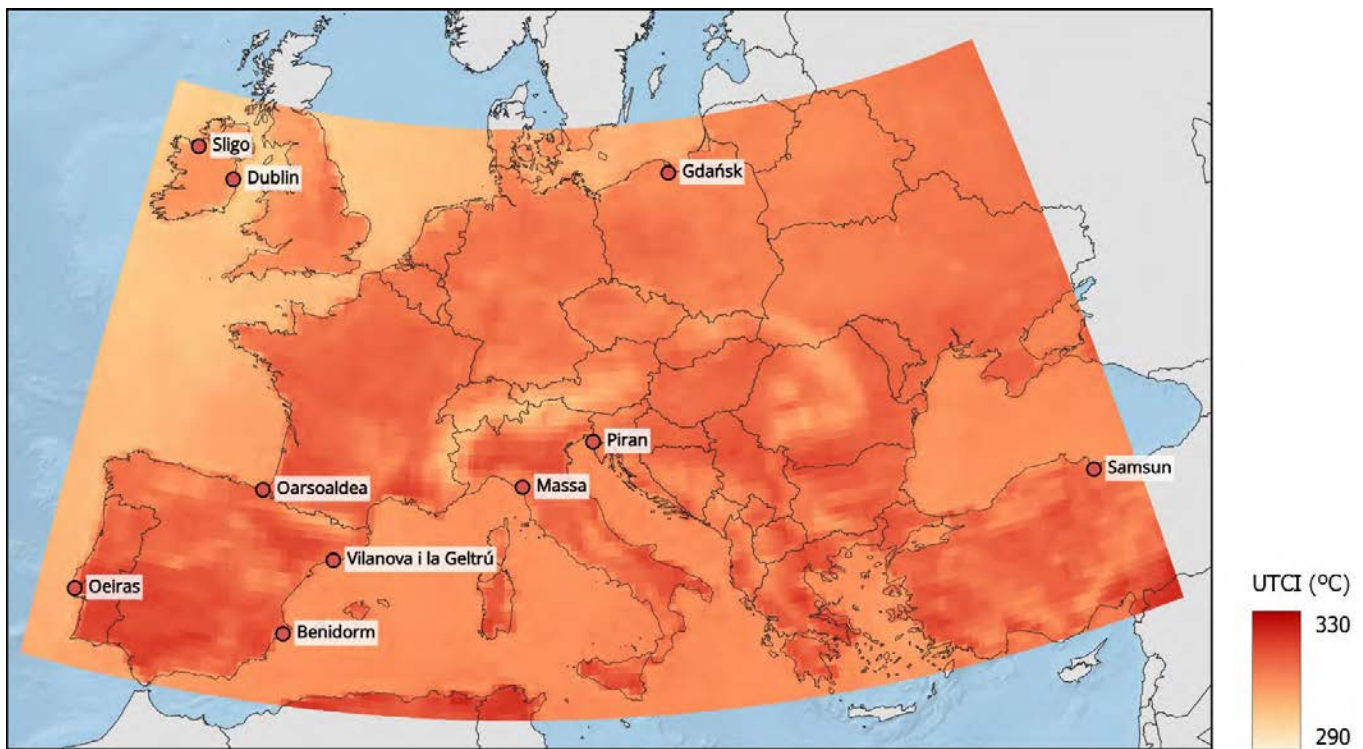
UTCI data was obtained from the ERA5-HEAT dataset. It includes modelled hourly data computed using environmental parameters provided by the ERA5 reanalysis from the European Centre for Medium-Range Forecasts (ECMWF), which combines model and observational data worldwide to provide a global and consistent description of the Earth's climate and its evolution in recent decades (Barnard, 2022). UTCI data from 01/01/1980 to 31/07/2022 were used to perform statistical analyses on the time series based on which a single score could be derived for each CCLL, as described in Section 3.1.4.

Figure 11 shows the 99th percentile of UTCI daily maxima computed for each grid cell in a spatial domain covering SCORE's ten CCLLs. The underlying data and additional information are available at the Copernicus Climate Data Store (<https://cds.climate.copernicus.eu/cdsapp#!/dataset/derived-utci-historical>).





Figure 11: UTCI daily maxima: 99th percentile for each grid cell over a spatial domain covering SCORE's ten CCLs.



2.2.6. Coastal erosion

The assessment of coastal erosion is based on the EUROSION version 2 dataset. EUROSION was a project commissioned by the Environment Directorate-General of the European Commission, which had as one of its objectives the development of a European geographical coastal erosion database according to standards laid down by the European Environmental Agency (Lenôtre et al., 2004). This database aimed to enable the identification of risks arising from potential coastal erosion problems on a Europe-wide scale. The design approach was an update of the 1990 CORINE Coastal Erosion methodology in which three criteria were used: 1) morpho-sedimentology (e.g., rocky coasts, beaches, muddy coasts); 2) evolutionary trends (i.e., erosion, aggradation, stability); and 3) presence or not of coastal defence works. The data were provided by national or local contact organisations and were merged into a seamless coastline database.

The database comprises around 34,000 coast segments, which represents approximately 100,000 km of coastline. Turkey is not covered, meaning the Samsun CCLL is not included in the analysis for this hazard. Each coast segment is characterised by a CEEVV2 (i.e., Coastal Erosion EVolutionary trend Version 2) code representing its evolutionary trend, as shown in Table 7. The ten code items are divided into four main classes: 1) Absence of information, 2) Stability, 3) Erosion and 4) Aggradation. The evolutionary trends are described qualitatively; according with Lenôtre N. (2004), owing to disparities in available data, it is not possible to have quantitative information on evolutionary trends at European scale. Moreover, the rate of erosion is far from constant in terms of time, and inversions can occur in the trend. For each coast segment, the EUROSION dataset also contains information on the presence of coastal defences (longitudinal or transversal, built on the strand or offshore), which is provided in a binary format (i.e., Yes/No).





Table 7: Erosion evolutionary trend code descriptions in the EUROSION dataset.

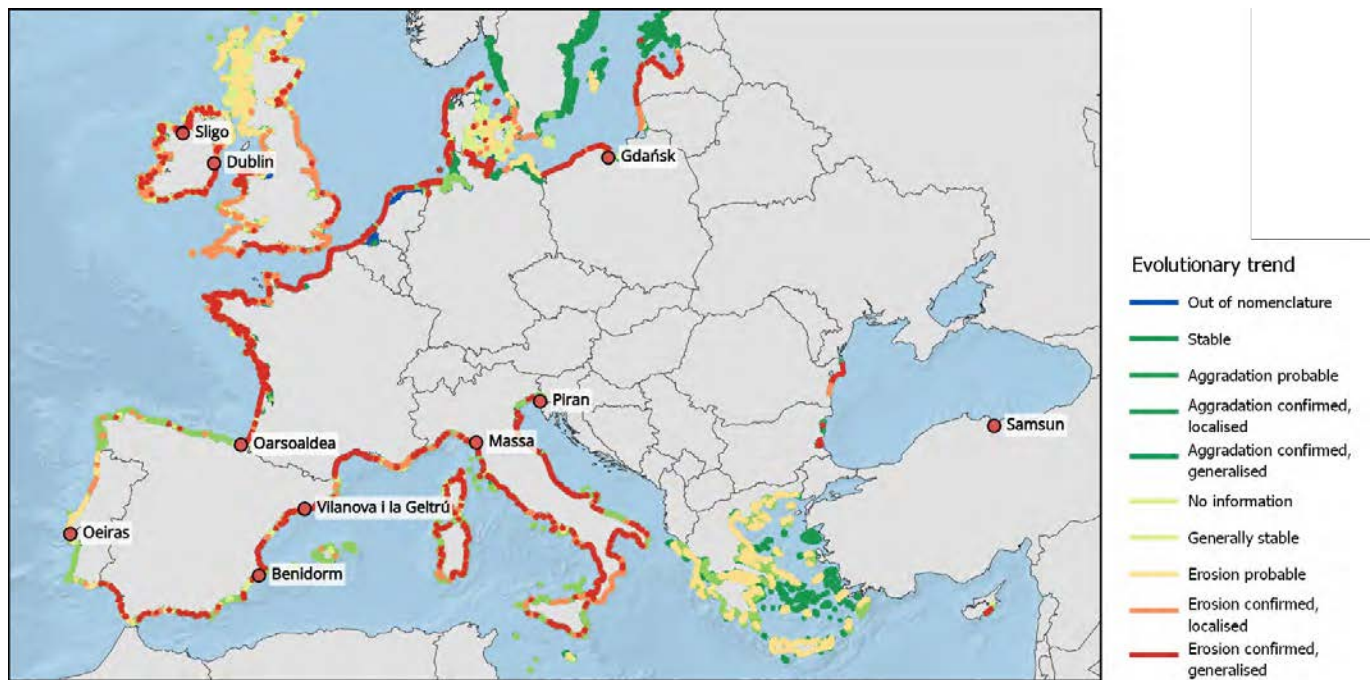
CEEV2 code	Description
Absence of information	
0	Not in nomenclature
1	No information on evolution
Stability	
2	Stable: evolution almost imperceptible at human scale
3	Generally stable: small "isolated" variations around a stable position – the evolutionary trend is uncertain
Erosion	
4	Erosion probable, but not documented
50	Erosion confirmed (available data) along parts of the segment
51	Erosion confirmed (available data) along almost the whole length of the segment
Aggradation	
6	Aggradation probable, but not documented
70	Aggradation confirmed (available data) along parts of the segment
71	Aggradation confirmed (available data) along almost the whole length of the segment

Figure 12 shows the extension covered by the EUROSION dataset, classified according to the evolutionary trends described above. The data are available at <https://www.eea.europa.eu/data-and-maps/data/geomorphology-geology-erosion-trends-and-coastal-defence-works>.





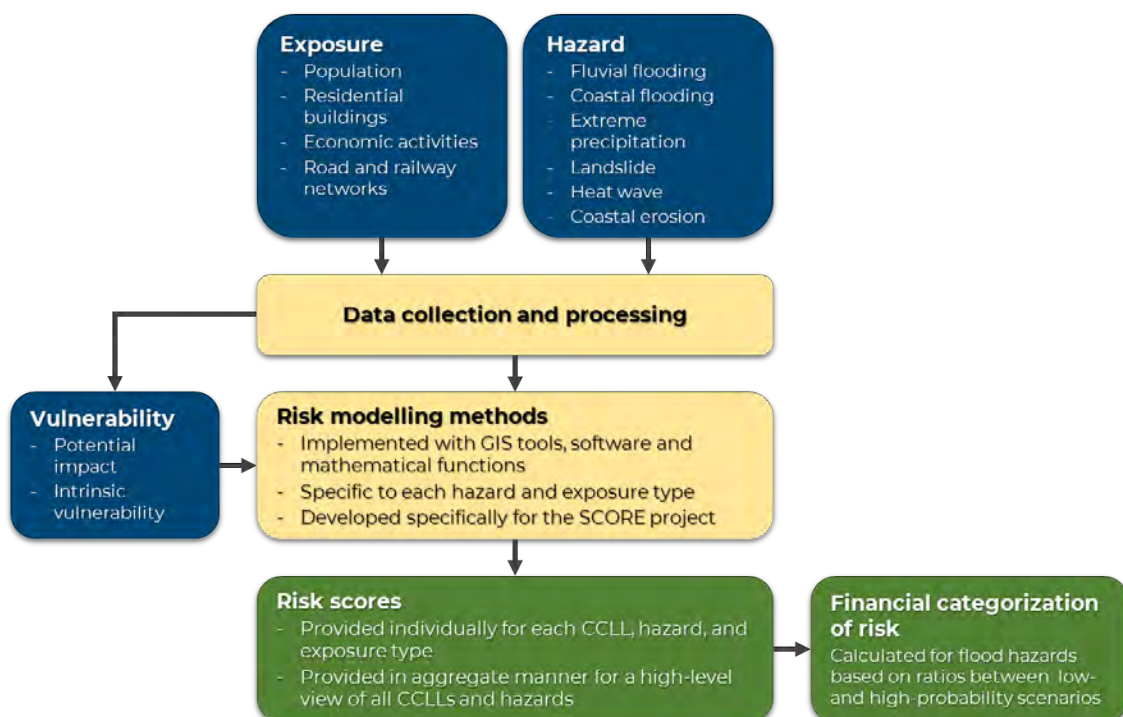
Figure 12: EUROSION coastal erosion dataset with coast segments classified according to their evolutionary trend.



3. METHODOLOGY

This section describes the methodology developed in the context of Task 6.1 for the characterization of the different risks that the CCLs are exposed to. The general methodological framework is represented in Figure 13. Note that the risk score computation methodology varies depending on the hazard, as described in the following subsection.

Figure 13: Methodological framework.





3.1. Risk scores

The developed methodologies for computing risk scores for the six hazards considered in the present task are designed to provide results which, even if semi-quantitative, have an underlying physically-based meaning and support from the risk modelling viewpoint (i.e., combining hazard, exposure and vulnerability components). In addition, they are designed such that the scores among types of exposed elements and/or hazards have a common scale and can be compared in a straightforward manner. In this regard, a scale between 0 (i.e., no risk or negligible) and 10 (i.e., very high risk) was adopted to quantify the risks.

Notwithstanding, it should be noted that the methodologies, described in the following subsections, are necessarily different due to differences in their physical properties and the hazard models adopted to describe them. In this regard, two main aspects can be distinguished: the type of variable used to characterize the hazard, and its spatial variability at the scale of the CCLLs. Regarding the former, a hazard can be characterized through either an intensity measure, which is a measure of a physical property of the hazard (typically associated with a probability of exceedance) that is informative for estimating its potential consequences, or a susceptibility class describing the tendency of an area to undergo the effects of a certain hazard. In terms of spatial variability, while certain phenomena tend to have large footprints without abrupt intensity variations in space (e.g., heat waves) and a single hazard value can be adopted for the whole area covered by the CCLL, others tend to have narrower and more irregularly shaped footprints where intensity can significantly change among nearby areas (e.g., floods) and therefore the spatial variability of the hazard within the city has to be taken into account. Table 8 summarizes these properties for each hazard.

Table 8: hazard properties (variable adopted for hazard quantification and spatial variability of the hazard at the scale of a CCLL).

Hazard	Hazard variable		Spatial variability at CCLL scale	
	Intensity measure	Susceptibility class	Heterogeneous	Single value
Fluvial flooding	●		●	
Coastal flooding	●		●	
Extreme precipitation	●			●
Landslide		●	●	
Heat wave	●			●
Coastal erosion		●	●	

3.1.1. Fluvial and coastal flooding

Floods tend to have irregularly-shaped spatial footprints, and their intensity – typically expressed in terms of water depth – can vary substantially over small areas. Therefore, the estimation of risk scores for this spatially heterogeneous hazard is based on a conceptual framework where potential impacts are first expressed on a grid-cell basis, and then combined to obtain overall risk scores. Fluvial and coastal flood hazard map corresponding to a 100-year return period were adopted, since the 1-in-100 years event is representative of a damaging event which typically has a significant impact. The methodology to estimate and combine risk scores for the four types of elements





considered – population, residential buildings, economic activities, and road and railway networks – is described in the following subsections.

3.1.1.1. Population

The risk score for population S_{pop} is given by

$$S_{pop} = \min \{S'_{pop}, 10\} \quad (1)$$

and

$$S'_{pop} = I_{pop} \times V_{pop} \quad (2)$$

where I_{pop} is the potential impact sub-score and V_{pop} is the intrinsic vulnerability factor. The I_{pop} sub-score reflects the amount of exposed population in the CCLL and the hazard intensities to which they are exposed, linked to potential impacts through a simplified vulnerability function. It is given by the average of the potential impacts over the cells of a regular grid covering the CCLL, weighted by the population in each cell:

$$I_{pop} = \frac{1}{t} \sum_g i_{pop,g} \times f_{pop,g} \quad (3)$$

where $i_{pop,g}$ is the potential impact index to population in the g th grid cell affected by flooding and $f_{pop,g}$ is the fraction of the CCLL population therein based on WorldPop data. The $i_{pop,g}$ index is obtained as a function of water depth through a simplified vulnerability model given by

$$i_{pop,g} = \begin{cases} 10x_g/w, & x_g < w \\ 10 & , x_g \geq w \end{cases} \quad (4)$$

where x_g is the water depth at the g th grid cell and w corresponds to the water depth threshold at which the maximum value for the potential impact index (i.e., $i_{pop,g}=10$) is obtained. This formulation assumes that a linear relationship between water depth and flood impact up to a certain water depth threshold (in the case of population, $w=1.5$ m is used), at which a very high level of impact is reached (e.g., Figueiredo et al., 2020). Lastly, in Eq. (3), t is a factor that adjusts the sub-score to the fact that a flood event is considered disastrous not only when the entire CCLL is affected (i.e., when the fraction of population affected sums to 1), but at a significantly lower threshold. Here, $t=0.05$ was adopted, meaning that I_{pop} can potentially reach a value of 10 when 5% of the population in a CCLL is affected by a flood.

The second variable of Eq.(2) (V_{pop}) is defined as a factor that captures the intrinsic vulnerability of the elements under analysis as a function of certain characteristics. In the case of population, the age structure was adopted, i.e., the fractions of population belonging to different age ranges, as follows:

$$V_{pop} = \sum_j v_{age,j} \times f_{pop,j} \quad (5)$$

In Eq.(5), $v_{age,j}$ is the vulnerability index for the j th age range (see Table 2) and $f_{pop,j}$ is the fraction of population in the CCLL belonging to that range, based on Eurostat data. Table 9 shows the vulnerability indices $v_{age,j}$ considered for each age range. Based on this formulation, V_{pop} works as a factor that increases the potential physical impact sub-score I_{pop} depending on the age structure of the population, whereby both the younger and the older groups of population are considered more vulnerable to negative hazard impacts (e.g., Kaynia et al., 2008).





Table 9: Vulnerability indices considered for different age ranges.

Age range	Vulnerability index
0 – 4	2.0
5 – 14	1.2
15 – 64	1.0
65 – 74	1.2
>= 75	2.0

3.1.1.2. Residential buildings

The formulation of the risk score for residential buildings $S_{resbldg}$ is analogous to the one for population:

$$S_{resbldg} = \min \{S'_{resbldg}, 10\} \quad (6)$$

$$S'_{resbldg} = I_{resbldg} \times V_{resbldg} \quad (7)$$

$$I_{resbldg} = \frac{1}{t} \sum_g i_{resbldg,g} \times f_{pop,g} \quad (8)$$

Note that in Eq. (8), the spatial distribution of building fractions within a CCLL is assumed to follow the same spatial distribution of population fractions therein, and therefore $f_{pop,g}$ is used. This is a robust assumption, which is particularly suitable in this case because the adopted WorldPop constrained dataset uses building footprints to spatially distribute population in the first place (see Section 2.1.1.1).

The potential impact index at grid cell level for residential buildings $i_{resbldg,g}$ is computed similarly to the index for population, as defined in Eq. (4). Here, the threshold w at which the vulnerability function is assumed to reach its maximum value is 2.5 m:

$$i_{resbldg,g} = \begin{cases} 10x_g/w, & x_g < w \\ 10 & , x_g \geq w \end{cases} \quad (9)$$

As for population, in Eq.(9), $V_{resbldg}$ is a factor that captures the intrinsic vulnerability of residential buildings in the CCLL, amplifying the potential physical impact sub-score $I_{resbldg}$. In this case, $V_{resbldg}$ is a function of the distributions of building material types and building heights in the CCLL, which are two properties that are known to affect to vulnerability of buildings to this type of hazard (Dottori et al., 2016b). It is given by

$$V_{resbldg} = \left(\sum_j v_{mat,j} \times f_{resbldg,j} + \sum_k v_{height,k} \times f_{resbldg,k} \right) / 2 \quad (10)$$

where $v_{mat,j}$ is the vulnerability index for the j th building material class, $v_{height,k}$ is the vulnerability index for the k th building height class, and $f_{resbldg,j}$ and $f_{resbldg,k}$ are the fractions of residential buildings belonging to those two classes, respectively. Table 10 shows the considered vulnerability indices for each class, which were defined based on expert engineering knowledge.





Table 10: Vulnerability indices considered for different classes of building properties.

Building property	Class	Vulnerability index
Construction material	Reinforced concrete	1.0
	Masonry	1.1
	Wood	1.5
Height	Low rise	1.4
	Mid rise	1.1
	High rise	1.0

3.1.1.3. Economic activities

The risk score for economic activities S_{econ} is estimated from the combination of the risk sub-scores for three selected sectors: agriculture, industry, and tourism. The sub-score combination is performed based on the geometric mean to avoid the full compensability of linear aggregation methods, i.e., the possibility of offsetting a high risk score for one sector with a low risk score for another (OECD, 2008). Specifically, the formulation is based on a weighted geometric mean, where the weights are given by the relative contributions of each sector to the GVA of the region, as defined in Section 2.1.4. Accordingly,

$$S_{econ} = - \left(\prod_j (-I_j + 11)^{w_j} \right)^{1/\sum_j c_j} + 11 \quad (11)$$

with

$$I_j = \min \{I'_j, 10\} \quad (12)$$

where I'_j is the potential impact sub-score for the j th economic activity and c_j is its respective weight given by the corresponding GVA fraction (Table 5). The I'_j sub-score for each individual economic activity reflects the estimated areas of associated land cover in the CCLL and the hazard intensities to which they are exposed, linked to impacts through a simplified vulnerability function. It is given by

$$I'_j = \frac{1 \sum_g i_{j,g}}{t N_j} \quad (13)$$

where $i_{j,g}$ is the potential impact index to the j th economic activity in the g th grid cell affected by flooding, N_j is the number of grid cells associated with that activity within the CCLL, and t is a modifying factor as described in Section 3.1.1.1 that takes the value of 0.05. Here, the definition of grid cells associated with each of the three economic activities is based on CLC geospatial data through a correspondence between those activities (and underlying NACE classes) and CLC classes, as shown in Table 11. Note that Eq. (13) assumes that the economic activities are homogeneously distributed within each CLC polygon, which may not always be the case. Nevertheless, this is considered an adequate assumption given the scope of the present study.





Table 11: Correspondence between economic activities and CLC classes.

Economic activity	CLC class	CLC description
Agriculture	211	Non-irrigated arable land
	212	Permanently irrigated land
	213	Rice fields
	221	Vineyards
	222	Fruit trees and berry plantations
	223	Olive groves
	231	Pastures
	241	Annual crops associated with permanent crops
	242	Complex cultivation patterns
	243	Land principally occupied by agriculture with significant areas of natural vegetation
	244	Agro-forestry areas
Industry	121	Industrial or commercial units
	131	Mineral extraction sites
Tourism	111	Continuous urban fabric
	112	Discontinuous urban fabric
	124	Airports
	141	Green urban areas
	142	Sport and leisure facilities

The $i_{j,g}$ index is obtained, following the same rationale as for population and residential buildings, as a function of water depth through a simplified vulnerability model given by

$$i_{j,g} = \begin{cases} 10x_g/w_j, & x_g < w_j \\ 10 & , x_g \geq w_j \end{cases} \quad (14)$$

where x_g is the water depth at the g th grid cell and w_j corresponds to the water depth threshold for the j th economic activity at which the maximum value for the potential impact index is obtained (i.e., $i_{j,g}=10$). A water depth threshold of 1.5 m is considered for agriculture, while a threshold of 1.0 m is considered for industry and tourism. The different thresholds reflect the assumption that agriculture is typically more resilient to flood than the two other sectors.

3.1.1.4. Road and railway networks

The risk score for land transportation networks S_{transp} is calculated as a combination of potential impact sub-scores for the road and railway networks (I_{road} and I_{rail} , respectively), using a geometric mean-based approach to avoid full sub-score compensability, as explained in the previous subsection. S_{transp} is therefore given by





$$S_{transp} = -((-I_{road} + 11) \times (-I_{rail} + 11))^{1/2} + 11 \quad (15)$$

where

$$I_{road} = \min \{I'_{road}, 10\} \quad (16)$$

$$I_{rail} = \min \{I'_{rail}, 10\} \quad (17)$$

and

$$I'_{road} = \frac{1}{t} \frac{\sum_g l_{pri,g} i_{pri,g} + \sum_g l_{sec,g} i_{sec,g}}{L_{road}} \quad (18)$$

$$I'_{rail} = \frac{1}{t} \frac{\sum_g l_{rail,g} i_{rail,g}}{L_{rail}} \quad (19)$$

The variables $l_{pri,g}$, $l_{sec,g}$ and $l_{rail,g}$ are, respectively, the length of primary roads, secondary roads and railways in the g th grid cell, $i_{pri,g}$, $i_{sec,g}$ and $i_{rail,g}$ are the respective potential impact indices, L_{road} and L_{rail} are the total road and railway lengths in the CCLL, and t is the modifying factor described in previous subsections. Concerning the estimation of potential impact indices, indirect losses caused by the disruption of transportation networks can be very significant and typically larger than direct losses to roads and railways, and should be considered in risk assessments. Disruption in a road or railway segment can be assumed to occur when water depth exceeds a certain threshold at its location, at which it is rendered unusable, affecting network functionality. Therefore, in the case of roads and railways, the impact index is given by

$$i_{j,g} = \begin{cases} 0 & , \quad x_g < w_j \\ y_j & , \quad x_g \geq w_j \end{cases} \quad (20)$$

where y_j is the impact index for the j th element type (i.e., primary road, secondary road or railway) that occurs when water depth at the g th grid cell where it is located exceeds the water depth threshold w_j for that type, as shown in Table 12. Here, a maximum value of 8 – rather than 10 – is used in order to reflect the limited flood direct damage that is expected to occur to these elements compared to the indirect damage, as explained above. The lower value considered for secondary roads reflects their lower value and relevance for the network. In Eqs. (18) and (19), t is a modifying factor to the sub-scores analogous to the one used in Eqs. (3), (8) and (13), which in this case is equal to the fraction of affected road or railway lengths that would lead to a very high level of network disruption; a value of 0.05 was adopted.

Table 12: Flood potential impact indices for road and railway network elements.

Element type	Impact index y_j	Water depth threshold w_j
Primary road	8	0.2
Secondary road	6	0.2
Railway	8	0.1

3.1.2. Extreme precipitation

Extreme precipitation tends to cause damage and losses mainly due to disaster events that it triggers rather than in a direct manner, as discussed in Section 2.2.3. In addition, its intensity also tends to present less spatial variability





over small areas when compared with floods. Reder et al. (2022), for example, developed an extreme precipitation dataset for a selected number of cities based on a downscaling of ERA5 reanalysis data, which is considered by the authors to have a very high spatial resolution at 0.02° (≈ 2.2 km). In contrast, flood hazard models require a much higher resolution (i.e., 100 m or higher) in order to allow for accurate impact modelling at city-scale (e.g., Bates, 2022). For these reasons, and taking into account the spatial resolution of the adopted GPEX data (i.e., 0.1° , or approximately 11 km), the methodology for computing extreme precipitation risk scores is necessarily different than the one presented in the previous subsection. Here, performing a spatial overlap between precipitation estimates and exposed assets – which are represented at much higher spatial resolutions – would not be meaningful. Accordingly, in this case, the risk score for extreme precipitation is defined directly as a function of its estimated intensity. This intensity is calculated as the mean precipitation over the CCLL, which is considered a suitable approach because of the generally low number of precipitation grid cells over the CCLLs and the fact that their values have low variability.

The risk score for extreme precipitation in the CCLLs is intended to express damage caused by short and intense rainfall events that typically result in urban pluvial floods, as mentioned in Section 2.2.3. Accordingly, GPEX precipitation data for a duration of 24 hours was adopted. The translation of precipitation intensity p into a risk score S is performed as follows:

$$S = \min \left\{ \frac{(p - 30) \times 10}{60}, 10 \right\} \quad (21)$$

This corresponds to a linear interpolation whereby a precipitation intensity of 30mm corresponds to a risk score of 0 and a precipitation intensity of 90mm or above corresponds to a risk score of 10. These thresholds were defined taking into account sources that translate quantitative rainfall estimates into qualitative intensity descriptions, such as (ARPA Piemonte, n.d.). The 5-year return period GPEX dataset was used considering the design return periods that are typically used for urban surface drainage systems.

3.1.3. Landslide

Landslides are expressed in terms of susceptibility levels which have sub-CCLL spatial variability, as shown in Table 8. Therefore, the calculation of landslide risk scores requires a conceptual framework where hazard and exposure are combined at grid-cell level. However, in the case of landslides, a relationship between hazard variable and potential impact cannot be established, as the susceptibility index is not a measure of hazard intensity but instead reflects the tendency of a landslide to occur at every grid cell in the CCLL (as explained in Section 3.1). The computation of the landslide risk scores reflects these specificities and is described in the following subsections.

3.1.3.1. Population

The risk score for population S_{pop} is given by Eq. (1), with

$$S'_{pop} = U_{pop} \times V_{pop} \quad (22)$$

where U_{pop} is the susceptibility sub-score and V_{pop} is the intrinsic vulnerability factor. The U_{pop} sub-score reflects the amount of exposed population in the CCLL and the hazard susceptibilities to which they are exposed, and is given by





$$U_{pop} = \frac{1}{t} \sum_g u_g \times f_{pop,g} \quad (23)$$

where u_g is the susceptibility index in the g th grid cell and $f_{pop,g}$ is the fraction of the CCLL population therein based on WorldPop data. For landslides, the u_g index is obtained by converting the qualitative description of landslide susceptibility in the ELSUS and LHASA datasets into a semi-quantitative scale ranging from 0 to 10, as shown in Table 13, such that it can be used for obtaining risk scores that are comparable among different hazards and CCLLs.

Table 13: Correspondence between qualitative landslide susceptibility classes and semi-quantitative susceptibility indices.

Original susceptibility class	Susceptibility index u_g
Very low	0
Low	2.5
Medium	5.0
High	7.5
Very high	10

In Eq. (23), t is a sub-score adjusting factor that enables U_{pop} to potentially reach a value of 10 not only if the entire population in the CCLL is located in areas of very high susceptibility (i.e., $u_g=10$), but at a lower threshold of exposed population. Here, $t=0.75$ was adopted. Lastly, the population intrinsic vulnerability factor V_{pop} in Eq. (22) is described in Section 3.1.1.1 and is given by Eq. (5).

3.1.3.2. Residential buildings

Analogously to the case of population, the risk score for residential buildings $S_{resbldg}$ is given by Eq. (6), with

$$S'_{resbldg} = U_{resbldg} \times V_{resbldg} \quad (24)$$

$$U_{resbldg} = U_{pop} \quad (25)$$

As explained in Section 3.1.1.2, the spatial distribution of building fractions within a CCLL is assumed to follow the same spatial distribution of population fractions. Therefore, and because in the case of landslides the $U_{resbldg}$ sub-score reflects landslide susceptibility rather than impact, $U_{resbldg}$ is equal to U_{pop} , as expressed in Eq. (25). The $V_{resbldg}$ factor is described in Section 3.1.1.2 and is given by Eq. (10)

3.1.3.3. Economic activities

The risk score for economic activities S_{econ} is given by:

$$S_{econ} = - \left(\prod_j (-U_j + 11)^{w_j} \right)^{1/\sum_j c_j} + 11 \quad (26)$$

with





$$U_j = \min \{U'_j, 10\} \quad (27)$$

where U'_j is the susceptibility sub-score for the j th economic activity and c_j is its respective weight given by the corresponding GVA fraction (Table 5). The U'_j sub-score for each individual economic activity reflects the estimated areas of associated land cover in the CCLL and their landslide susceptibilities. It is given by

$$U'_j = \frac{1}{t} \frac{\sum_g u_{j,g}}{N_j} \quad (28)$$

where $u_{j,g}$ is the susceptibility index in the g th grid cell where the j th economic activity is considered to be developed, N_j is the number of grid cells associated with that activity within the CCLL, and t is a modifying factor as described in Section 3.1.1.1, which in the case of landslides is defined as equal to 0.75. The definition of grid cells associated with each of the three economic activities is described in Section 3.1.1.3.

3.1.3.4. Road and railway networks

The risk score for road and railway networks is given by

$$S_{transp} = -((-U_{road} + 11) \times (-U_{rail} + 11))^{1/2} + 11 \quad (29)$$

where

$$I_{road} = \min \{U'_{road}, 10\} \quad (30)$$

$$I_{rail} = \min \{U'_{rail}, 10\} \quad (31)$$

and

$$U'_{road} = \frac{1}{t} \frac{\sum_g l_{pri,g} u_g + \sum_g l_{sec,g} u_g}{L_{road}} \quad (32)$$

$$U'_{rail} = \frac{1}{t} \frac{\sum_g l_{rail,g} u_g}{L_{rail}} \quad (33)$$

Equations (29) to (33) are analogous to the ones presented in Section 3.1.1.4, adjusted for the fact that the landslide hazard is expressed in terms of susceptibility at grid cell level u_g rather than intensity. As previously mentioned, in the case of landslides, t is considered to be equal to 0.75.

3.1.4. Heat wave

Risk associated with unusual heat stress conditions arises mainly when such conditions persist over time. Therefore, in the development of a UTCI-based risk score for heat waves, it is necessary to take into account not only the highest values of UTCI that can be expected at a given location, but also to perform time-series analyses in order to characterize the potential for prolonged heat stress periods to occur, considering both day-time and night-time UTCI values. To achieve this, in this study, the heat wave risk score is defined as a weighted sum of two components, as follows:





$$S = \frac{1}{3}H_{q99} + \frac{2}{3}H_{freq} \quad (34)$$

H_{q99} is the heat wave UTCI extremes sub-score, H_{freq} is the heat wave frequency sub-score. The larger weight assigned to the frequency sub-score has the purpose of assigning larger risk scores to CCLLs where heatwaves are frequent rather to CCLLs where temperature are high, given that frequent, relatively mild, heatwaves are more impactful than infrequent extreme heatwaves, especially on economic activities and productivity. Nevertheless, both aspects should be taken into consideration.

H_{q99} is given by

$$H_{q99} = \begin{cases} 0 & , z \leq 30^{\circ}C \\ \frac{(z - 30) \times 10}{8} & , 30^{\circ}C < z \leq 38^{\circ}C \\ 10 & , z > 38^{\circ}C \end{cases} \quad (35)$$

where z is the 99th percentile of the distribution of UTCI daily maxima within CCLL boundaries. This corresponds to a linear interpolation between $z=30^{\circ}C$ and $z=38^{\circ}C$, with the former corresponding to a sub-score of 0 and the latter corresponding to a sub-score of 10. The UTCI lower and upper thresholds were defined based on Błazejczyk et al. (2010), according to which a UTCI of $30^{\circ}C$ corresponds to moderate heat stress, whereby and $38^{\circ}C$ corresponds to a limit value between strong and very strong heat stress, at which very significant physiological responses occur.

H_{freq} is given by

$$H_{freq} = \min \{H'_{freq}, 10\} \quad (36)$$

where H'_{freq} is calculated based on the observed average annual frequency of heat waves during the period of the analysed dataset, i.e., between 1980 and 2022:

$$H'_{freq} = \frac{N_h}{N_y} \times 10 \quad (37)$$

N_h is the number of heat waves and N_y is the number of years covered by the the UTCI dataset. Here, a heat wave is defined as a period of at least 2 consecutive days where the UTCI daily maxima exceeds $33^{\circ}C$ and the UTCI daily minima exceed $13^{\circ}C$. Considering not only daily maxima but also daily minima in the definition of a heat wave event is important as high night-time temperatures are known to exacerbate heat stress conditions. The thresholds for UTCI daily maxima and minima were defined based on Di Napoli et al. (2019), which analyses the relationship between UTCI and observed periods of excess mortality.

3.1.5. Coastal erosion

Coastal erosion is expressed in terms of susceptibility classes (see Table 7) that have sub-CCLL scale variability. Therefore, the computation of CCLL coastal erosion risk scores calls for a conceptual framework where the geospatial hazard layer, expressed in terms of coast segment susceptibility, is combined with exposure. Here, the original hazard layer consists of line segments along the coast. In order to allow for a geospatial analysis of coastal erosion risk, elements located within a buffer area of 300 m of the coast segments in the EUROSION dataset were assumed to be within the area of influence of the phenomenon.





3.1.5.1. Population

The risk score for population S_{pop} is given by

$$S_{pop} = \min \{U_{pop}, 10\} \quad (38)$$

where U_{pop} is the susceptibility sub-score, which is given by

$$U_{pop} = \frac{1}{t} \sum_g u_g \times d_g \times f_{pop,g} \quad (39)$$

Here, u_g is the susceptibility index in the g th grid cell, which in the case of coastal erosion is obtained by converting the qualitative description of susceptibility in the EUROSION dataset into a semi-quantitative scale ranging from 0 to 10, as shown in Table 14, such that it can be used for obtaining risk scores that are compatible with those adopted for other hazards. Susceptibility indices ranging from 5 to 10 correspond to coast segments where coastal erosion is probable or confirmed, whereas an index of 2.5 is assigned to coast segments where the erosion evolutionary trend is uncertain or there is insufficient information available. An index value of 0 corresponds to no susceptibility, referring to coast segments where there is no observable erosion or that are outside nomenclature (e.g., harbour areas).

Table 14: Correspondence between qualitative coastal erosion susceptibility classes and semi-quantitative susceptibility indices.

Susceptibility class (CEEV2 code)	Susceptibility index u_g
0 2 6 70 71	0
1 3	2.5
4	5
50	7.5
51	10

In Eq. (39), d_g is the coastal defence index, which takes the value of 1 if defences are not present in the coast segment associated with g th grid cell and 0.25 otherwise. This corresponds to a reduction of the risk sub-score by 75% in segments where coastal defences exist, which is deemed a reasonable assumption in the absence of specific information on the effectiveness of the defences in the EUROSION dataset. The $f_{pop,g}$ variable represents the fraction of the CCLL population located in the g th grid cell, and t is the sub-score adjusting factor, which in the case of coastal erosion is considered equal to 0.05. As previously explained in the subsections referring to flooding and landslides, this allows S_{pop} to potentially reach a value of 10 when 5% of the population is within the area of influence of coastal erosion, if that area has a very high susceptibility and no defences. It should be noted that due to the slow-onset nature of coastal erosion, the intrinsic vulnerability of exposed elements considered for other hazards is assumed not to be relevant for the calculation of risk scores.





3.1.5.2. Residential buildings

In the case of coastal erosion, the risk score for residential buildings is $S_{resbldg}$ is equal to the risk score for population S_{pop} because 1) there is no differentiation in terms of the intrinsic vulnerability of exposed elements (as mentioned in the previous subsection), and 2) the spatial distribution of building fractions within a CCLL is assumed to follow the same spatial distribution of population fractions (as described for flooding and landslide hazards).

3.1.5.3. Economic activities

The coastal erosion risk score for economic activities is calculated similarly to the respective landslide risk score, i.e., it is given by Eqs. (26) to (28). In this case, in Eq. (28), $u_{j,g}$ is the susceptibility index in the g th grid cell, located within the area of influence of a coast segment, where the j th economic activity is considered to be developed. The t modifying factor is set to 0.05 (see Section 3.1.5.1).

3.1.5.1. Road and railway networks

The risk score for roads and railway networks is given by Eqs. (29) to (33). In the case of coastal erosion, the variables $l_{pri,g}$, $l_{sec,g}$ and $l_{rail,g}$ in Eqs. (32) and (33) are, respectively, the length of primary roads, secondary roads and railways in the g th coast segment, and u_g is the respective susceptibility index intensity; t is equal to 0.05.

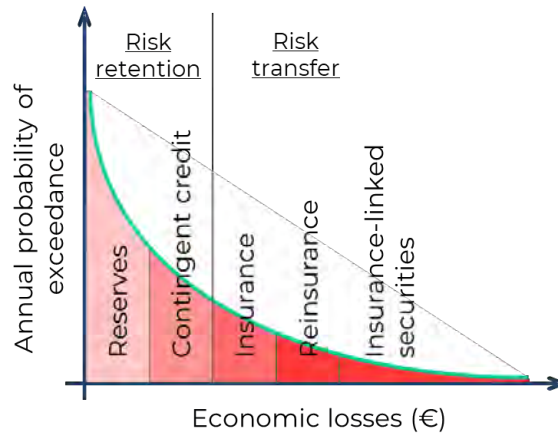
3.2. Financial categorization of risk

The development and analysis of risk management strategies, particularly those related with risk transfer, require the support of quantitative risk assessments where disaster losses and risk are estimated in monetary terms. Accordingly, in the context of SCORE, WP6 focuses essentially on a sequence of quantitative risk modelling activities that are expected to result in the assessment of alternative strategies to improve the financial resilience of three frontrunner CCLLs. Nevertheless, within the objective of Task 6.1, which is to develop a preliminary, semi-quantitative characterization of risk for all CCLLs, it is also relevant to perform a simplified categorization of risk from a financial viewpoint. This categorization is meant to provide a first screening of different possible situations that each CCLL may find itself in in terms of risk management and risk financing, i.e., whether the CCLL is subject to a low-frequency high-loss risk and should therefore look for risk transfer schemes, or if the risk is mostly high-frequency low-loss and therefore should preferentially be managed internally. Note that the cost of risk transfer is calculated such that the premium will always be higher than what the insurer or risk carrier expects to pay out on average, in order to cover operating costs and profit margins. Thus, risk transfer is particularly useful to provide payouts for extreme events – which a CCLL may not be financially equipped to deal with – rather than covering the losses of average events (see Figure 14).





Figure 14: Schematic representation of the suitability of risk transfer mechanisms to different layers of risk.



The methodology adopted to perform the categorization of risk consists in first estimating semi-quantitative risk scores – which can be assumed to serve as a proxy for economic losses – for two hazard scenarios with high and low annual probabilities of occurrence, respectively. Then, by calculating the ratio between the two scores, it is possible to have a preliminary understanding of the order of magnitude of the most extreme loss events relative to the most frequent events, and consequently of whether the implementation of risk transfer schemes may be warranted. This approach requires that the hazard can be evaluated quantitatively in terms of intensities associated to certain event frequencies. In this study, this can be done for the two hazards that are characterized in terms of intensities and associated probabilities of occurrence: fluvial flooding and coastal flooding. For other hazards, either this analysis is not relevant (for example, for slow-onset processes such as coastal erosion) or cannot be done due to the lack of quantitative hazard assessments (for example, in the case of landslides). The analysis is performed separately for three selected types of exposure that would, in a practical situation, likely be covered by different policies in the context of risk transfer mechanisms: residential buildings, agricultural assets, and industrial assets.

4. RESULTS

4.1. Risk scores

This section presents the risk scores for each hazard and CCLL, obtained following the methodology presented in Section 3.1. In the subsections concerning the four hazards with intra-CCLL spatial heterogeneity for which the computation of risk scores involves a geospatial overlap between hazard and exposure (i.e., fluvial flooding, coastal flooding, landslide, and coastal erosion), the results are organized as follows. First, a table is provided containing the risk scores for each CCLL and type of exposure (i.e., population, residential buildings, economic activities, and land transportation networks), and an overall risk score that is obtained by combining them. This combination is performed through a geometric mean-based approach as described in Section 3.1:

$$S = - \left((-S_{pop} + 11) \times (-S_{resbldg} + 11) \times (-S_{econ} + 11) \times (-S_{transp} + 11) \right)^{1/4} + 11 \quad (40)$$

Results are then presented for each exposure type, including sub-scores that are used in the computation of the risk scores (as described in the respective Methodology sections), as well as maps showing the relevant spatially-





disaggregated variables. The latter are illustrative and are provided here mainly to facilitate the interpretation of the methods and results. For brevity, for each hazard, maps for a selected CCLL are provided.

In the subsections concerning the two hazards without intra-CCLL spatial heterogeneity (i.e., extreme precipitation and heat wave), the risk scores and underlying variables are presented in a single table.

The risk scores for each hazard and CCLL are summarized in Table 15.

Table 15: Risk scores S for each hazard and CCLL.

CCLL	Fluvial flooding	Coastal flooding	Extreme precipitation	Landslide	Heat wave	Coastal erosion
Benidorm	0.0	0.0	5.1	4.7	2.4	0.0
Dublin	6.1	2.4	0.7	1.6	0.2	0.0
Gdańsk	10.0	8.2	1.1	0.6	1.5	0.2
Massa	0.0	0.0	10.0	3.8	5.8	1.0
Oarsoaldea	0.0	0.6	6.1	4.9	8.1	0.0
Oeiras	0.0	3.2	6.7	6.8	0.3	4.7
Piran	0.0	4.9	9.6	3.7	9.1	8.4
Samsun	4.5	0.0	4.2	5.4	8.4	*
Sligo	1.8	1.9	1.6	4.8	0.0	3.4
Vilanova i la Geltrú	0.0	0.0	7.7	2.5	3.3	1.5

* Coastal erosion score not available for Samsun (Turkey).

4.1.1. Fluvial flooding

Table 16: Fluvial flooding risk scores both for each type of exposed element and combined into a single risk score for each CCLL.

CCLL	S_{pop}	$S_{resbldg}$	S_{econ}	S_{transp}	$S_{fluvflood}$
Benidorm	0.0	0.0	0.0	0.0	0.0
Dublin	6.2	5.6	1.9	8.7	6.1
Gdańsk	10.0	10.0	10.0	10.0	10.0
Massa	0.0	0.0	0.0	0.0	0.0
Oarsoaldea	0.0	0.0	0.0	0.0	0.0
Oeiras	0.0	0.0	0.0	0.0	0.0
Piran	0.0	0.0	0.0	0.0	0.0
Samsun	3.3	2.6	2.3	7.9	4.5
Sligo	1.0	0.8	1.0	4.1	1.8
Vilanova i la Geltrú	0.0	0.0	0.0	0.0	0.0





4.1.1.1. Disaggregated by exposure type

Figure 15: Fluvial flooding potential impact indices $i_{pop,g}$ at grid cell level for population in the Gdańsk CCLL.

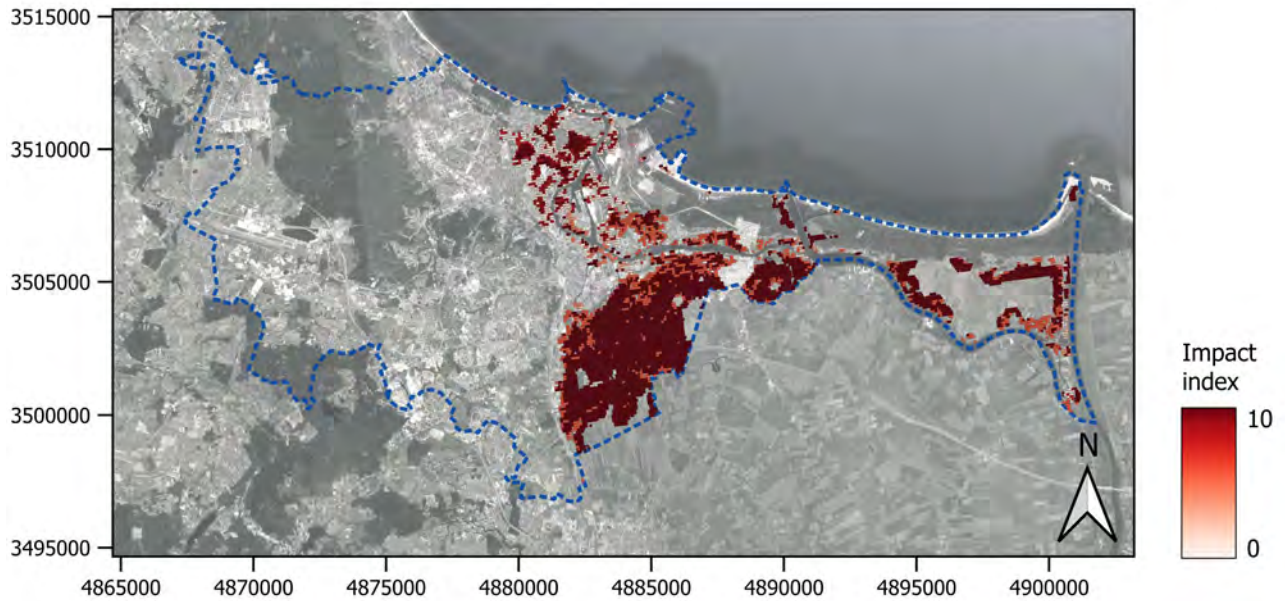


Table 17: Fluvial flooding potential impact sub-scores I_{pop} and risk scores S_{pop} for population.

CCLL	I_{pop}	S_{pop}
Benidorm	0.0	0.0
Dublin	5.3	6.2
Gdańsk	24.2	10.0
Massa	0.0	0.0
Oarsoaldea	0.0	0.0
Oeiras	0.0	0.0
Piran	0.0	0.0
Samsun	2.9	3.3
Sligo	0.8	1.0
Vilanova i la Geltrú	0.0	0.0





Figure 16: Fluvial flooding potential impact indices $i_{resbldg,g}$ at grid cell level for residential buildings in the Gdańsk CCLL.

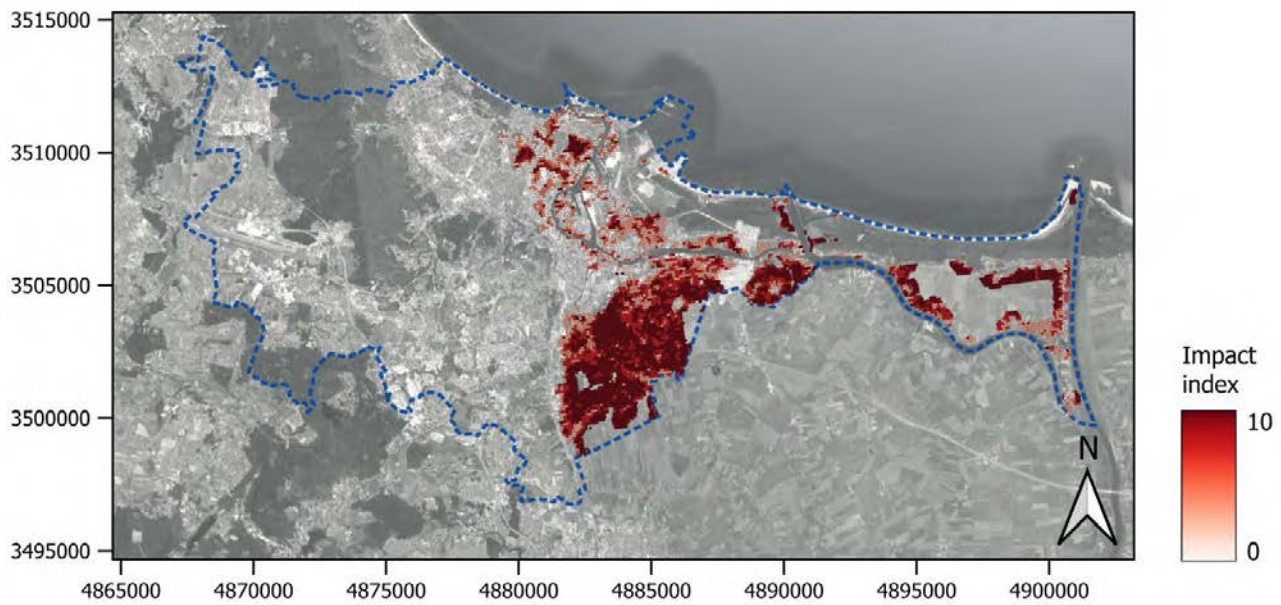


Table 18: Fluvial flooding potential impact sub-scores $I_{resbldg}$ and risk scores $S_{resbldg}$ for residential buildings.

CCLL	$I_{resbldg}$	$S_{resbldg}$
Benidorm	0.0	0.0
Dublin	4.6	5.6
Gdańsk	19.7	10.0
Massa	0.0	0.0
Oarsoaldea	0.0	0.0
Oeiras	0.0	0.0
Piran	0.0	0.0
Samsun	2.2	2.6
Sligo	0.7	0.8
Vilanova i la Geltrú	0.0	0.0





Figure 17: Fluvial flooding potential impact indices $i_{agr,g}$ at grid cell level for agriculture in the Gdańsk CCLL.

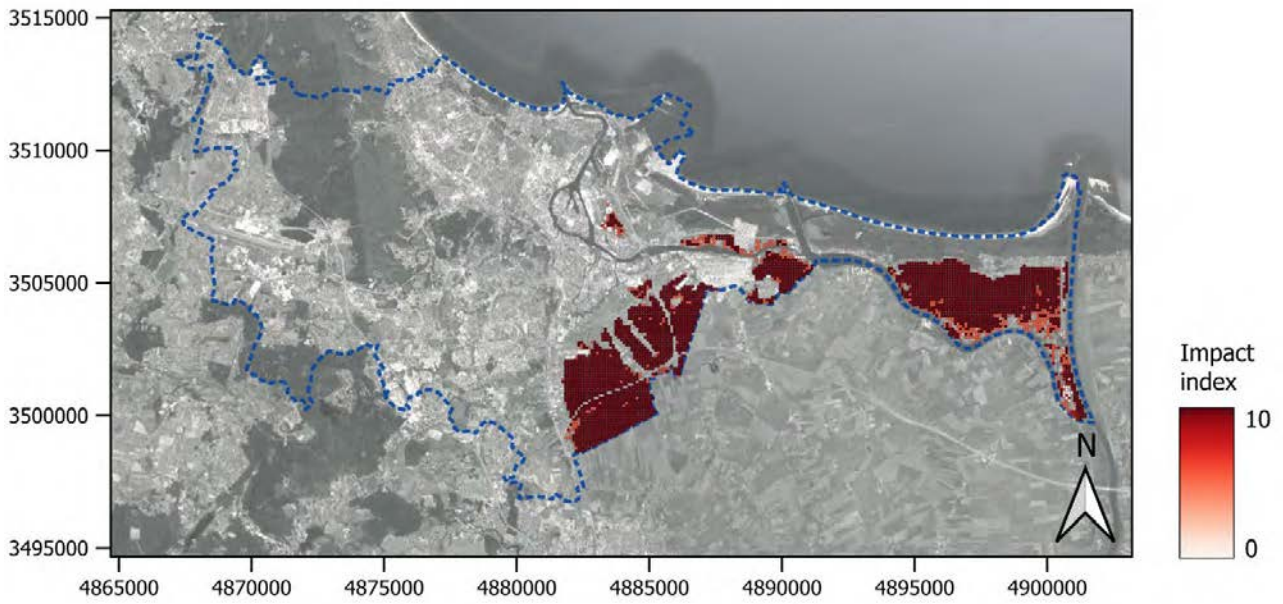


Figure 18: Fluvial flooding potential impact indices $i_{ind,g}$ at grid cell level for industry in the Gdańsk CCLL.

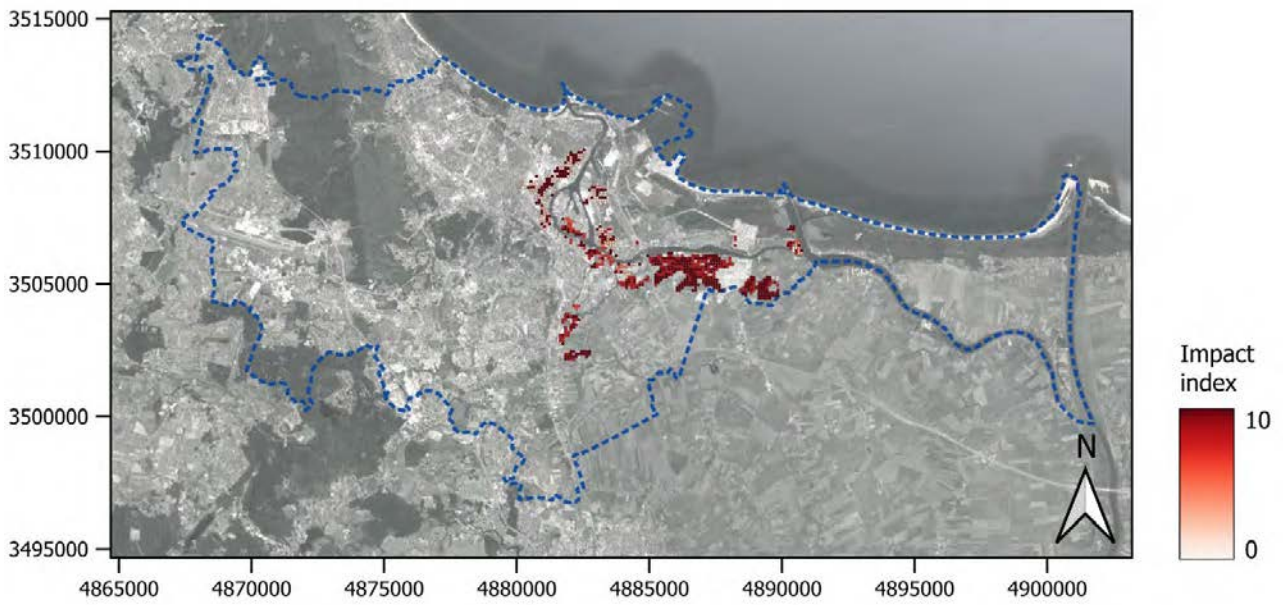




Figure 19: Fluvial flooding potential impact indices $i_{tou,g}$ at grid cell level for tourism in the Gdańsk CCLL.

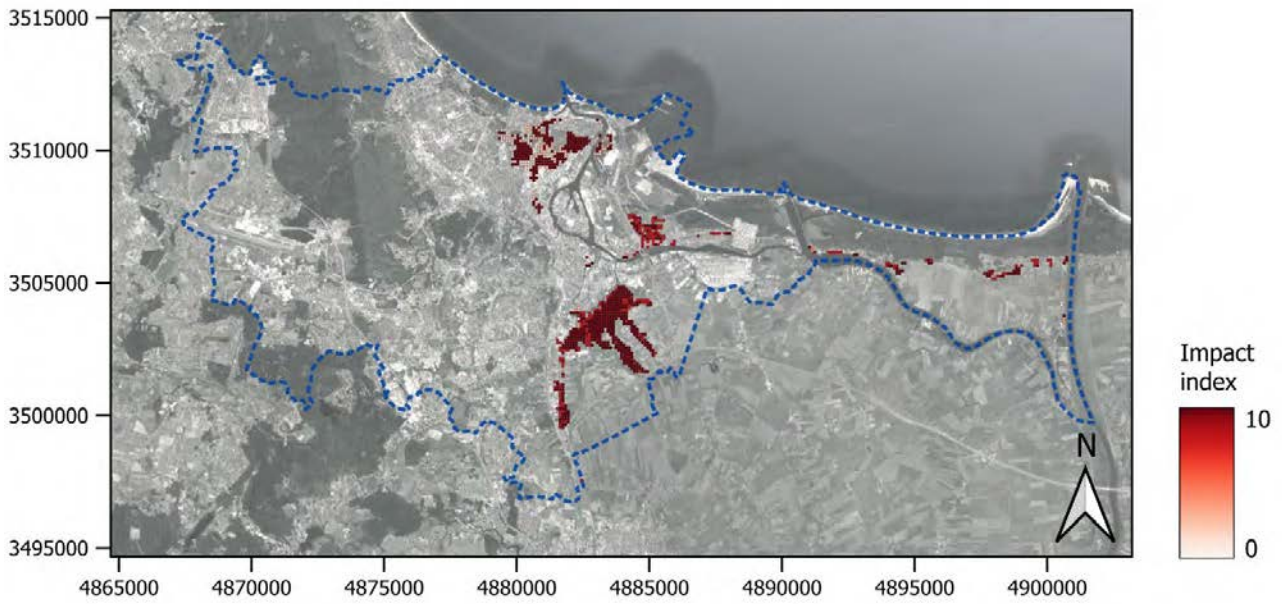


Table 19: Fluvial flooding potential impact sub-scores I'_j and risk scores S_{econ} for economic activities.

CCLL	I'_{agr}	I'_{ind}	I'_{tou}	S_{econ}
Benidorm	0.0	0.0	0.0	0.0
Dublin	0.0	1.5	4.3	1.9
Gdańsk	94.8	50.8	18.5	10.0
Massa	0.0	0.0	0.0	0.0
Oarsoaldea	0.0	0.0	0.0	0.0
Oeiras	0.0	0.0	0.0	0.0
Piran	0.0	0.0	0.0	0.0
Samsun	1.1	3.1	1.7	2.3
Sligo	0.1	1.2	0.6	1.0
Vilanova i la Geltrú	0.0	0.0	0.0	0.0





Figure 20: Fluvial flooding potential impact indices for the road network in the Gdańsk CCLL.



Figure 21: Fluvial flooding potential impact indices for the railway network in the Gdańsk CCLL.





Table 20: Fluvial flooding potential impact sub-scores I'_j and risk scores S_{transp} for road and railway networks.

CCLL	I'_{road}	I'_{rail}	S_{transp}
Benidorm	0.0	0.0	0.0
Dublin	5.5	15.6	8.7
Gdańsk	17.3	45.6	10.0
Massa	0.0	0.0	0.0
Oarsoaldea	0.0	0.0	0.0
Oeiras	0.0	0.0	0.0
Piran	0.0	0.0	0.0
Samsun	1.1	12.1	7.9
Sligo	0.6	6.4	4.1
Vilanova i la Geltrú	0.0	0.0	0.0

4.1.2. Coastal flooding

Table 21: Coastal flooding risk scores both for each type of exposed element and combined into a single risk score for each CCLL.

CCLL	S_{pop}	$S_{resbldg}$	S_{econ}	S_{transp}	$S_{coastflood}$
Benidorm	0.0	0.0	0.0	0.0	0.0
Dublin	0.8	0.5	5.9	1.1	2.4
Gdańsk	7.0	4.1	9.9	8.9	8.2
Massa	0.0	0.0	0.0	0.0	0.0
Oarsoaldea	0.5	0.4	0.2	1.1	0.6
Oeiras	0.1	0.1	1.0	7.9	3.2
Piran	7.3	4.2	3.9	3.0	4.9
Samsun	0.0	0.0	0.0	0.0	0.0
Sligo	1.5	1.3	4.1	0.0	1.9
Vilanova i la Geltrú	0.0	0.0	0.0	0.0	0.0





4.1.2.1. Disaggregated by exposure type

Figure 22: Coastal flooding potential impact indices $i_{pop,g}$ at grid cell level for population in the Piran CCLL.



Table 22: Coastal flooding potential impact sub-scores I_{pop} and risk scores S_{pop} for population.

CCLL	I_{pop}	S_{pop}
Benidorm	0.0	0.0
Dublin	0.7	0.8
Gdańsk	6.1	7.0
Massa	0.0	0.0
Oarsoaldea	0.5	0.5
Oeiras	0.1	0.1
Piran	6.2	7.3
Samsun	0.0	0.0
Sligo	1.3	1.5
Vilanova i la Geltrú	0.0	0.0





Figure 23: Coastal flooding potential impact indices $i_{resbldg,g}$ at grid cell level for residential buildings in the Piran CCLL.



Table 23: Coastal flooding potential impact sub-scores $I_{resbldg}$ and risk scores $S_{resbldg}$ for residential buildings.

CCLL	$I_{resbldg}$	$S_{resbldg}$
Benidorm	0.0	0.0
Dublin	0.4	0.5
Gdańsk	3.6	4.1
Massa	0.0	0.0
Oarsoaldea	0.4	0.4
Oeiras	0.1	0.1
Piran	3.7	4.2
Samsun	0.0	0.0
Sligo	1.1	1.3
Vilanova i la Geltrú	0.0	0.0





Figure 24: Coastal flooding potential impact indices $i_{agr,g}$ at grid cell level for agriculture in the Piran CCLL.



Figure 25: Coastal flooding potential impact indices $i_{tou,g}$ at grid cell level for tourism in the Piran CCLL.





Table 24: Coastal flooding potential impact sub-scores I'_j and risk scores S_{econ} for economic activities.

CCLL	I'_{agr}	I'_{ind}	I'_{tou}	S_{econ}
Benidorm	0.0	0.0	0.0	0.0
Dublin	0.0	6.4	1.1	5.9
Gdańsk	34.6	15.2	6.9	9.9
Massa	0.0	0.0	0.0	0.0
Oarsoaldea	0.0	0.0	1.0	0.2
Oeiras	0.0	0.0	2.2	1.0
Piran	1.0	0.0	9.0	3.9
Samsun	0.0	0.0	0.0	0.0
Sligo	0.6	4.6	4.2	4.1
Vilanova i la Geltrú	0.0	0.0	0.0	0.0

Figure 26: Coastal flooding potential impact indices for the road network in the Piran CCLL.





Table 25: Coastal flooding potential impact sub-scores I'_j and risk scores S_{transp} for road and railway networks.

CCLL	I'_{road}	I'_{rail}	S_{transp}
Benidorm	0.0	0.0	0.0
Dublin	0.8	1.3	1.1
Gdańsk	6.6	24.1	8.9
Massa	0.0	0.0	0.0
Oarsoaldea	0.1	2.0	1.1
Oeiras	1.3	21.6	7.9
Piran	5.2	0.0	3.0
Samsun	0.0	0.0	0.0
Sligo	0.0	0.0	0.0
Vilanova i la Geltrú	0.0	0.0	0.0

4.1.3. Extreme precipitation

Table 26: Extreme precipitation intensities and risk scores.

CCLL	ρ	S_{prec}
Benidorm	60.6	5.1
Dublin	34.3	0.7
Gdańsk	36.4	1.1
Massa	124.0	10.0
Oarsoaldea	66.5	6.1
Oeiras	70.0	6.7
Piran	87.5	9.6
Samsun	55.3	4.2
Sligo	39.8	1.6
Vilanova i la Geltrú	76.2	7.7





4.1.4. Landslide

Table 27: Landslide risk scores both for each type of exposed element and combined into a single risk score for each CCLL.

CCLL	S_{pop}	$S_{resbldg}$	S_{econ}	S_{transp}	$S_{landslide}$
Benidorm	5.1	5.3	3.8	4.2	4.7
Dublin	1.8	1.9	1.2	1.7	1.6
Gdańsk	0.6	0.6	0.6	0.5	0.6
Massa	3.8	3.8	4.8	2.9	3.8
Oarsoaldea	5.1	5.0	4.9	4.6	4.9
Oeiras	7.9	7.6	6.0	5.0	6.8
Piran	5.1	4.8	1.5	2.9	3.7
Samsun	6.1	6.3	6.5	1.8	5.4
Sligo	5.2	5.4	4.0	4.3	4.8
Vilanova i la Geltrú	2.7	2.8	3.2	1.4	2.5

4.1.4.1. Disaggregated by exposure type

Figure 27: Landslide susceptibility indices at grid cell level for population and residential buildings in the Oeiras CCLL.

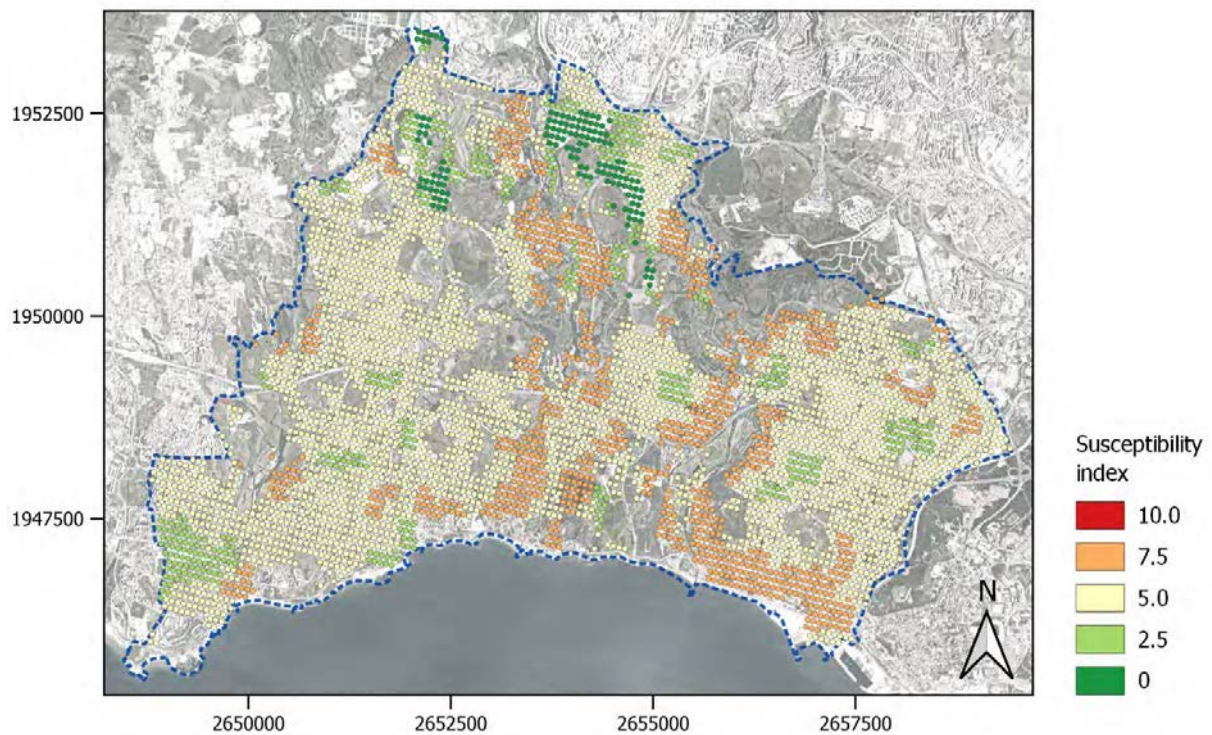




Table 28: Landslide susceptibility sub-scores and risk scores S_{pop} and $S_{resbldg}$ for population and residential buildings, respectively.

CCLL	U	S_{pop}	$S_{resbldg}$
Benidorm	4.4	5.1	5.3
Dublin	1.5	1.8	1.9
Gdańsk	0.6	0.6	0.6
Massa	3.1	3.8	3.8
Oarsoaldea	4.2	5.1	5.0
Oeiras	6.6	7.9	7.6
Piran	4.3	5.1	4.8
Samsun	5.3	6.1	6.3
Sligo	4.4	5.2	5.4
Vilanova i la Geltrú	2.3	2.7	2.8

Figure 28: Landslide susceptibility indices $u_{agr,g}$ at grid cell level for agriculture in the Oeiras CCLL.

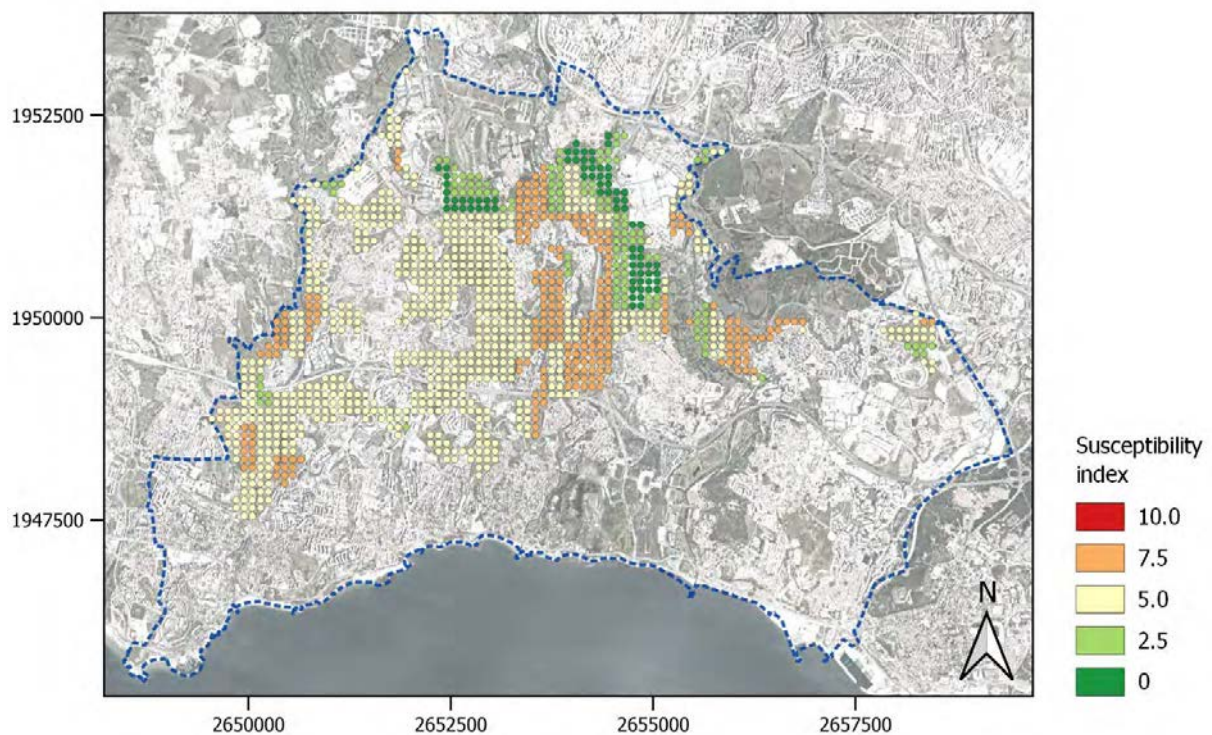




Figure 29: Landslide susceptibility indices $u_{ind,g}$ at grid cell level for industry in the Oeiras CCLL.

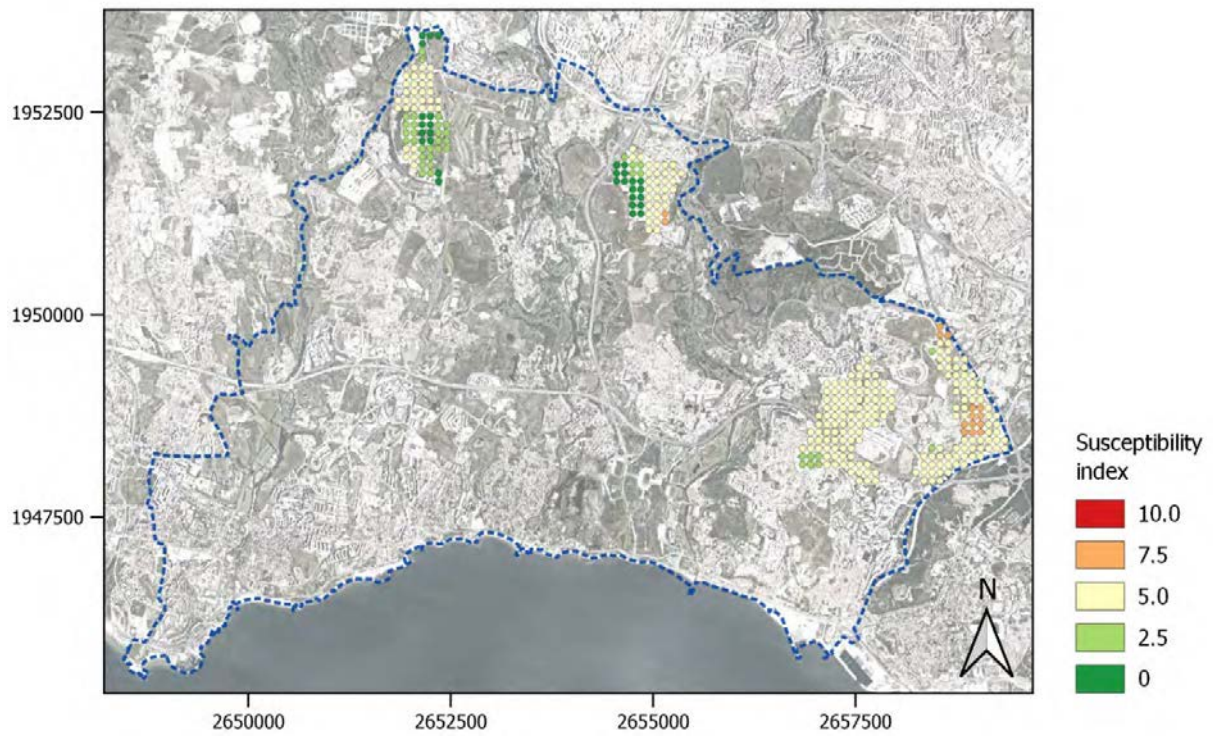


Figure 30: Landslide susceptibility indices $u_{tou,g}$ at grid cell level for tourism in the Oeiras CCLL.

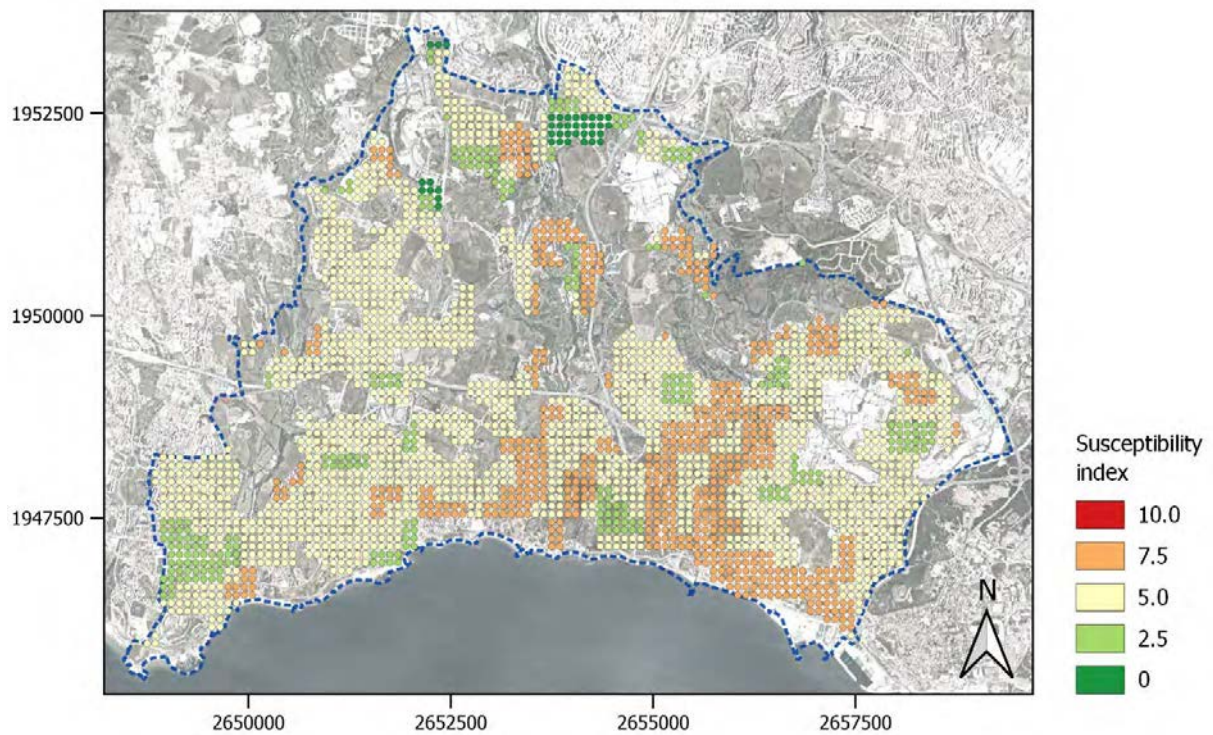




Table 29: Landslide susceptibility sub-scores U'_j and risk scores S_{econ} for economic activities.

CCLL	U'_{agr}	U'_{ind}	U'_{tou}	S_{econ}
Benidorm	3.3	3.6	4.2	3.8
Dublin	1.5	1.1	1.6	1.2
Gdańsk	0.8	0.6	0.5	0.6
Massa	4.8	5.3	2.0	4.8
Oarsoaldea	5.8	4.9	4.9	4.9
Oeiras	6.5	5.6	6.5	6.0
Piran	6.0	0.0	3.8	1.5
Samsun	8.5	4.7	5.2	6.5
Sligo	4.6	3.9	3.6	4.0
Vilanova i la Geltrú	3.1	3.4	2.5	3.2

Figure 31: Landslide susceptibility indices for the road network in the Oeiras CCLL.

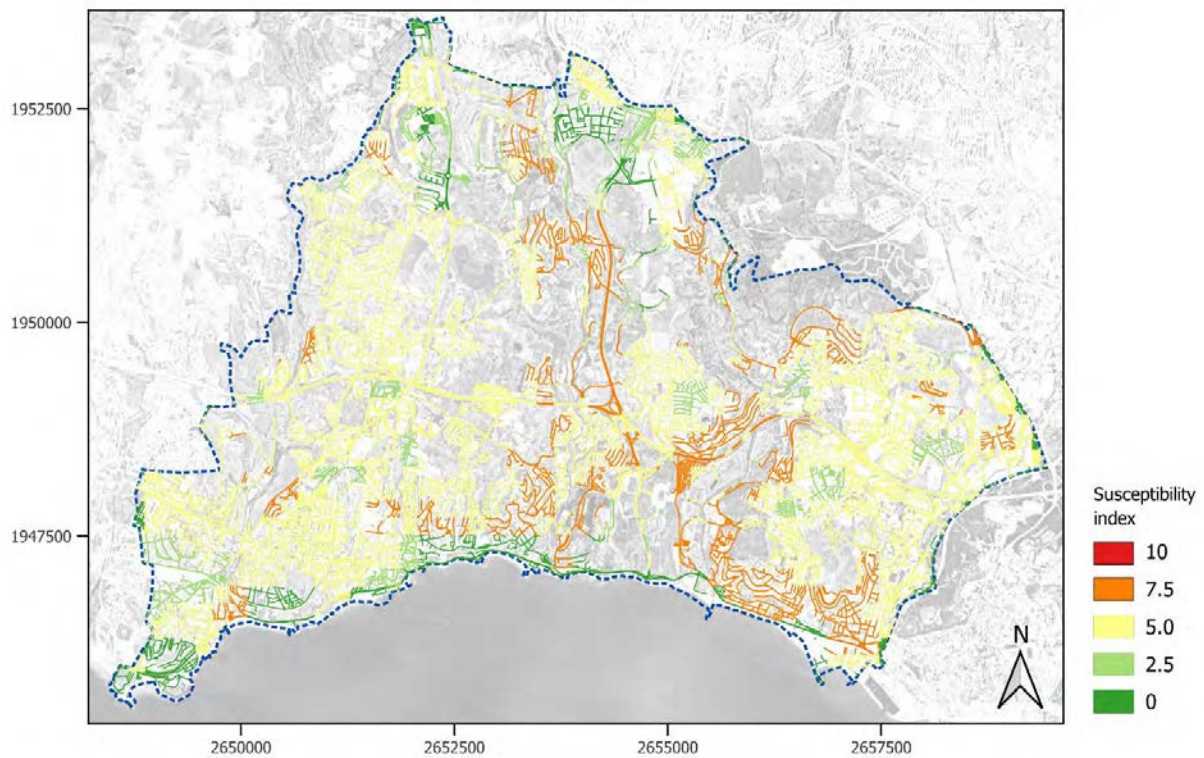




Figure 32: Landslide susceptibility indices for the railway network in the Oeiras CCLL.

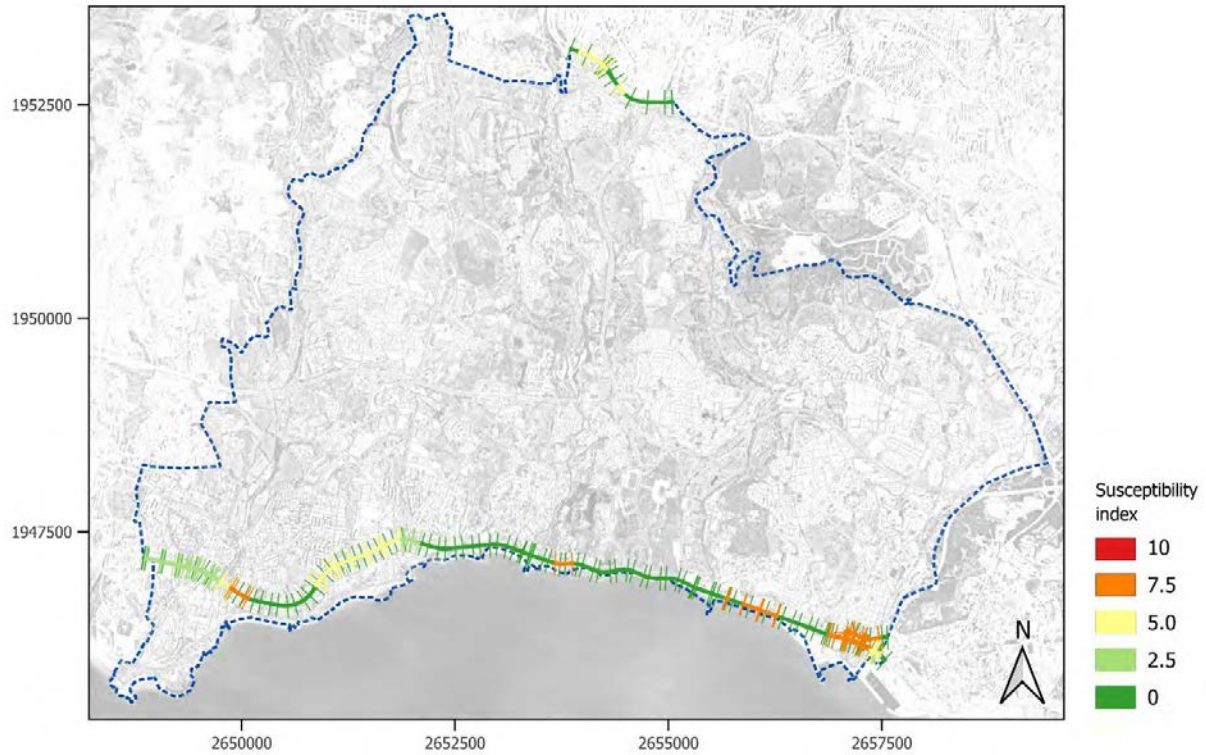


Table 30: Landslide susceptibility sub-scores U'_j and risk scores S_{transp} for road and railway networks.

CCLL	U'_{road}	U'_{rail}	S_{transp}
Benidorm	4.4	4.0	4.2
Dublin	1.5	2.0	1.7
Gdańsk	0.5	0.5	0.5
Massa	3.6	2.0	2.9
Oarsoaldea	5.3	3.9	4.6
Oeiras	6.2	3.4	5.0
Piran	5.0	0.0	2.9
Samsun	1.7	1.9	1.8
Sligo	4.6	4.1	4.3
Vilanova i la Geltrú	2.6	0.2	1.4





4.1.5. Heat wave

Table 31: Heat wave sub-scores and risk scores.

CCLL	H_{q99}	H_{freq}	S_{heat}
Benidorm	3.6	1.9	2.4
Dublin	0.0	0.2	0.2
Gdańsk	2.2	1.2	1.5
Massa	4.2	6.6	5.8
Oarsoaldea	7.7	8.2	8.1
Oeiras	1.0	0.0	0.3
Piran	7.2	14.8	9.1
Samsun	6.5	9.4	8.4
Sligo	0.0	0.0	0.0
Vilanova i la Geltrú	3.9	3.1	3.3

4.1.6. Coastal erosion

Table 32: Coastal erosion risk scores both for each type of exposed element and combined into a single risk score for each CCLL.

CCLL	S_{pop}	$S_{resbldg}$	S_{econ}	S_{transp}	$S_{erosion}$
Benidorm	0.0	0.0	0.0	0.0	0.0
Dublin	0.0	0.0	0.0	0.0	0.0
Gdańsk	0.4	0.4	0.0	0.1	0.2
Massa	0.0	0.0	1.3	2.6	1.0
Oarsoaldea	0.0	0.0	0.0	0.0	0.0
Oeiras	2.4	2.4	2.5	8.4	4.7
Piran	10.0	10.0	3.9	4.2	8.4
Samsun	0.0	0.0	0.0	0.0	0.0
Sligo	2.5	2.5	6.5	0.9	3.4
Vilanova i la Geltrú	0.0	0.0	0.3	4.7	1.5





4.1.6.1. Disaggregated by exposure type

Figure 33: Coastal erosion susceptibility indices at grid cell level for population and residential buildings in the Sligo CCLL.

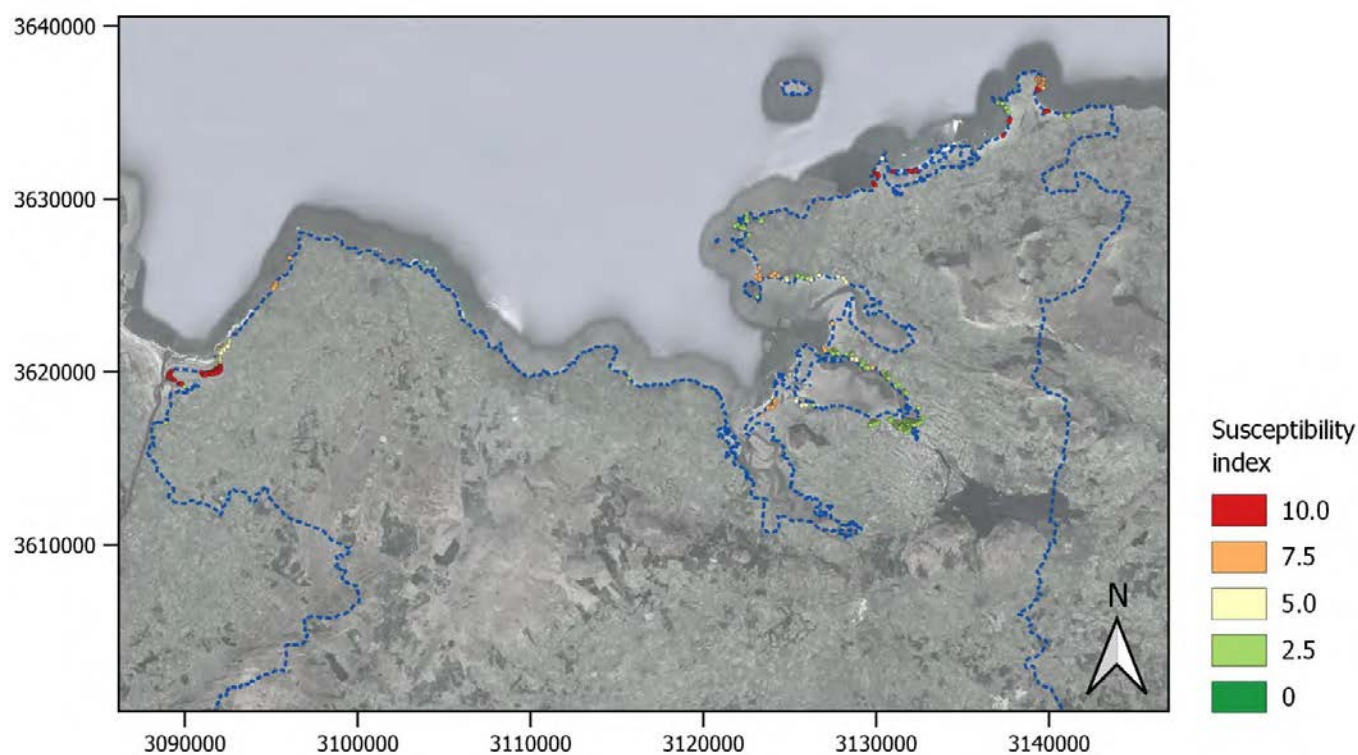


Table 33: Coastal erosion susceptibility sub-scores and risk scores for population and residential buildings.

CCLL	U	S_{pop}	$S_{resbldg}$
Benidorm	0.0	0.0	0.0
Dublin	0.0	0.0	0.0
Gdańsk	0.4	0.4	0.4
Massa	0.0	0.0	0.0
Oarsoaldea	0.0	0.0	0.0
Oeiras	2.4	2.4	2.4
Piran	11.1	10.0	10.0
Samsun	0.0	0.0	0.0
Sligo	2.5	2.5	2.5
Vilanova i la Geltrú	0.0	0.0	0.0





Figure 34: Coastal erosion susceptibility indices $u_{agr,g}$ at grid cell level for agriculture in the Sligo CCLL.

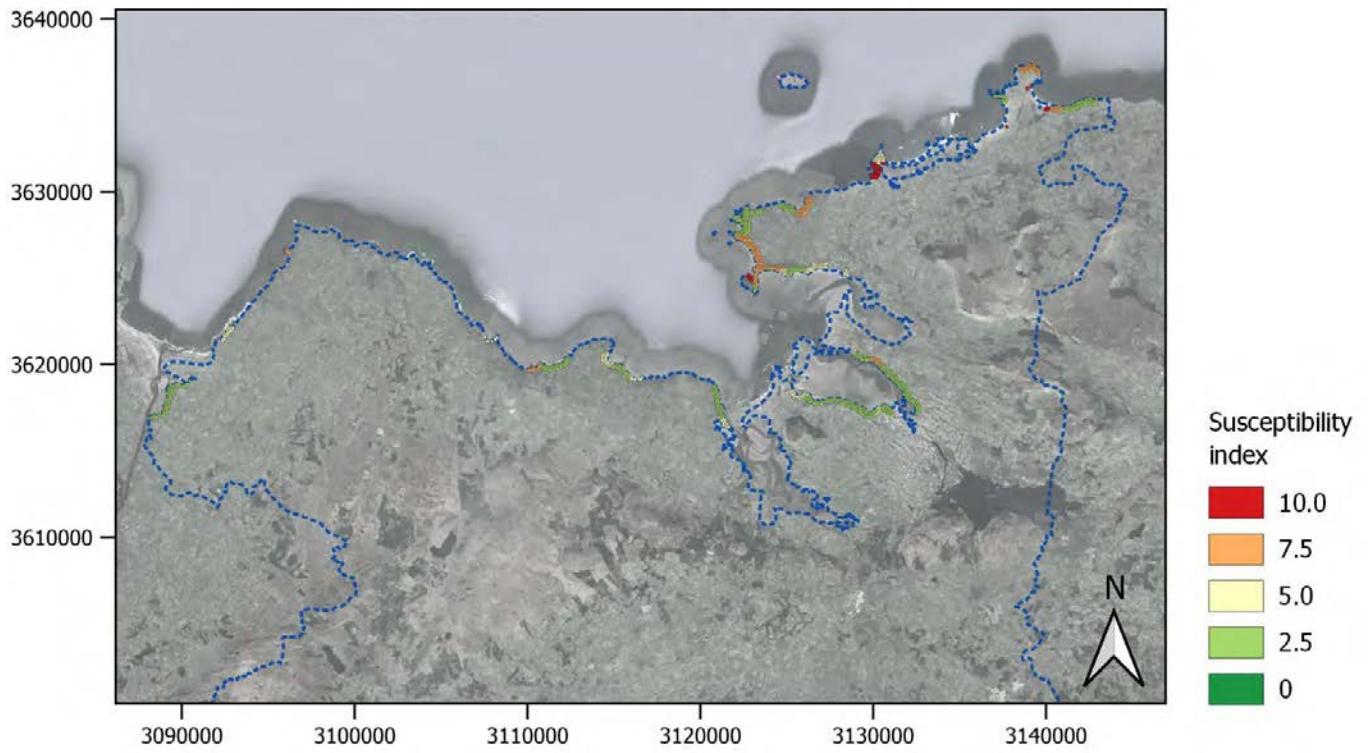


Figure 35: Coastal erosion susceptibility indices $u_{ind,g}$ at grid cell level for industry in the Sligo CCLL.

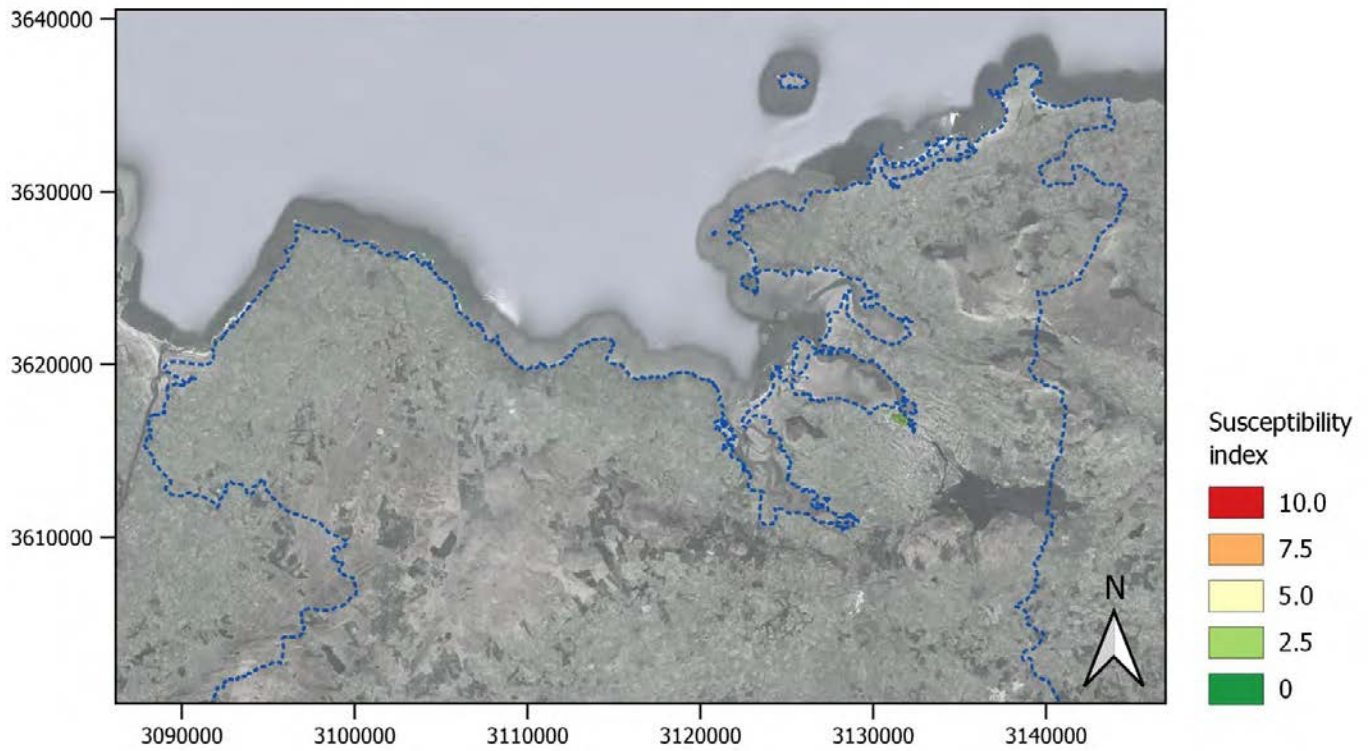




Figure 36: Coastal erosion susceptibility indices $u_{tou,g}$ at grid cell level for tourism in the Sligo CCLL.

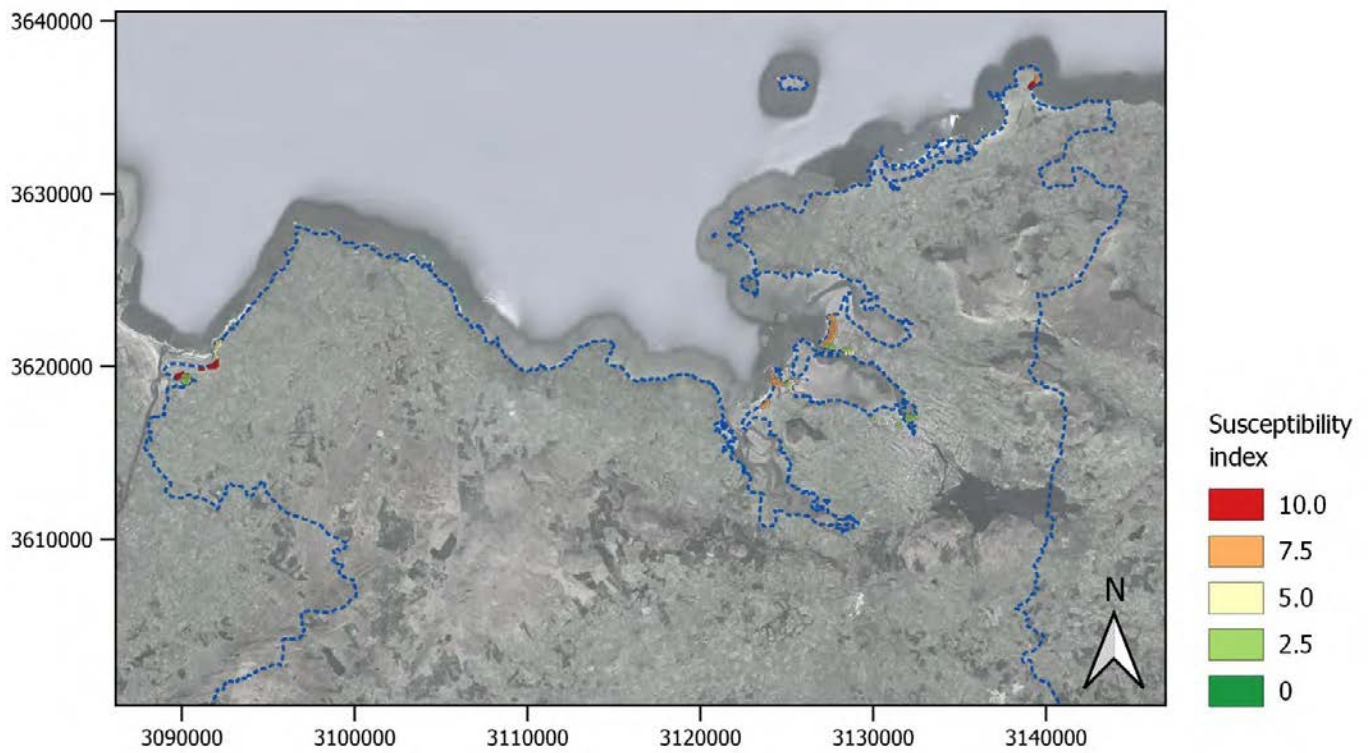


Table 34: Coastal erosion susceptibility sub-scores U'_j and risk scores S_{econ} for economic activities.

CCLL	U'_{agr}	U'_{ind}	U'_{tou}	S_{econ}
Benidorm	0.0	0.0	0.0	0.0
Dublin	0.0	0.0	0.0	0.0
Gdańsk	0.0	0.0	0.3	0.0
Massa	0.0	0.0	5.5	1.3
Oarsoaldea	0.0	0.0	0.0	0.0
Oeiras	0.0	0.0	5.3	2.5
Piran	2.8	0.0	8.9	3.9
Samsun	0.0	0.0	0.0	0.0
Sligo	0.9	6.6	14.7	6.5
Vilanova i la Geltrú	1.1	0.0	1.1	0.3





Figure 37: Coastal erosion susceptibility indices for the road network in the Sligo CCLL.

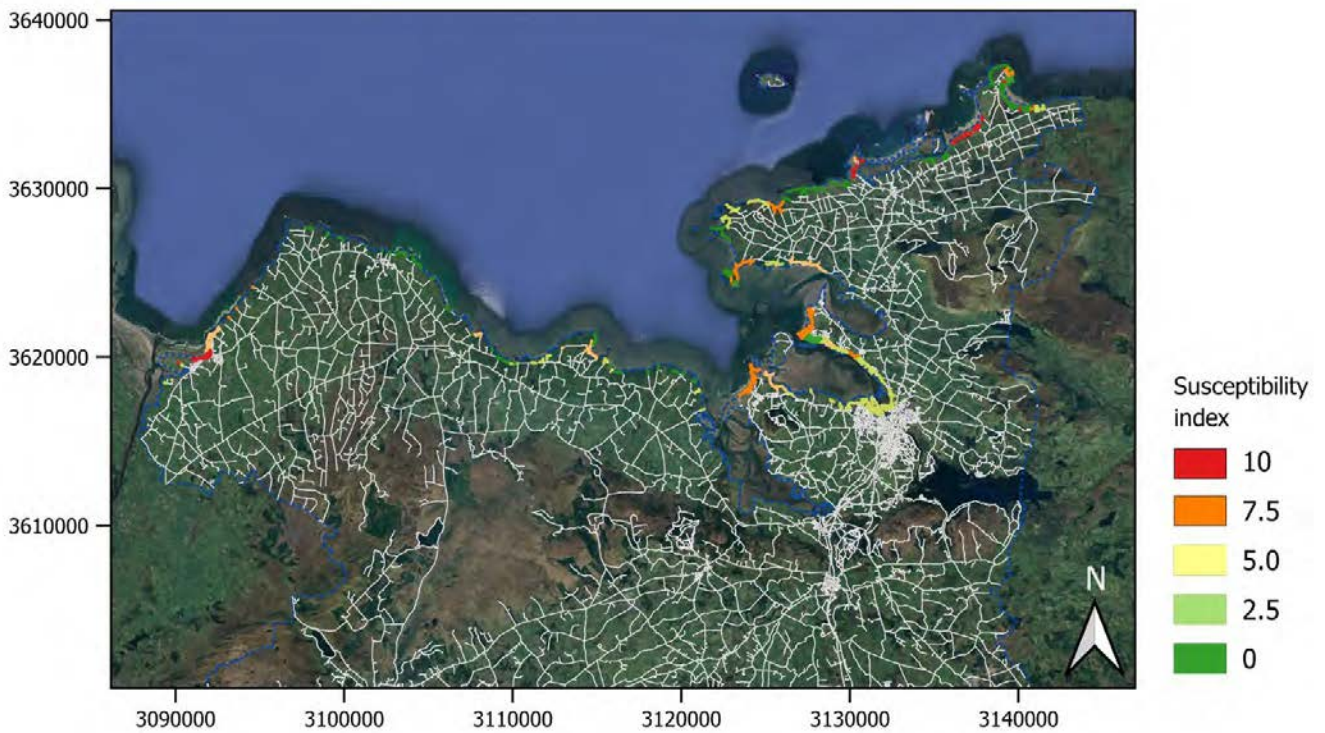


Table 35: Coastal erosion susceptibility sub-scores U'_i and risk scores S_{transp} for road and railway networks.

CCLL	U'_{road}	U'_{rail}	S_{transp}
Benidorm	0.0	0.0	0.0
Dublin	0.0	0.0	0.0
Gdańsk	0.3	0.0	0.1
Massa	4.7	0.0	2.6
Oarsoaldea	0.0	0.0	0.0
Oeiras	4.3	14.8	8.4
Piran	6.8	0.0	4.2
Samsun	0.0	0.0	0.0
Sligo	1.8	0.0	0.9
Vilanova i la Geltrú	1.0	7.0	4.7

4.2. Financial categorization of risk

As described in Section 3.2, the financial categorization of risk is performed based on ratios between the risk scores for low and high probability scenarios, both for fluvial flooding and coastal flooding. The analysis is limited to the CCLLs covered by the models adopted for these two hazards. Here, the limitation of the scores to a maximum value of 10 is removed, as the objective is to work with values that can be considered more representative of potential losses. Based on the data adopted to describe these two hazards in the present study, 500- and 20-year return period scenarios were selected; as previously mentioned, the analysis covers residential buildings, agriculture, and industry. It must be noted that the calculated ratios are merely indicative, as an analysis of this type necessarily requires the





support of more detailed, CCLL-specific quantitative risk assessments such as the one that will be developed for WP6's frontrunner CCLLs in subsequent project activities. Nevertheless, the simple framework adopted here can provide a first idea of the type of risk management strategy (i.e., risk retention and/or risk transfer) that may be more suitable for each CCLL. The results are shown in Table 36 and Table 37.

Table 36: Comparison of fluvial flooding risk scores with 20- and 500-year return periods for residential buildings, agriculture, and industry.

CCLL	Residential buildings			Agriculture			Industry		
	RP20	RP500	Ratio	RP20	RP500	Ratio	RP20	RP500	Ratio
Dublin	4.90	6.48	1.32	0.00	0.00	-	1.31	2.15	1.64
Gdańsk	13.21	26.18	1.98	56.34	98.53	1.75	28.48	61.91	2.17
Samsun	0.00	3.02	∞	0.00	1.13	∞	0.00	8.08	∞
Sligo	0.74	0.88	1.18	0.08	0.12	1.53	1.09	1.26	1.16

Table 37: Comparison of coastal flooding risk scores with 20- and 500-year return periods for residential buildings, agriculture, and industry.

CCLL	Residential buildings			Agriculture			Industry		
	RP20	RP500	Ratio	RP20	RP500	Ratio	RP20	RP500	Ratio
Dublin	0.43	0.57	1.32	0.00	0.00	-	5.62	7.24	1.29
Gdańsk	4.01	4.27	1.07	33.94	37.04	1.09	14.70	15.73	1.07
Oarsoaldea	0.40	0.47	1.17	0.00	0.00	-	0.00	0.00	-
Oeiras	0.11	0.11	1.05	0.00	0.00	-	0.00	0.00	-
Piran	3.77	4.68	1.24	0.72	1.35	1.88	0.00	0.00	-
Sligo	1.27	1.31	1.03	0.61	0.68	1.13	4.34	4.79	1.10

In terms of fluvial flooding, Dublin and Gdańsk, particularly the latter, present relatively high ratios between risk scores associated with the 500- and the 20-year return period scenarios. This is a relevant finding in the case of Gdańsk, as the risk scores – and therefore, potential losses – are quite high. In the case of Samsun, the 20-year RP fluvial flood hazard maps does not contain flood footprints; although the reason for this is unclear, it could suggest that such events in Samsun are not as frequent. For Sligo, notwithstanding the ratios (which are lower for residential buildings and industry and higher for agriculture), the risk scores are very low across all sectors and probabilities of occurrence, suggesting that fluvial flood losses in the CCLL are generally low. These results suggest that risk transfer mechanisms may be a particularly suitable option for Gdańsk, and possibly also for Dublin and Samsun; in the case of Sligo, risk retention would likely be a suitable option.

In the case of coastal flooding, the results are less conclusive. The differences between risk scores for scenarios with low and high probabilities of occurrence are not very marked, with low ratios between the two across the board. The highest ratios are found for Dublin and Piran; however, in Dublin, the risk scores for residential buildings are quite low, which is also the case for agriculture in Piran. Overall, this suggests that for coastal flooding, risk transfer could be a suitable strategy for industry in Dublin and residential buildings in Piran, whereas in other cases, risk retention might be preferable. Note that the relatively small differences found between most of the risk scores for low- and high-probability coastal flood scenarios could be due to the characteristics of the adopted hazard model, which would warrant further investigation in follow-up studies on this topic.





5. CONCLUSION

This report provides a characterization of hydro-meteorological and climate-related risks for SCORE's ten CCLLs. Its development comprised two main activities: first, a comprehensive data collection effort for open-access hazard and exposure datasets with continental coverage, and second, the development of a novel methodological framework for a semi-quantitative, score-based assessment of risks associated with multiple hazards. The report describes the adopted datasets and methodological framework in a complete and concise manner, such that it is understandable to stakeholders that are not familiar with risk modelling concepts while providing an adequate level of scientific and technical background.

The semi-quantitative risk scores for each hazard, CCLL and exposure type are provided in Section 4.1. The scores were designed to be easily interpretable, following a scale from 0 (i.e., no risk or negligible) to 10 (i.e., very high risk), as previously described. The results are presented such that readers are able to straightforwardly analyse them in terms of different dimensions and/or aggregation levels according to their interests. It is possible, for example, to easily compare risk scores for one hazard across all CCLLs, to compare risk scores for multiple hazards for one specific CCLL or analyse risk scores for specific exposure types.

Generally, it is observed that the highest risk scores for the different hazard are distributed in a heterogeneous manner among the CCLLs; in other words, considering all six hazards, there does not appear to be a specific CCLL that is significantly more at risk than the others. Nonetheless, in this regard, two CCLLs stand out: Gdańsk, which has the highest risk scores for both fluvial and coastal flooding, and Piran, which has the highest score for heat wave, coastal erosion, and the second highest score for extreme precipitation. Apart from these, the Dublin CCLL has a medium-high risk score for fluvial floods, while Massa and Vilanova i la Geltrú appear to be particularly at risk of extreme precipitation events. In terms of landslides, Oeiras has the highest risk score among all CCLLs, even if it is not particularly critical. Lastly, heat wave risk is also quite high in Oarsoaldea and Samsun. Results suggest that the Benidorm and Sligo CCLLs are generally at lower risk, even if some of the risk scores cannot be neglected.

A simple framework for the financial categorization of risk was also developed in the context of Task 6.1, which provides a first screening of different the type of risk management strategy that may be more suitable for each CCLL. The results are provided and briefly discussed in Section 4.2.

It should be noted that studies such as the one presented in this report necessarily involve a trade-off between accuracy and scale of application. Adopting large-scale datasets can provide a consistent, continental-level view of hazard and exposure – and subsequently risk – but this also involves a certain degree of uncertainty. Moreover, semi-quantitative risk estimates are also necessarily associated with some uncertainty due to the nature of the underlying methodological frameworks, which involve making certain assumptions to which results may be sensitive. In this study, this is minimized by supporting the analyses, to the maximum possible extent, by physically based, state-of-the-art exposure and hazard models, as well engineering-based and scientifically robust assumptions regarding the vulnerability of exposed assets. Nonetheless, analysing the sensitivity of the risk scores to variations in certain model parameters could be an interesting topic for a future follow-up study.

Ultimately, the present report provides a robust high-level characterization of the most critical risks for each CCLL, which can support stakeholders in prioritizing the development of more detailed, CCLL- and/or hazard-specific quantitative risk assessments.





6. REFERENCES

- Alfieri, L., Salamon, P., Bianchi, A., Neal, J., Bates, P., and Feyen, L. (2014). Advances in pan-European flood hazard mapping. *Hydrological Processes*, 28(13), 4067–4077. doi:10.1002/hyp.9947
- ARPA Piemonte. (n.d.). Agenzia Regionale per la Protezione Ambientale del Piemonte - Fenomeni meteo - Pioggia. Retrieved from https://www.arpa.piemonte.it/rischinaturali/approfondimenti/pericoli-meteo/fenomeni_meteo/pioggia.html
- Barnard, C. (2022). UTCL - User Guide. Retrieved from <https://confluence.ecmwf.int/display/CEMS/UTCL+-+User+Guide>
- Bashfield, A., and Keim, A. (2011). *Continent-wide DEM creation for the European Union. In 34th international symposium on remote sensing of environment. the GEOSS era: Towards operational environmental monitoring. Sydney, Australia.*
- Bates, P. D. (2022). Flood Inundation Prediction. *Annual Review of Fluid Mechanics*, 54(1), 287–315. doi:10.1146/annurev-fluid-030121-113138
- Błazejczyk, K., Broede, P., Fiala, D., Havenith, G., Holmér, I., Jendritzky, G., ... Kunert, A. (2010). Principles of the new universal thermal climate index (UTCI) and its application to bioclimatic research in European scale. *Miscellanea Geographica*, 14, 91–102. doi:10.2478/mgrsd-2010-0009
- Büttner, G., Kosztra, B., Maucha, G., Pataki, R., Kleeschulte, S., Hazeu, G., ... Littkop, A. (2021). *CORINE Land Cover User Manual.*
- Carrere, L., Lyard, F., Cancet, M., and Guillot, A. (2015). FES 2014, a new tidal model on the global ocean with enhanced accuracy in shallow seas and in the Arctic region. In Copernicus (Ed.), *EGU General Assembly* (Vol. 17). Vienna.
- Crowley, H., Despotaki, V., Rodrigues, D., Silva, V., Toma-Danila, D., Riga, E., ... Gamba, P. (2020). Exposure model for European seismic risk assessment. *Earthquake Spectra*, 36(1_suppl), 252–273. doi:10.1177/8755293020919429
- Dee, D. P., Uppala, S. M., Simmons, A. J., Berrisford, P., Poli, P., Kobayashi, S., ... Vitart, F. (2011). The ERA-Interim reanalysis: configuration and performance of the data assimilation system. *Quarterly Journal of the Royal Meteorological Society*, 137(656), 553–597. doi:10.1002/qj.828
- Di Napoli, C., Pappenberger, F., and Cloke, H. L. (2019). Verification of heat stress thresholds for a health-based heat-wave definition. *Journal of Applied Meteorology and Climatology*, 58(6), 1177–1194. doi:10.1175/JAMC-D-18-0246.1
- Dottori, F., Alfieri, L., Bianchi, A., Lorini, V., Feyen, L., and Salamon, P. (2016a). River flood hazard maps for Europe - version 1. European Commission, Joint Research Centre (JRC). Retrieved from <http://data.europa.eu/89h/8e49997c-ba99-4ed1-9aec-059bb440001b>
- Dottori, F., Alfieri, L., Bianchi, A., Skoien, J., and Salamon, P. (2021). River flood hazard maps for Europe and the Mediterranean Basin region. European Commission, Joint Research Centre (JRC). doi:10.2905/1D128B6C-A4EE-4858-9E34-6210707F3C81
- Dottori, F., Alfieri, L., Bianchi, A., Skoien, J., and Salamon, P. (2022). A new dataset of river flood hazard maps for Europe and the Mediterranean Basin. *Earth System Science Data*, 14(4), 1549–1569. doi:10.5194/essd-14-1549-2022
- Dottori, F., Figueiredo, R., Martina, M., Molinari, D., and Scorzini, A. R. (2016b). INSYDE: a synthetic, probabilistic flood damage model based on explicit cost analysis. *Natural Hazards and Earth System Sciences*, 16(12), 2577–2591. doi:10.5194/nhess-16-2577-2016
- Emberson, R., Kirschbaum, D., and Stanley, T. (2020). New global characterisation of landslide exposure. *Natural Hazards and Earth System Sciences*, 20(12), 3413–3424. doi:10.5194/nhess-20-3413-2020





- Eurostat. (2008). *NACE Rev. 2 – Statistical classification of economic activities in the European Community*. Luxembourg: Office for Official Publications of the European Communities.
- Figueiredo, R., Romão, X., and Paupério, E. (2020). Flood risk assessment of cultural heritage at large spatial scales: Framework and application to mainland Portugal. *Journal of Cultural Heritage*, 43, 163–174. doi:10.1016/j.culher.2019.11.007
- Gründemann, G. J., Zorzetto, E., Beck, H. E., Schleiss, M., van de Giesen, N., Marani, M., and van der Ent, R. J. (2023). Extreme precipitation return levels for multiple durations on a global scale. *Journal of Hydrology*, 621(July 2022), 129558. doi:10.1016/j.jhydrol.2023.129558
- Gründemann, G., Zorzetto, E., Beck, H., Schleiss, M., Giesen, N. Van de, Marani, M., and Ent, R. van der. (2021). GPEX: Global Precipitation EXtremes. 4TU.ResearchData. doi:doi.org/10.4121/12764429.v4
- IPCC. (2022). Annex II: Glossary [Möller, V., R. van Diemen, J.B.R. Matthews, C. Méndez, S. Semenov, J.S. Fuglestedt, A. Reisinger (eds.)]. In *Climate Change 2022: Impacts, Adaptation and Vulnerability. Contribution of Working Group II to the Sixth Assessment Report of the Intergovernmental Panel on Climate Change* (pp. 2897–2930). Cambridge, UK and New York, NY, USA: Cambridge University Press. doi:10.1017/9781009325844.029
- Jendritzky, G., de Dear, R., and Havenith, G. (2012). UTCI—Why another thermal index? *International Journal of Biometeorology*, 56(3), 421–428. doi:10.1007/s00484-011-0513-7
- Kaynia, A. M., Papathoma-Köhle, M., Neuhäuser, B., Ratzinger, K., Wenzel, H., and Medina-Cetina, Z. (2008). Probabilistic assessment of vulnerability to landslide: Application to the village of Lichtenstein, Baden-Württemberg, Germany. *Engineering Geology*, 101(1–2), 33–48. doi:10.1016/j.enggeo.2008.03.008
- Lenôtre, N., Thierry, P., Batkowski, D., and Vermeersch, F. (2004). *EUROSION project - The Coastal Erosion Layer - WP 2.6*.
- Muis, S., Verlaan, M., Winsemius, H. C., Aerts, J. C. J. H., and Ward, P. J. (2016). A global reanalysis of storm surges and extreme sea levels. *Nature Communications*, 7. doi:10.1038/ncomms11969
- OECD. (2008). *Handbook on Constructing Composite Indicators: Methodology and User Guide*. Retrieved from <https://www.oecd.org/els/soc/handbookonconstructingcompositeindicatorsmethodologyanduserguide.htm>
- OSM. (2023a). Contributors - OSM. Retrieved from <https://wiki.openstreetmap.org/wiki/Contributors>
- OSM. (2023b). OpenStreetMap. Retrieved from <https://www.openstreetmap.org/>
- Palla, A., Colli, M., Candela, A., Aronica, G. T., and Lanza, L. G. (2018). Pluvial flooding in urban areas: the role of surface drainage efficiency. *Journal of Flood Risk Management*, 11, S663–S676. doi:10.1111/jfr3.12246
- Reder, A., Raffa, M., Padulano, R., Rianna, G., and Mercogliano, P. (2022). Characterizing extreme values of precipitation at very high resolution: An experiment over twenty European cities. *Weather and Climate Extremes*, 35, 100407. doi:10.1016/j.wace.2022.100407
- Robinson, P. J. (2001). On the Definition of a Heat Wave. *Journal of Applied Meteorology*, 40(4), 762–775. doi:10.1175/1520-0450(2001)040<0762:OTDOAH>2.0.CO;2
- Schär, C., and Jendritzky, G. (2004). Hot news from summer 2003. *Nature*, 432(7017), 559–560. doi:10.1038/432559a
- Stanley, T., and Kirschbaum, D. B. (2017). A heuristic approach to global landslide susceptibility mapping. *Natural Hazards*, 87(1), 145–164. doi:10.1007/s11069-017-2757-y
- Stevens, F. R., Gaughan, A. E., Linard, C., and Tatem, A. J. (2015). Disaggregating census data for population mapping using Random forests with remotely-sensed and ancillary data. *PLoS ONE*, 10(2), 1–22. doi:10.1371/journal.pone.0107042
- Tatem, A. J. (2017). WorldPop, open data for spatial demography. *Scientific Data*, 4(1), 170004. doi:10.1038/sdata.2017.4
- Ward, P. J., Winsemius, H. C., Kuzma, S., Bierkens, M. F., Bouwman, A., De Moel, H., ... Gebremedhin, E. T. (2020).





Aqueduct floods methodology. Washington, D.C.

Wilde, M., Günther, A., Reichenbach, P., Malet, J.-P., and Hervás, J. (2018). Pan-European landslide susceptibility mapping: ELSUS Version 2. *Journal of Maps*, 14(2), 97–104. doi:10.1080/17445647.2018.1432511

WorldPop. (2023). Top-down estimation modelling: Constrained vs Unconstrained. Retrieved from https://www.worldpop.org/methods/top_down_constrained_vs_unconstrained/





APPENDIX 1 – CCLL-SPECIFIC EXPOSURE MAPS

A1.1. Population

Source: WorldPop

Figure A1.1-1: Population counts per grid cell for the Benidorm CCLL.

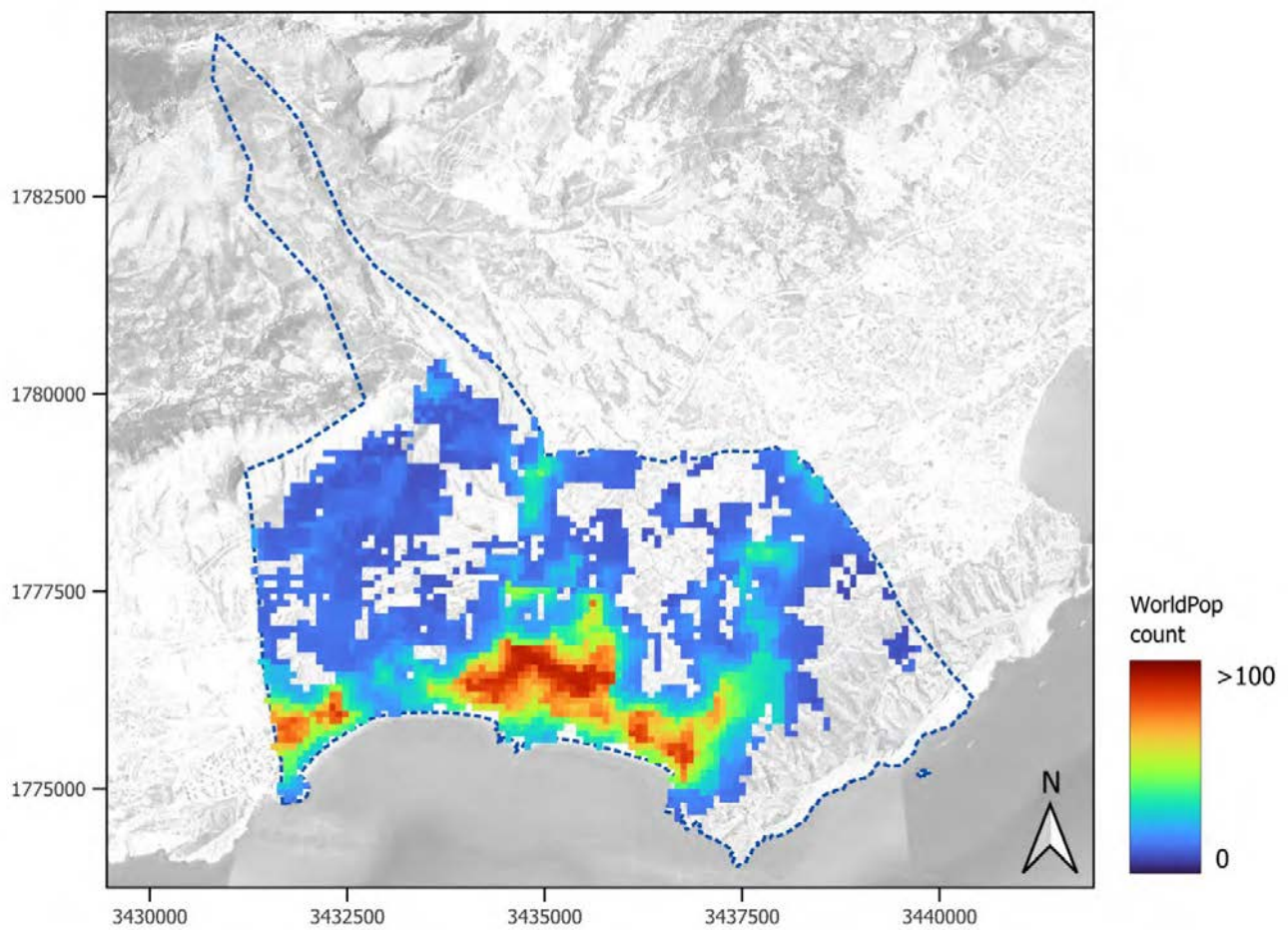




Figure A1.1-2: Population counts per grid cell for the Dublin CCLL.

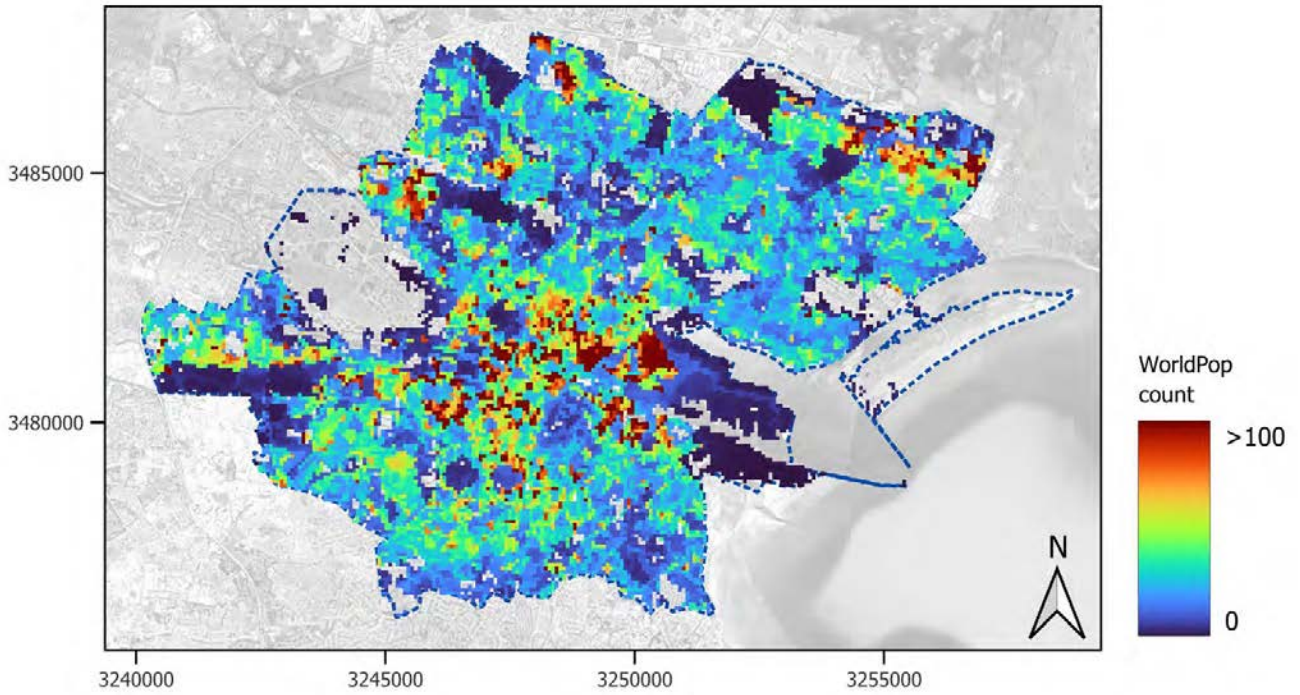


Figure A1.1-3: Population counts per grid cell for the Gdańsk CCLL.

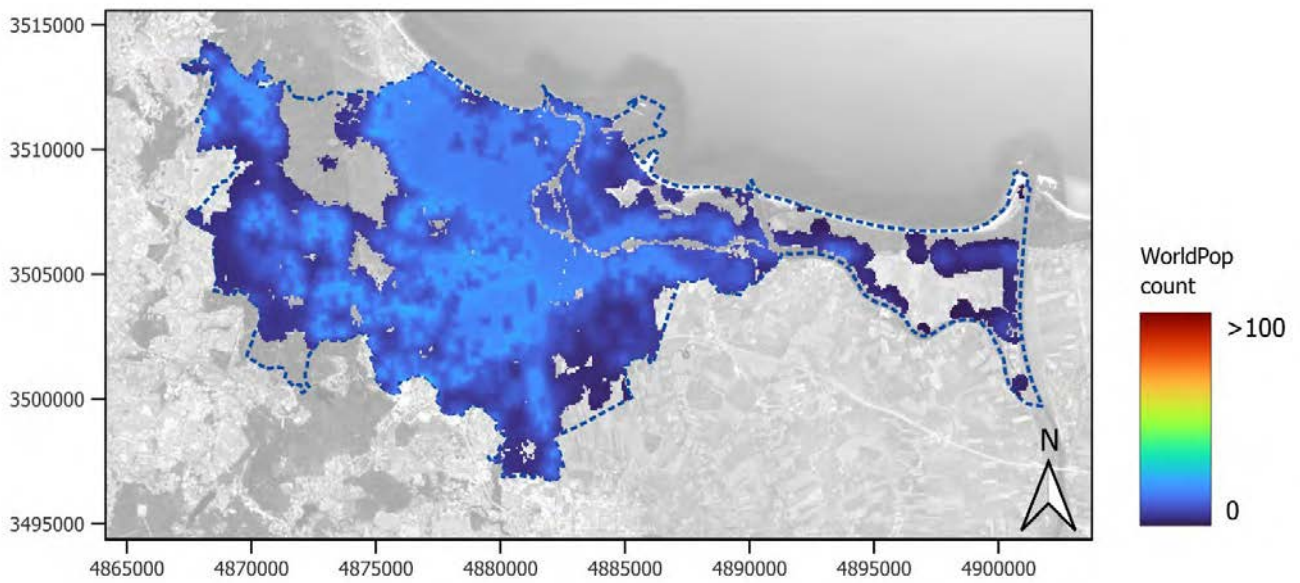




Figure A1.1-4: Population counts per grid cell for the Massa CCLL.

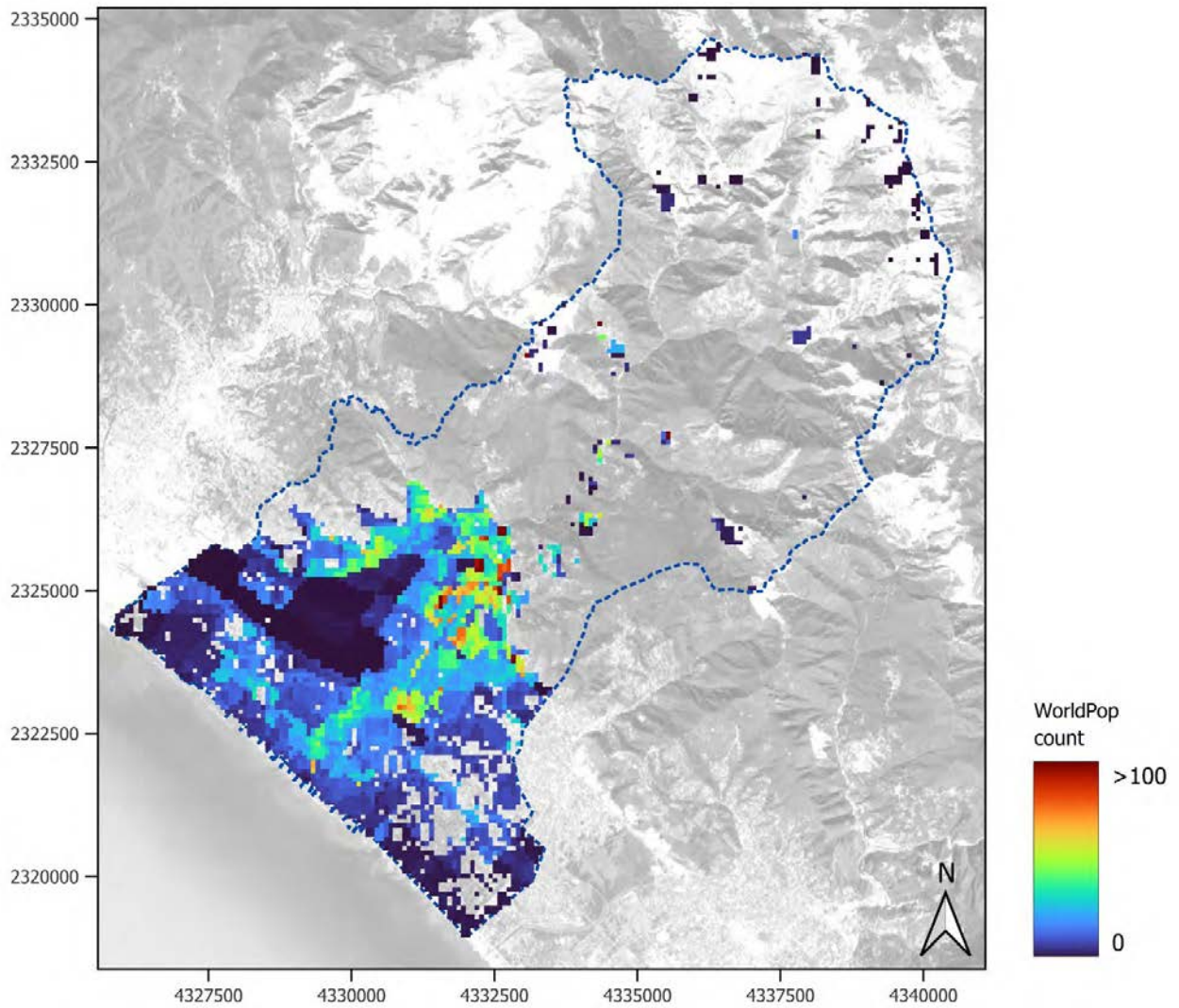




Figure A1.1-5: Population counts per grid cell for the Oarsoaldea CCLL.

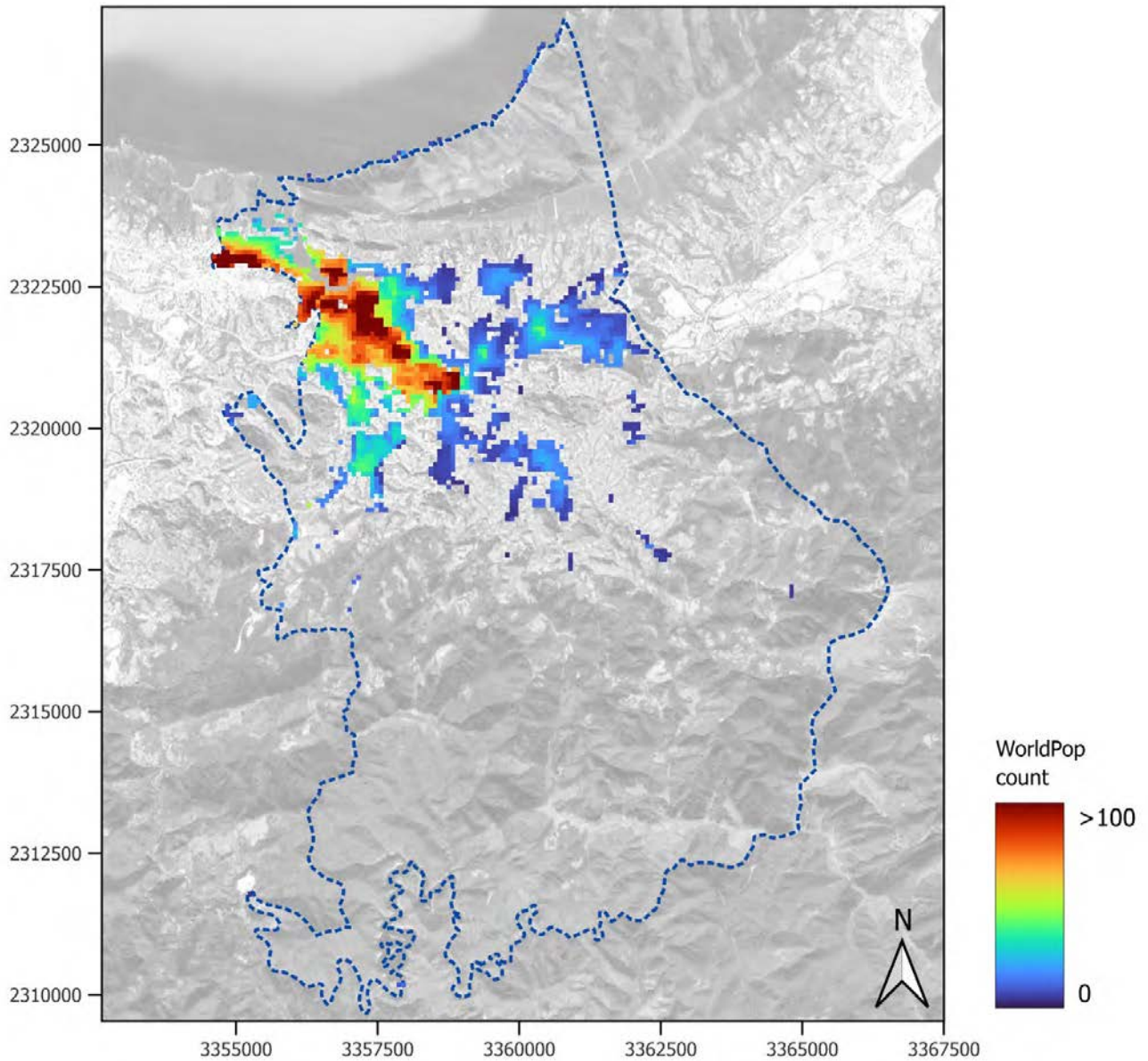




Figure A1.1-6: Population counts per grid cell for the Oeiras CCLL.

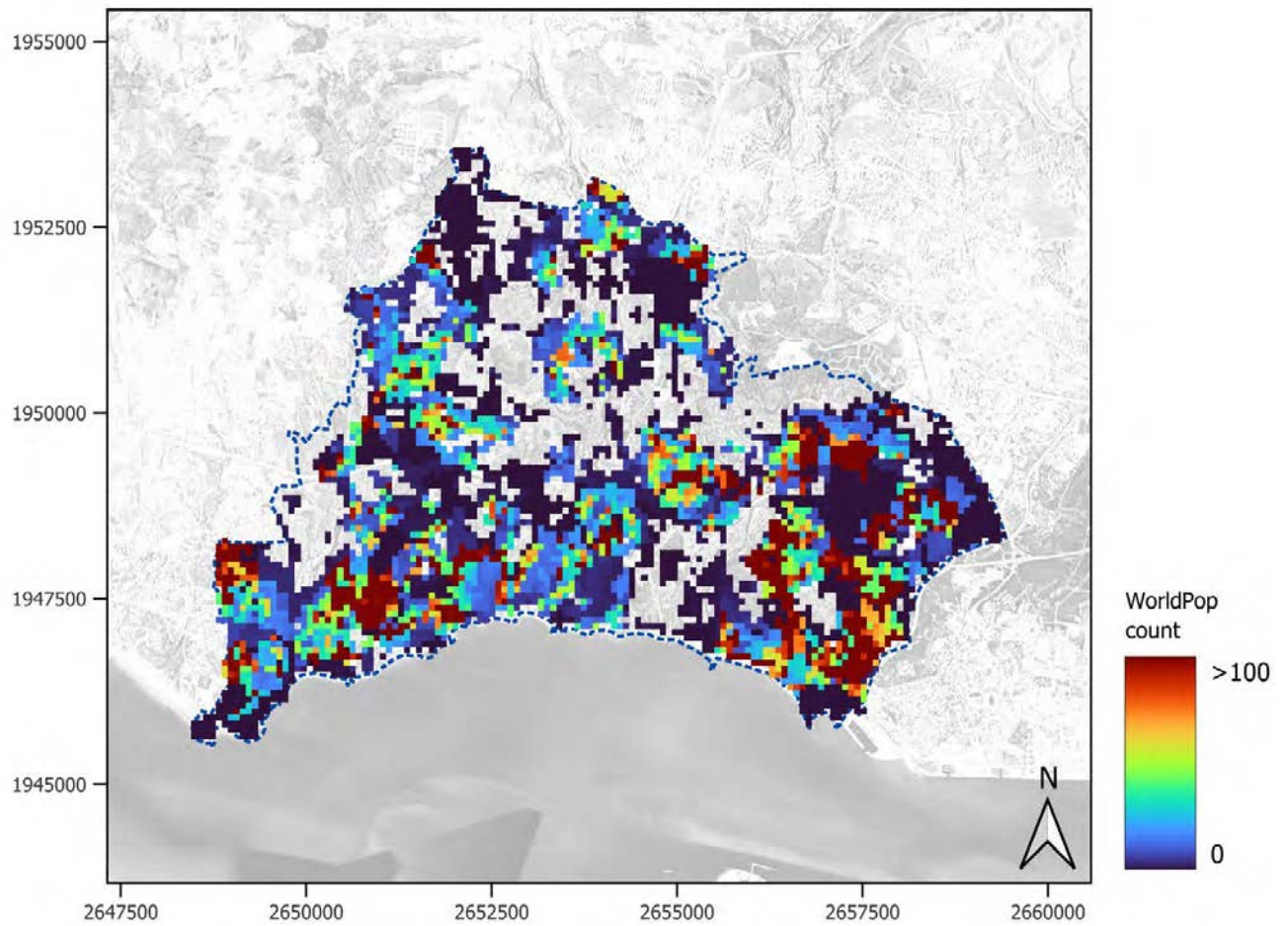




Figure A1.1-7: Population counts per grid cell for the Piran CCLL.

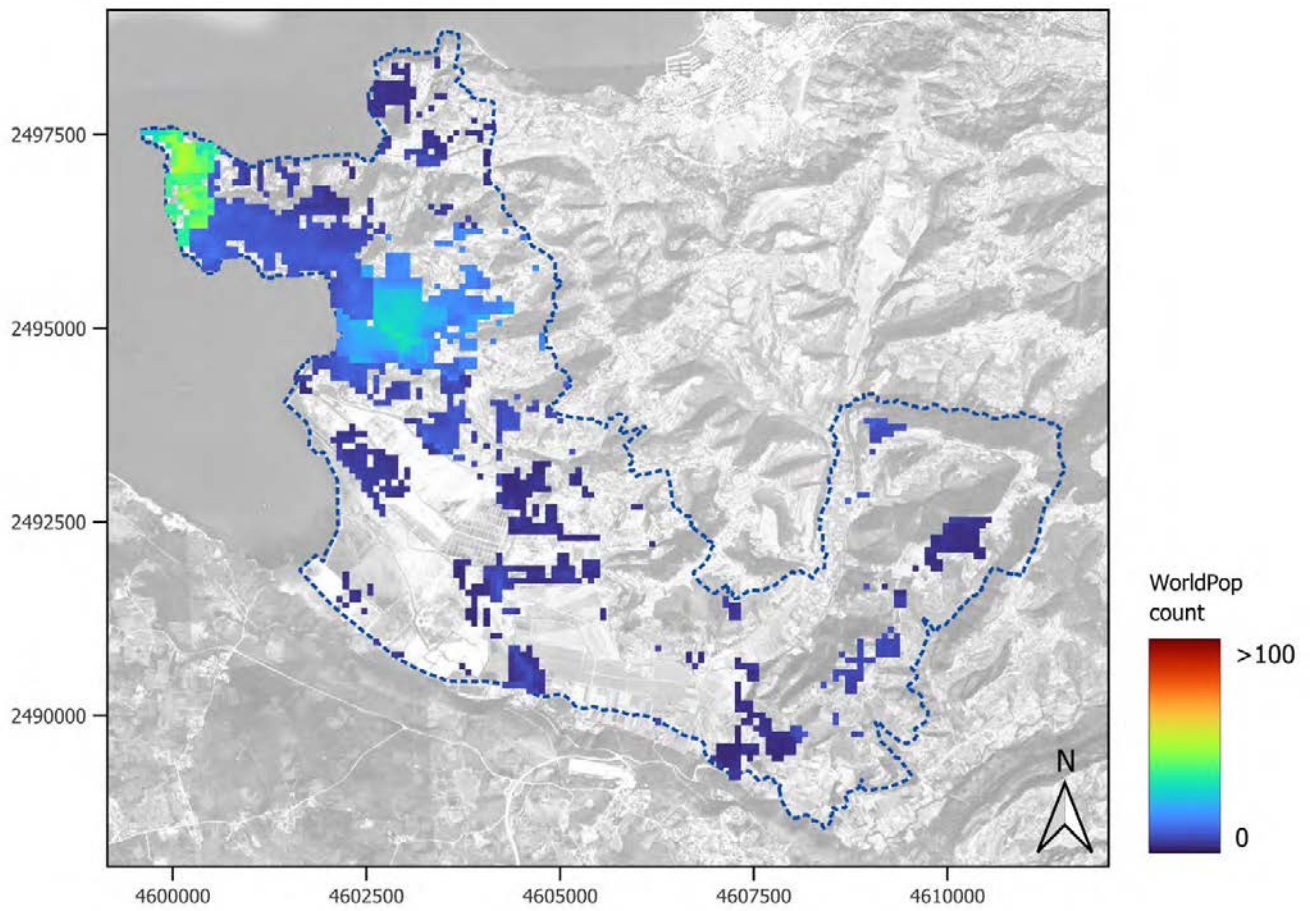




Figure A1.1-8: Population counts per grid cell for the Samsun CCLL.

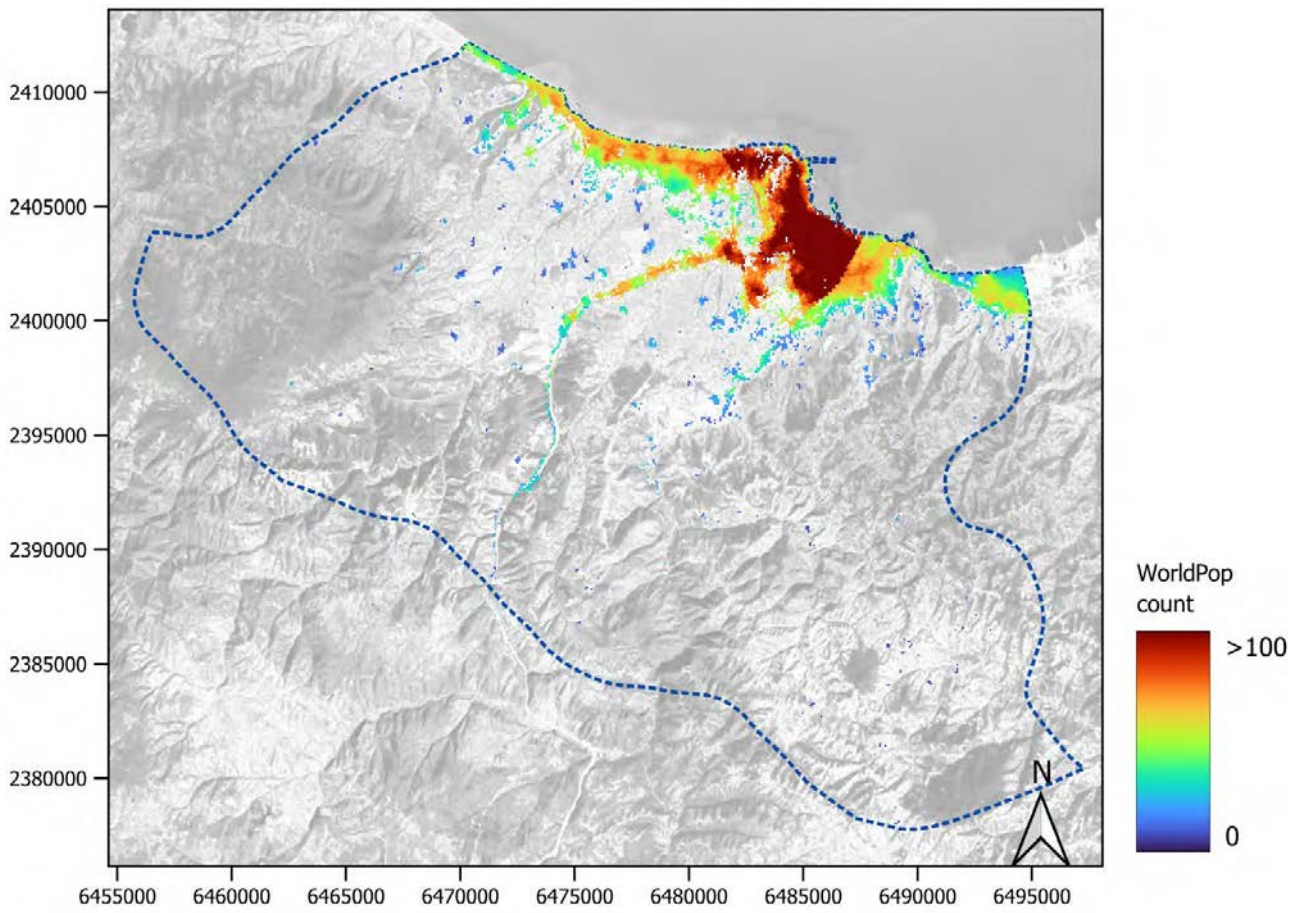




Figure A1.1-9: Population counts per grid cell for the Sligo CCLL.

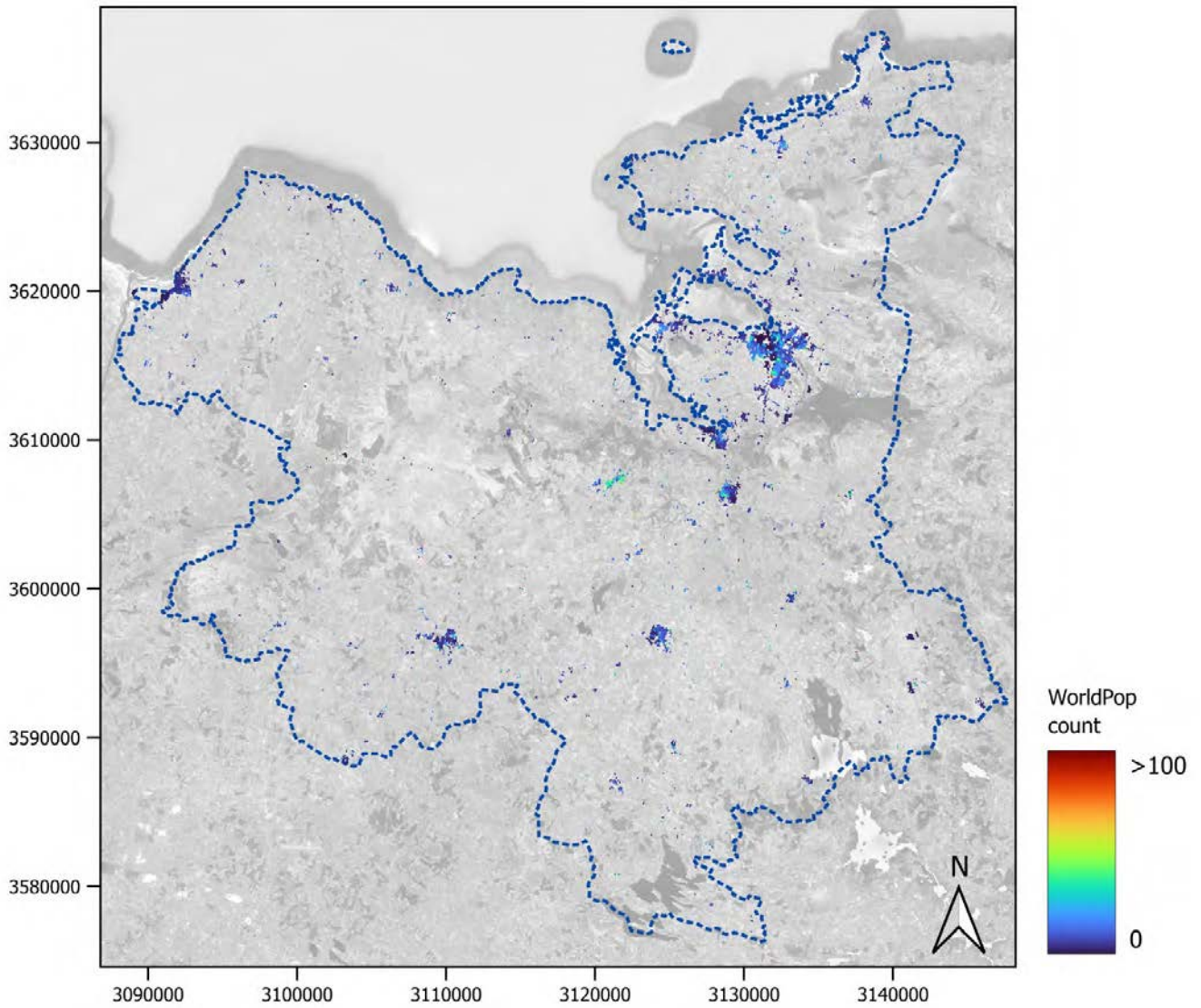
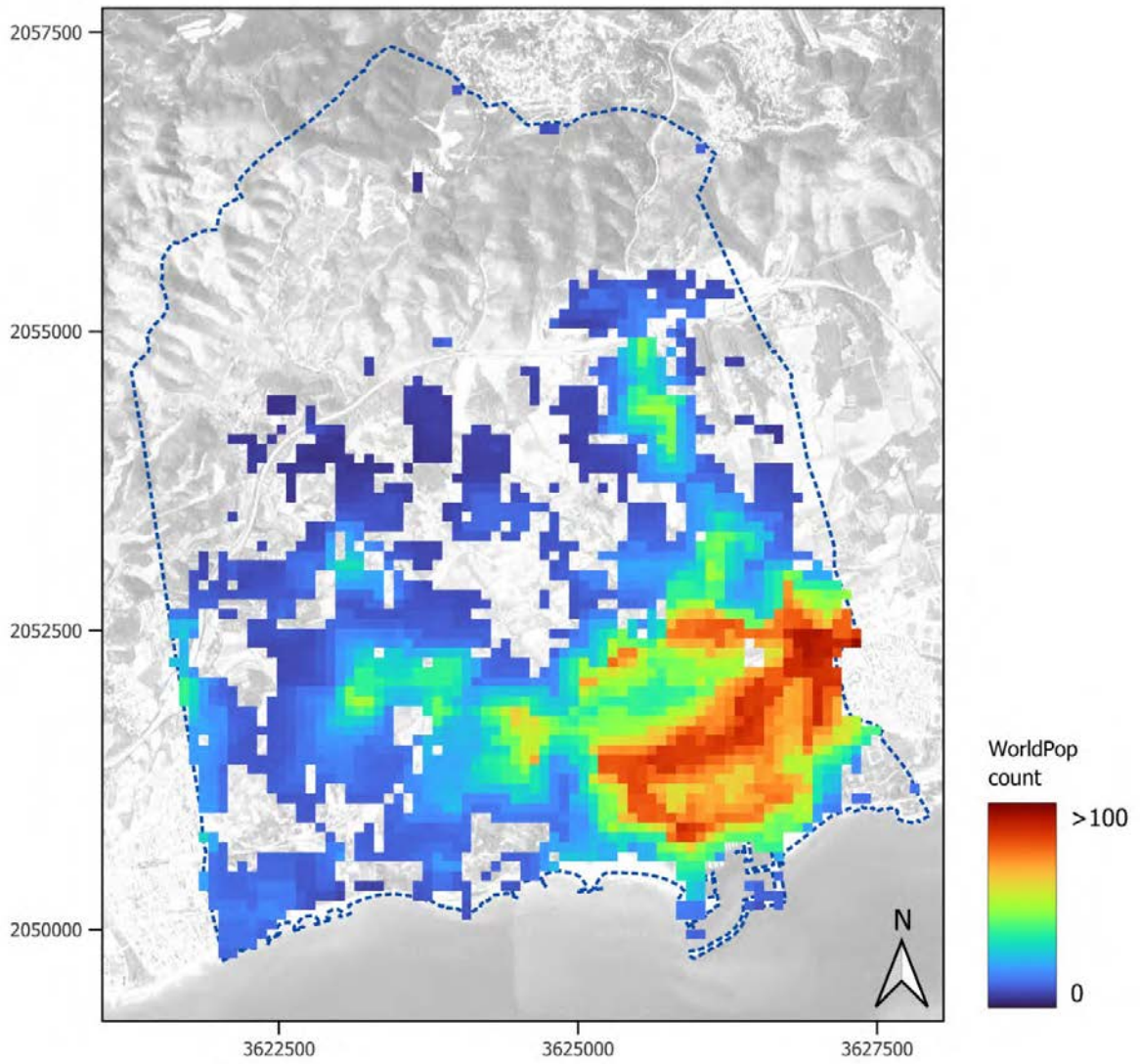




Figure A1.1-10: Population counts per grid cell for Vilanova i la Geltrú CCLL.





A1.2. Land cover

Source: CORINE Land Cover

For the legend, please refer to Figure A1.2-11.

Figure A1.2-1: Land cover map for the Benidorm CCLL.

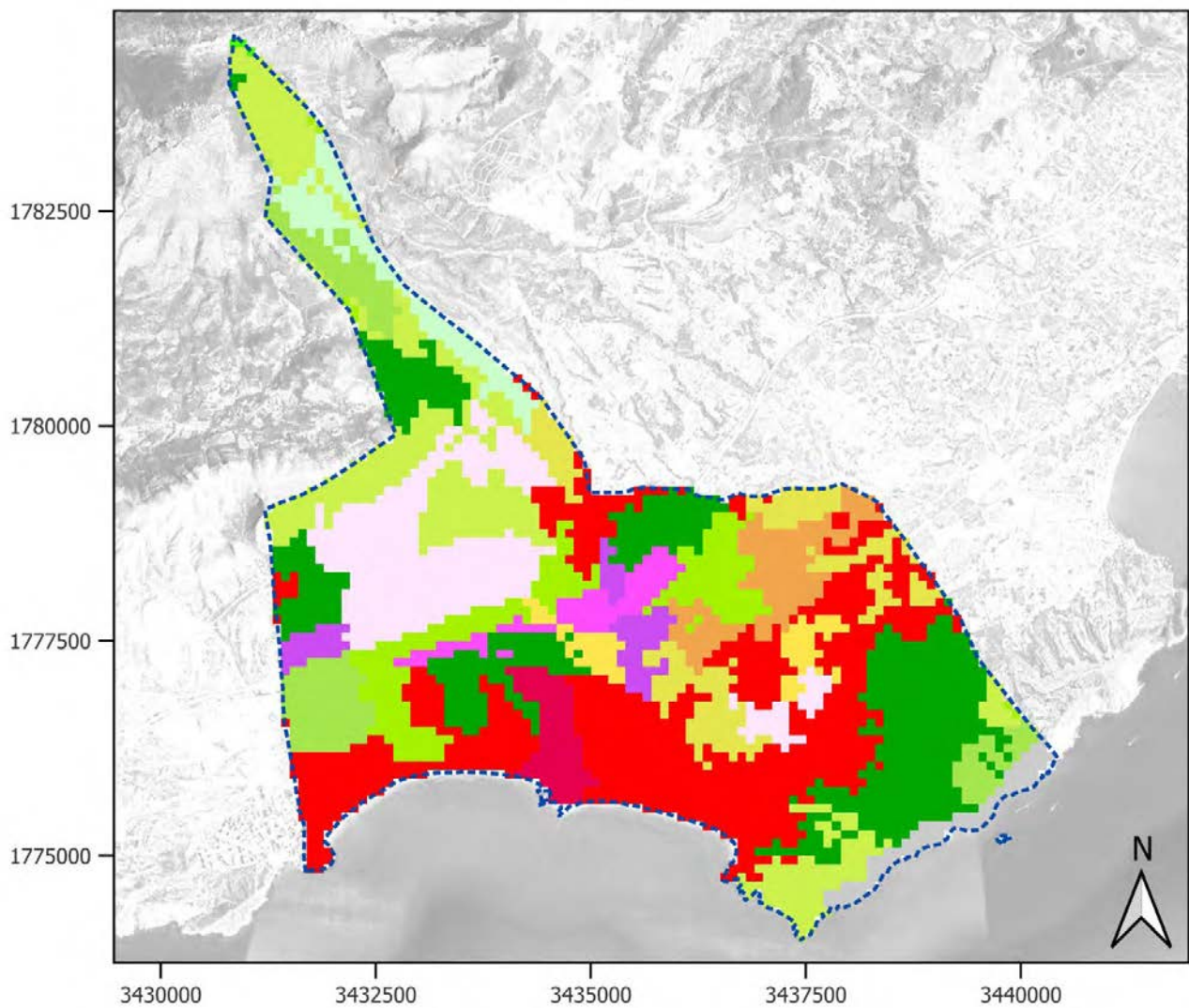




Figure A1.2-2: Land cover map for the Dublin CCLL.

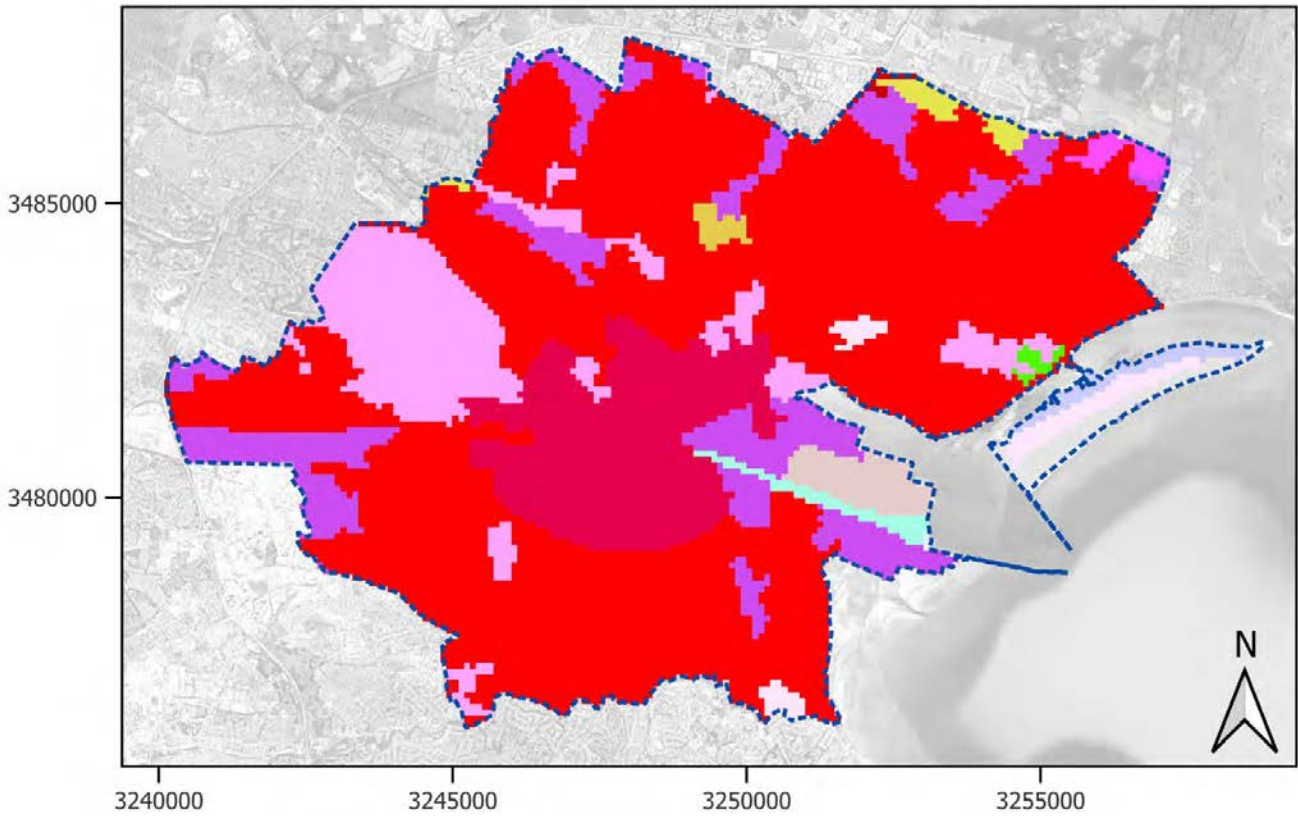


Figure A1.2-3: Land cover map for the Gdańsk CCLL.

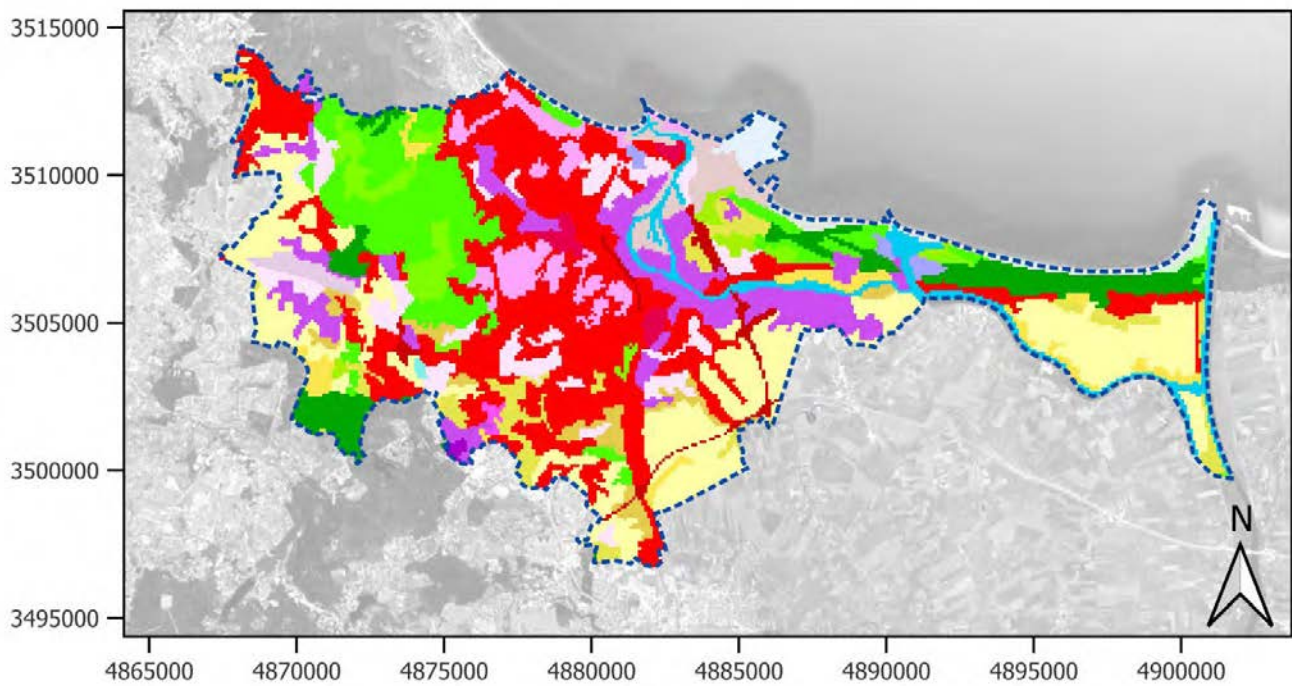




Figure A1.2-4: Land cover map for the Massa CCLL.

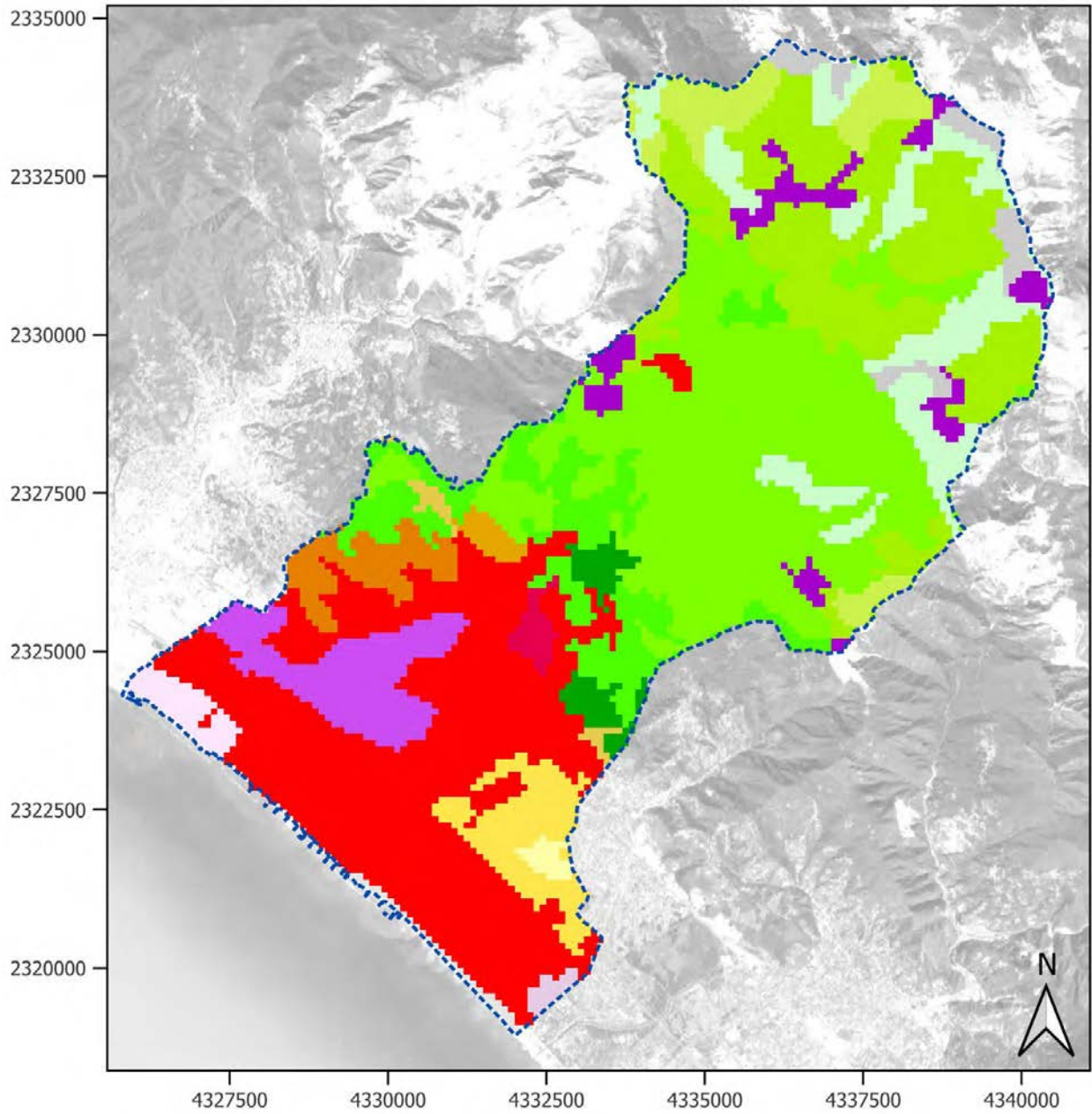




Figure A1.2-5: Land cover map for the Oarsoaldea CCLL.

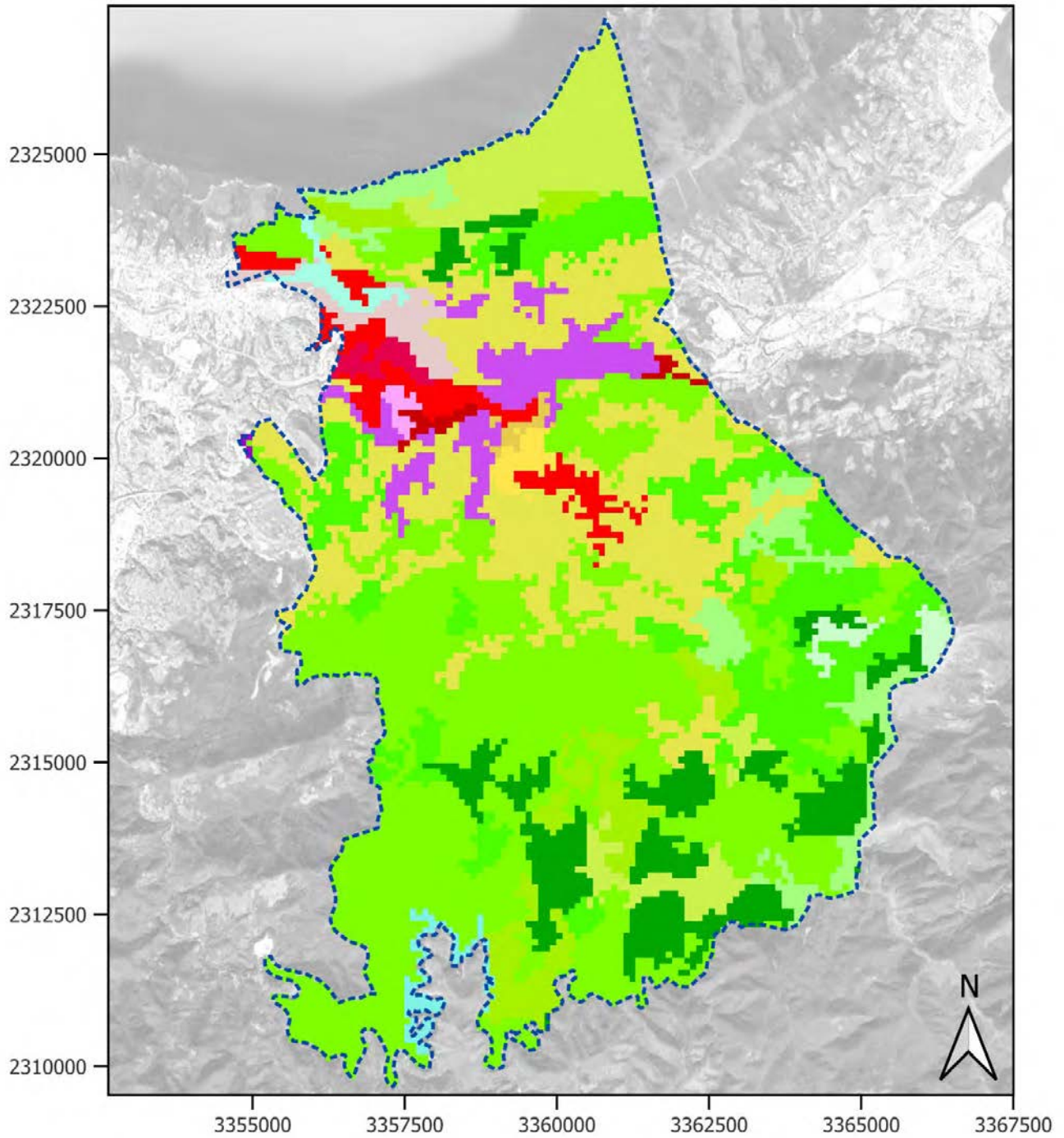




Figure A1.2-6: Land cover map for the Oeiras CCLL.

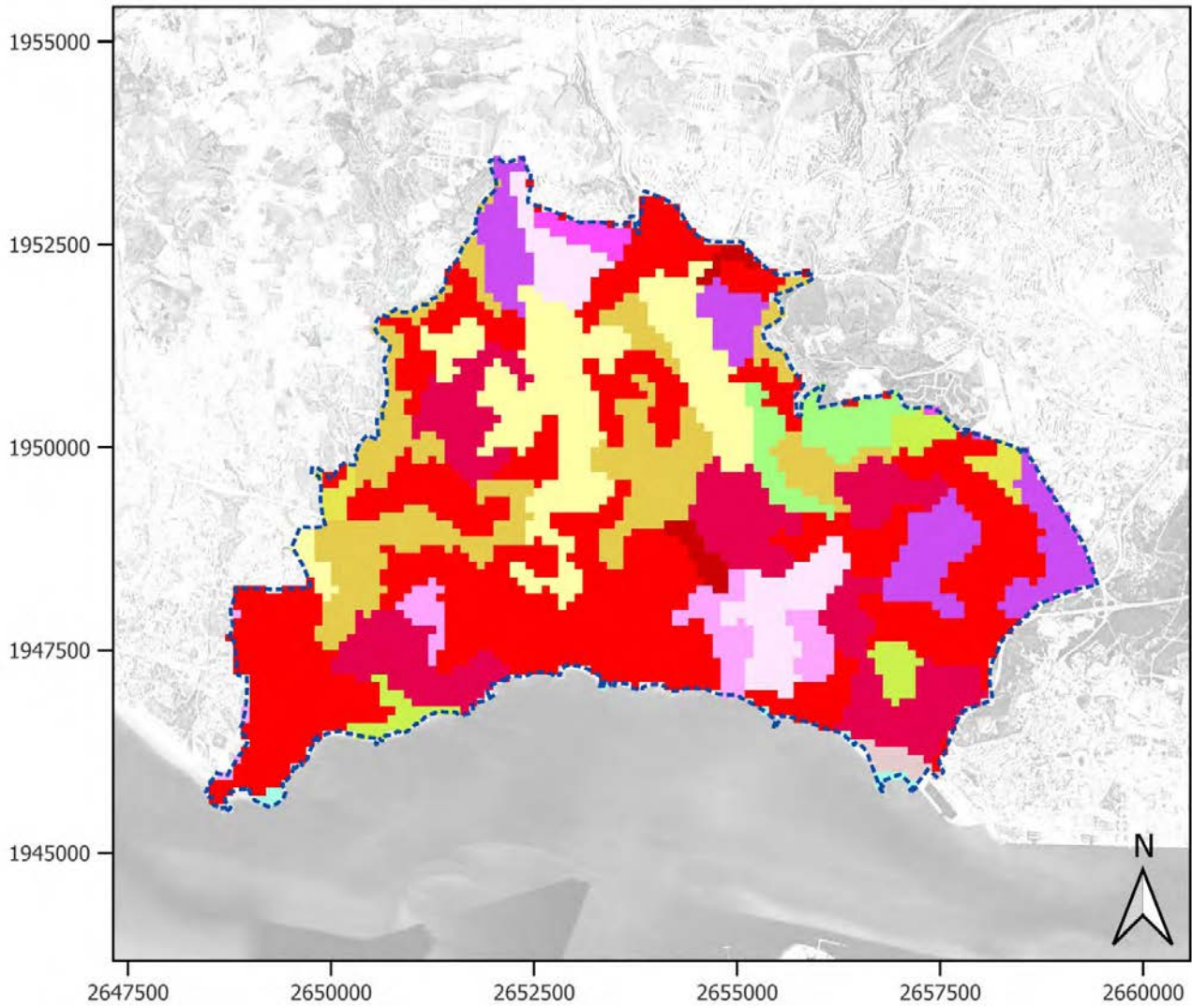




Figure A1.2-7: Land cover map for the Piran CCLL.

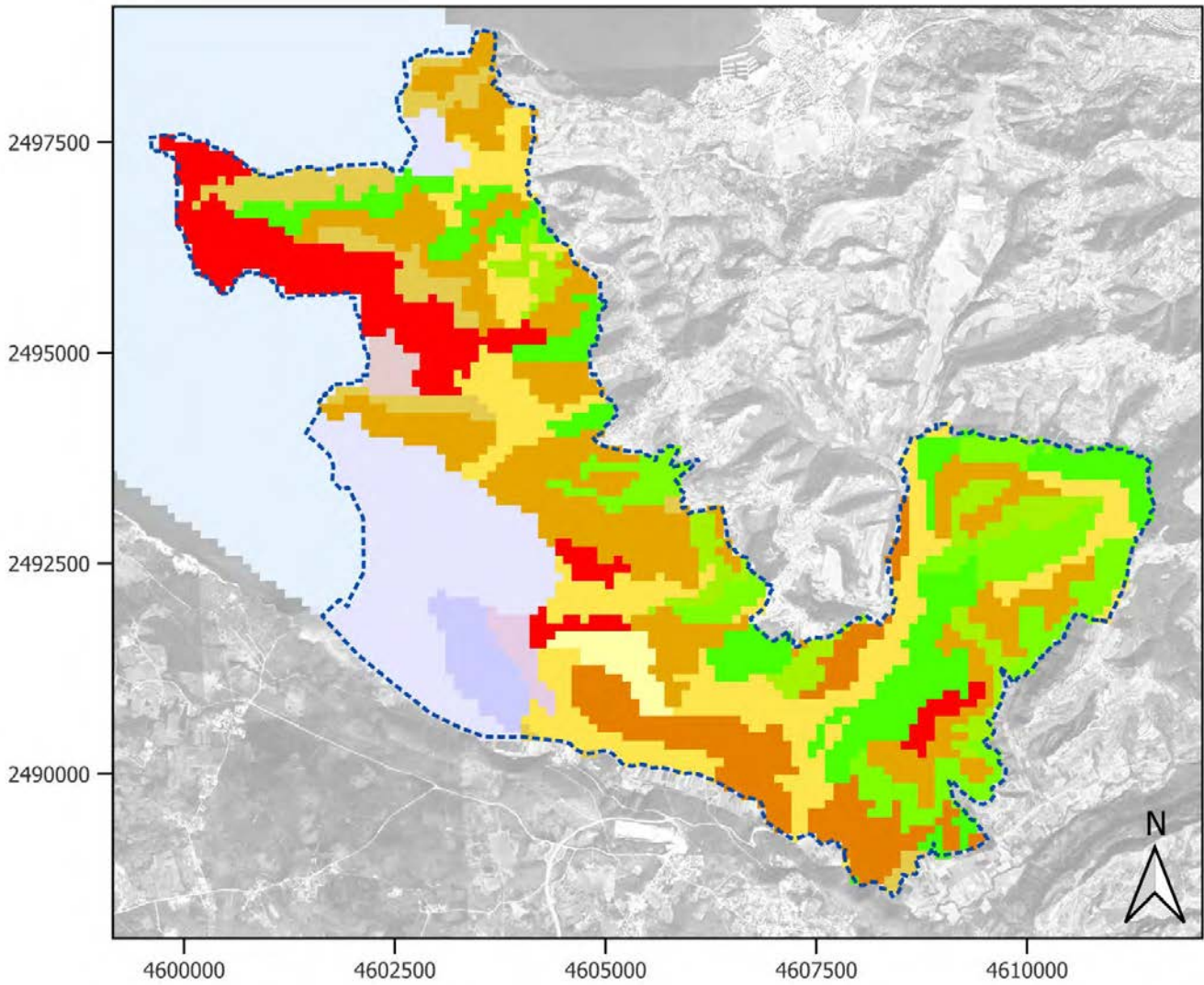




Figure A1.2-8: Land cover map for the Samsun CCLL.

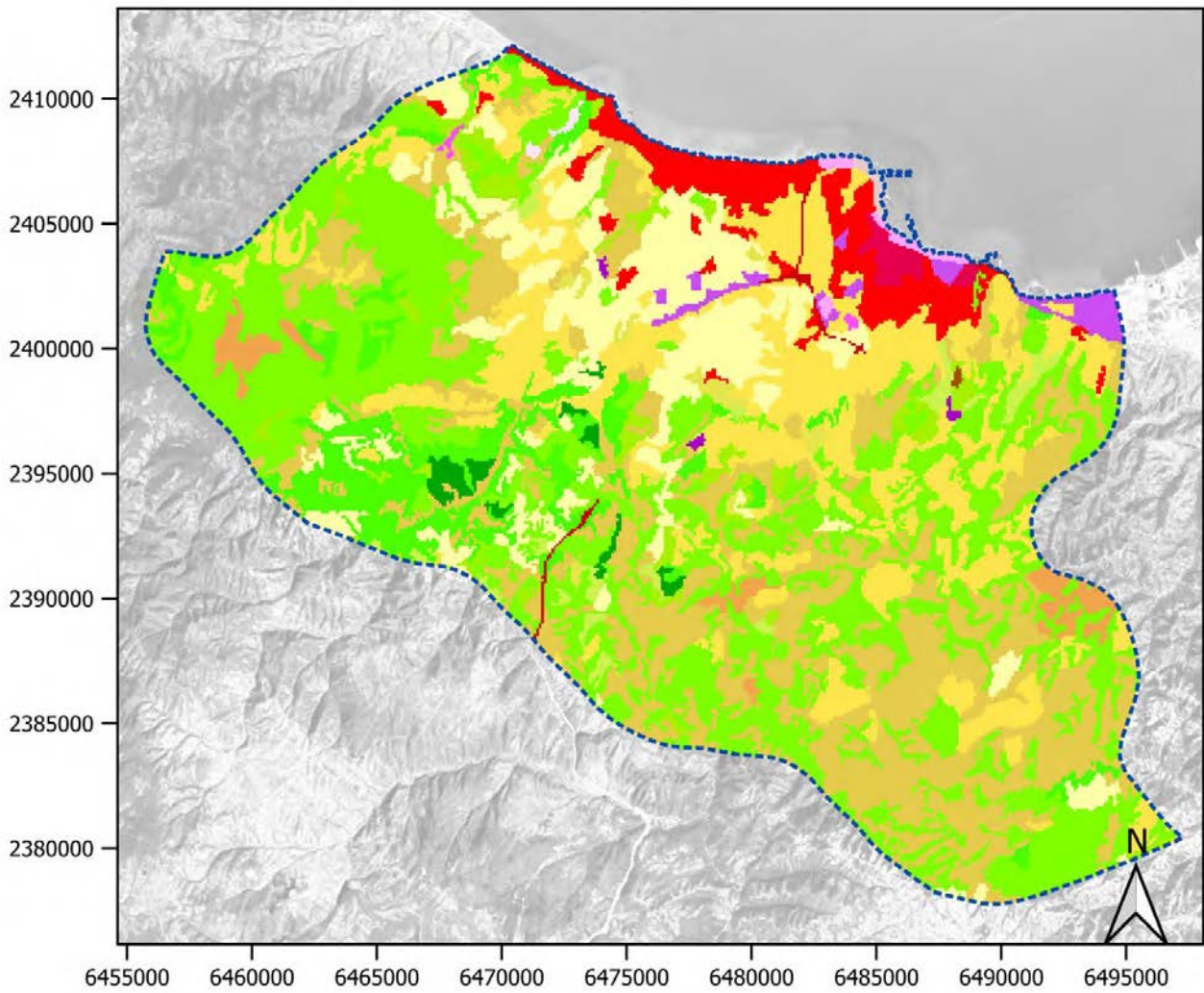




Figure A1.2-9: Land cover map for the Sligo CCLL.

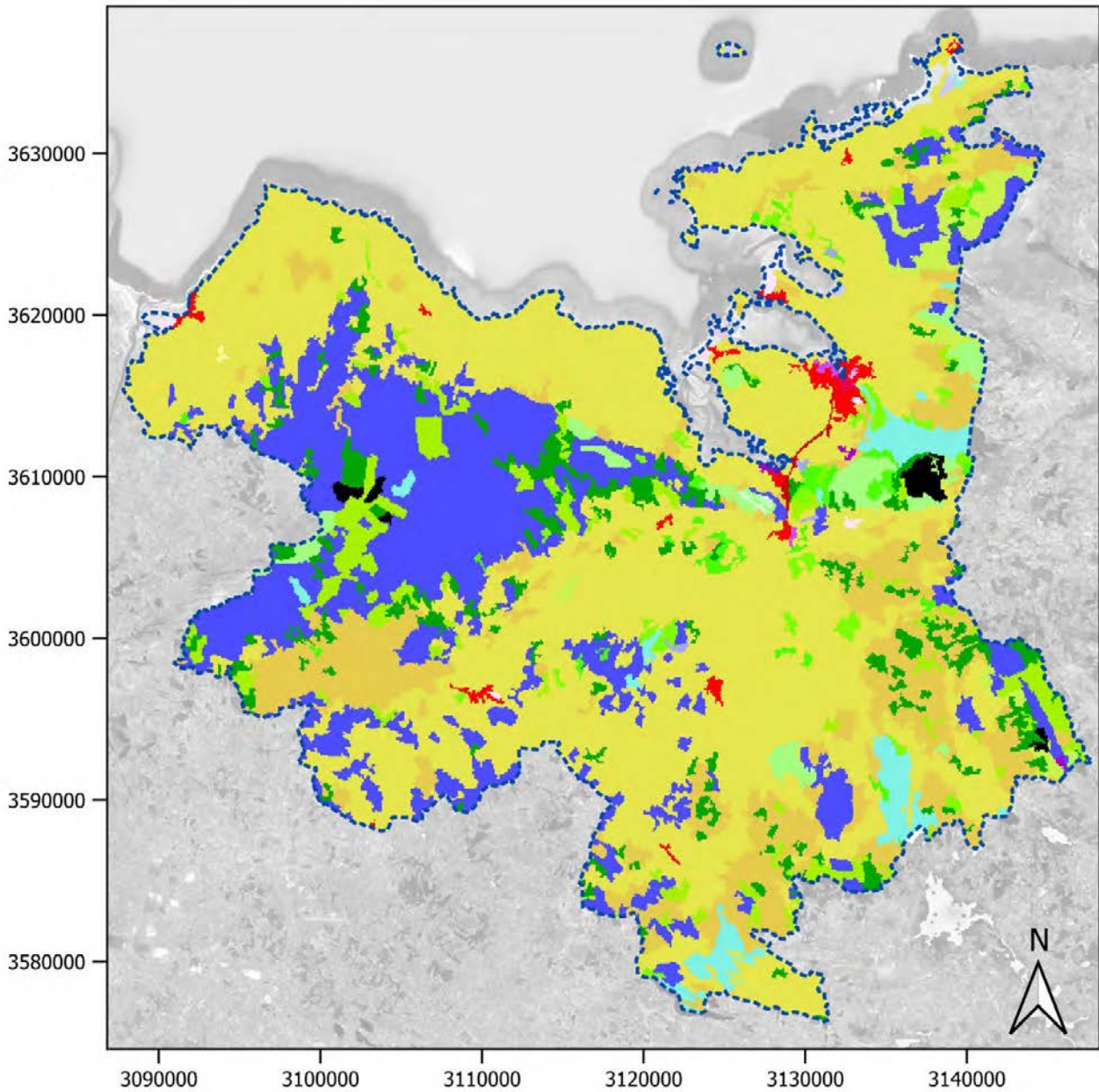




Figure A1.2-10: Land cover map for the Vilanova i la Geltrú CCLL.

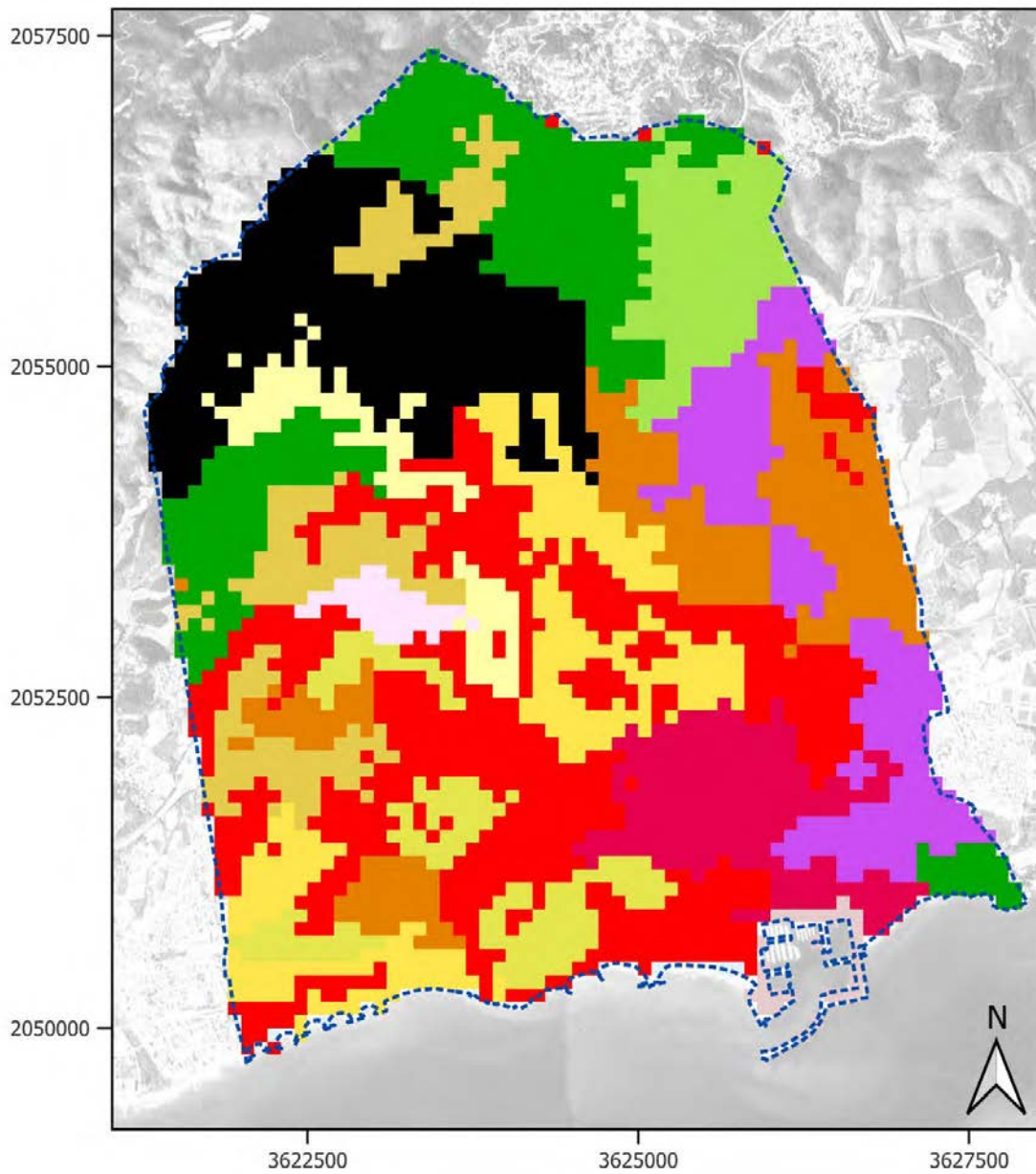




Figure A1.2-11: CORINE Land Cover map legend.

	111: Continuous urban fabric
	112: Discontinuous urban fabric
	121: Industrial or commercial units
	122: Road and rail networks and associated land
	123: Port areas
	124: Airports
	131: Mineral extraction sites
	132: Dump sites
	133: Construction sites
	141: Green urban areas
	142: Sport and leisure facilities
	211: Non-irrigated arable land
	212: Permanently irrigated land
	213: Rice fields
	221: Vineyards
	222: Fruit trees and berry plantations
	223: Olive groves
	231: Pastures
	241: Annual crops associated with permanent crops
	242: Complex cultivation patterns
	243: Land principally occupied by agriculture with significant areas of natural vegetation
	244: Agro-forestry areas
	311: Broad-leaved forest
	312: Coniferous forest
	313: Mixed forest
	321: Natural grasslands
	322: Moors and heathland
	323: Sclerophyllous vegetation
	324: Transitional woodland-shrub
	331: Beaches dunes sands
	332: Bare rocks
	333: Sparsely vegetated areas
	334: Burnt areas
	335: Glaciers and perpetual snow
	411: Inland marshes
	412: Peat bogs
	421: Salt marshes
	422: Salines
	423: Intertidal flats
	511: Water courses
	512: Water bodies
	521: Coastal lagoons
	522: Estuaries
	523: Sea and ocean





A1.3. Road and railway networks

Source: OpenStreetMap (reclassified according to Table 6)

Figure A1.3-1: Map of roads and railways in the Benidorm CCLL.

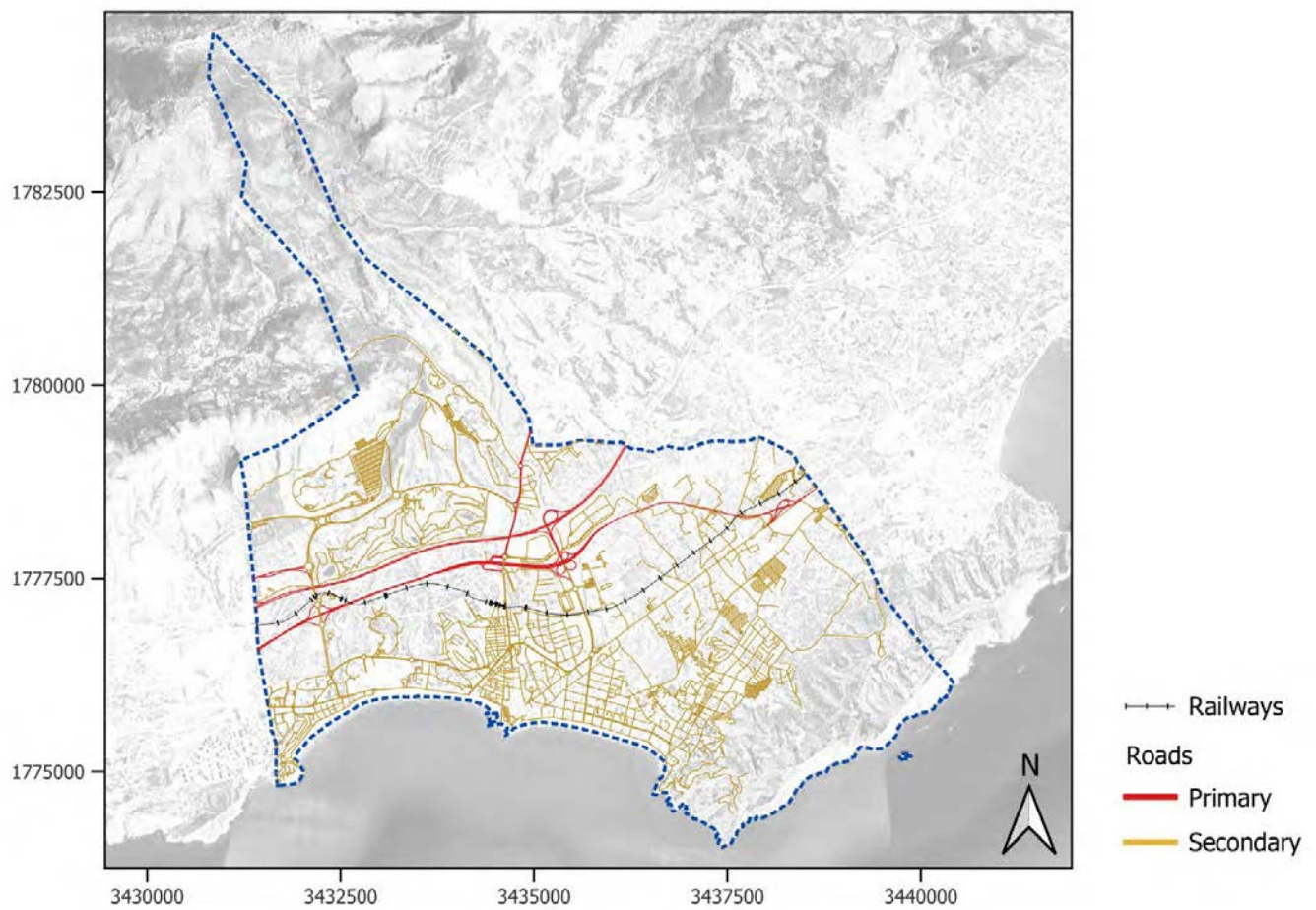




Figure A1.3-2: Map of roads and railways in the Dublin CCLL.

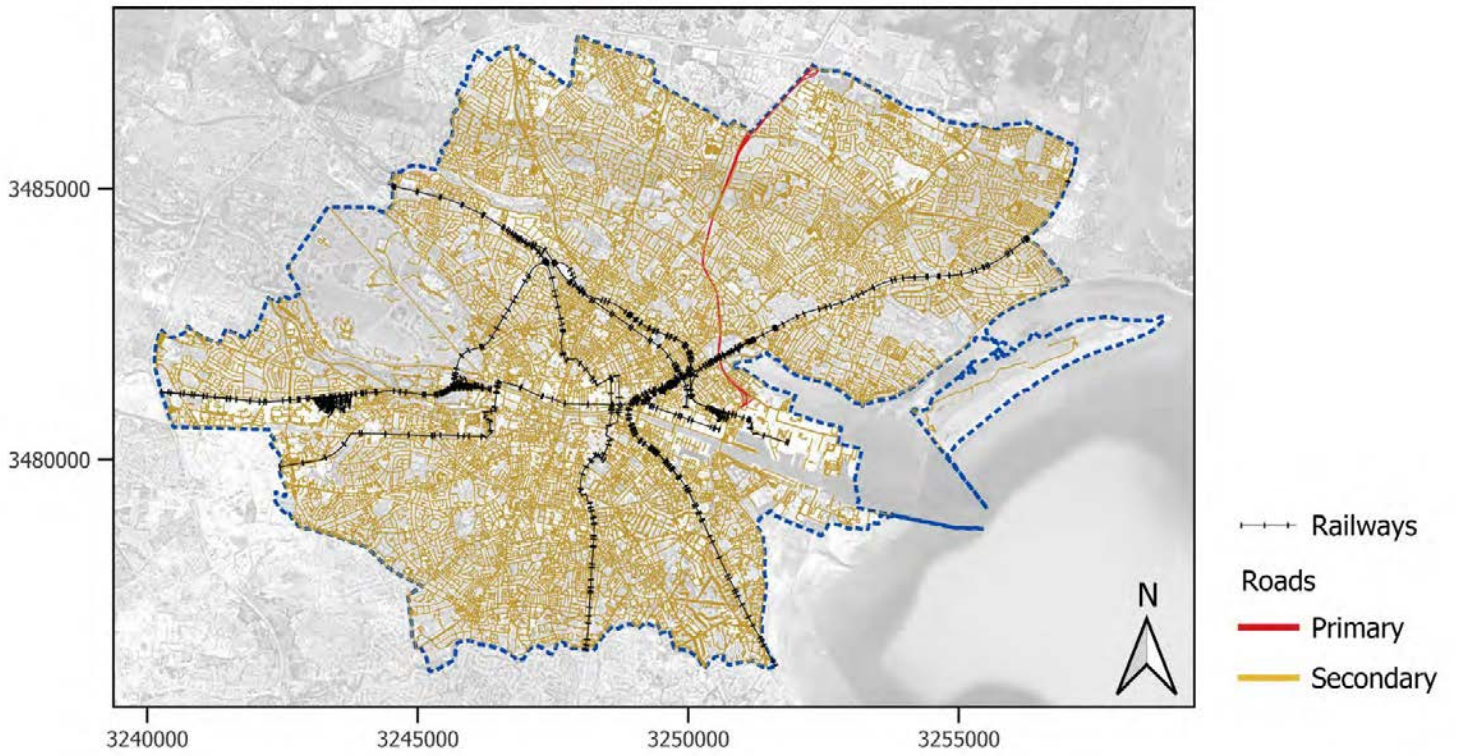


Figure A1.3-3: Map of roads and railways in the Gdańsk CCLL.

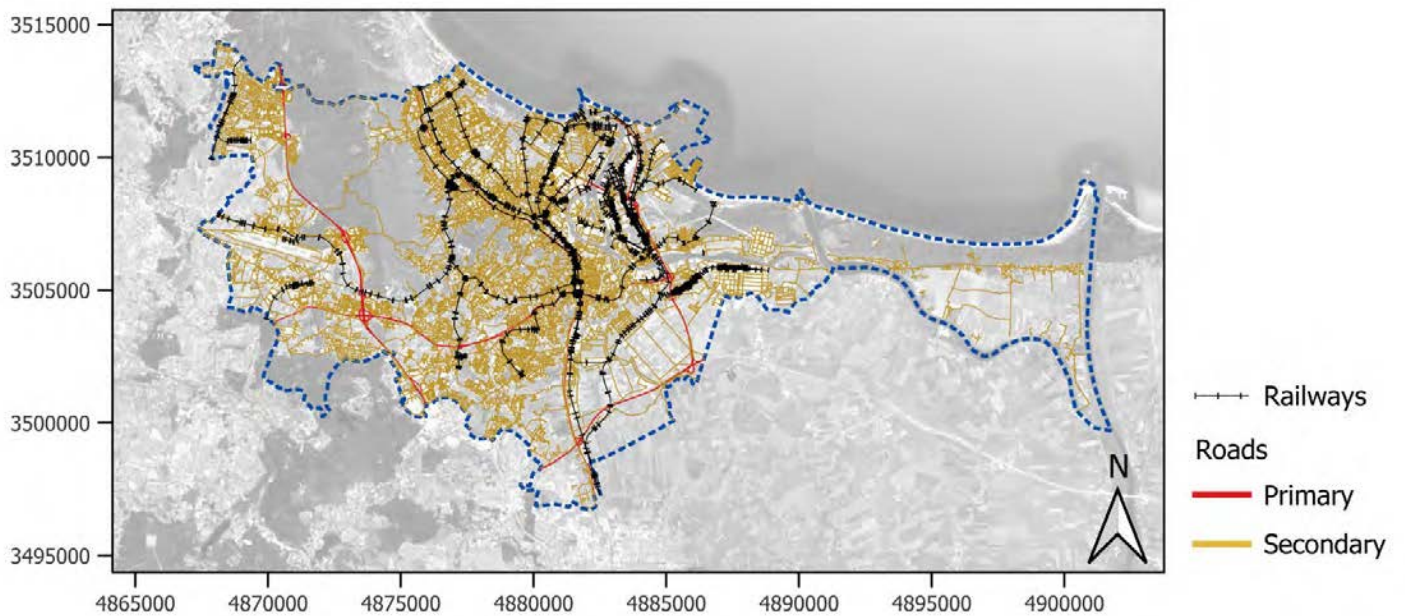




Figure A1.3-4: Map of roads and railways in the Massa CCLL.

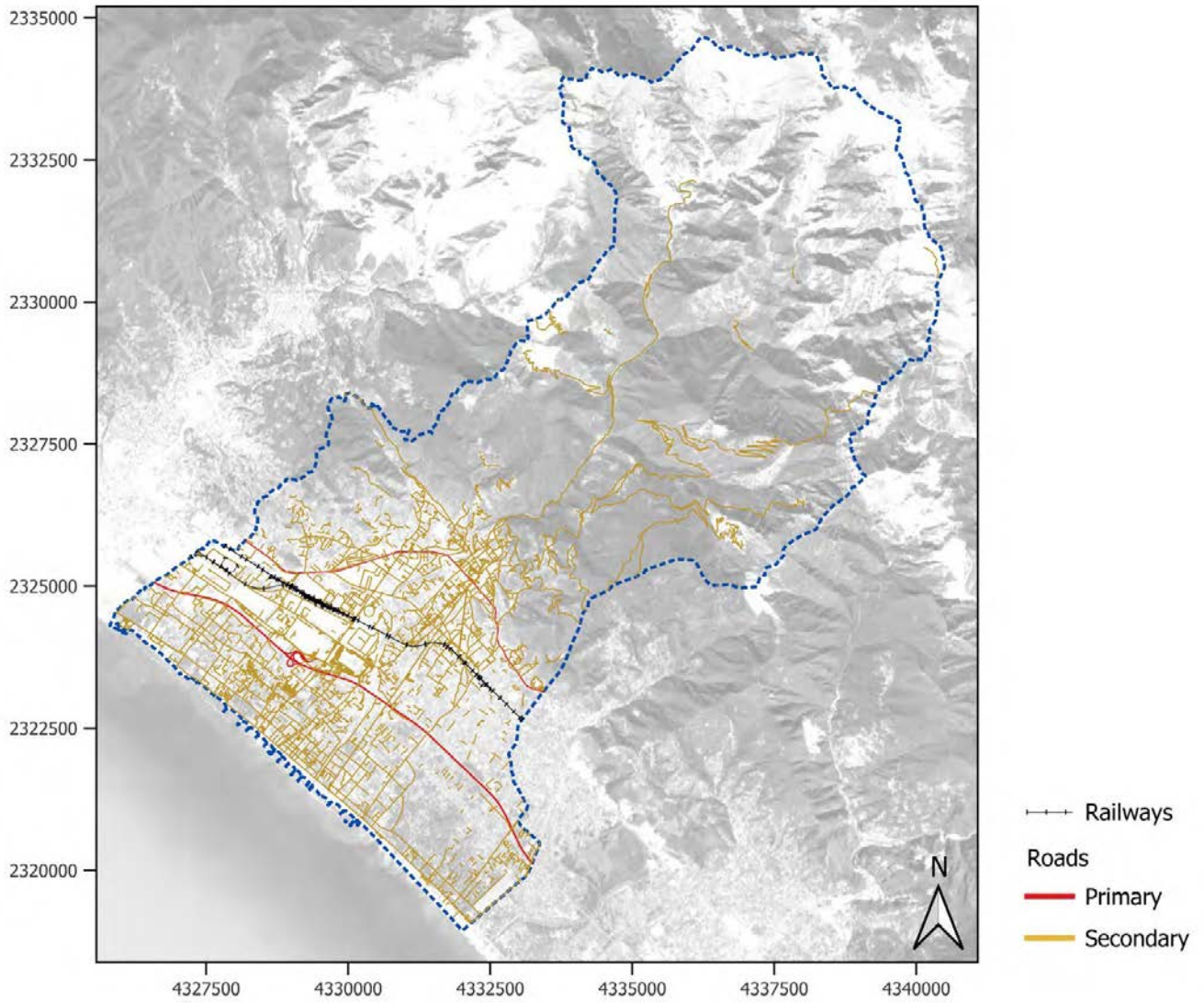




Figure A1.3-5: Map of roads and railways in the Oarsoaldea CCLL.

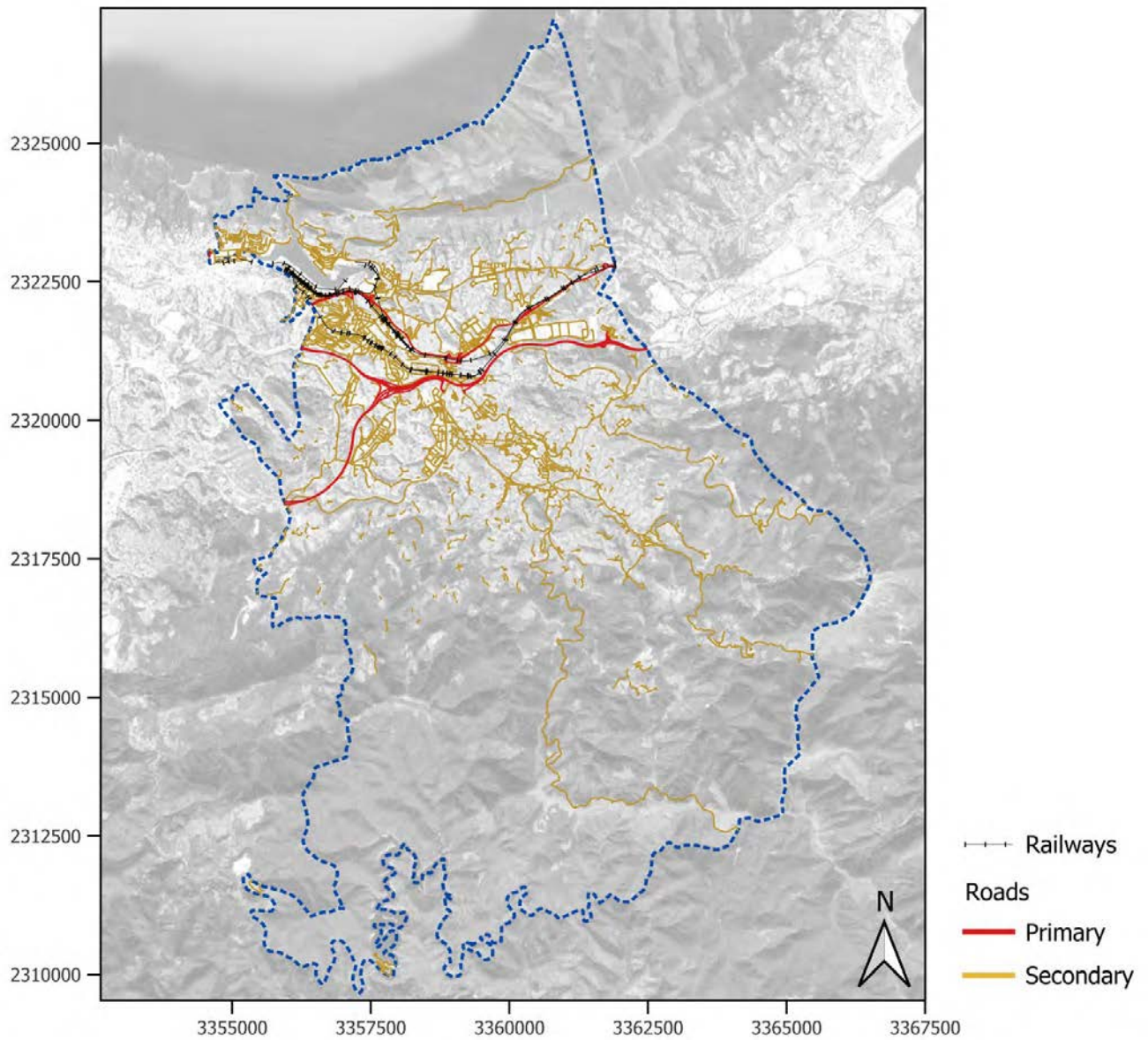




Figure A1.3-6: Map of roads and railways in the Oeiras CCLL.

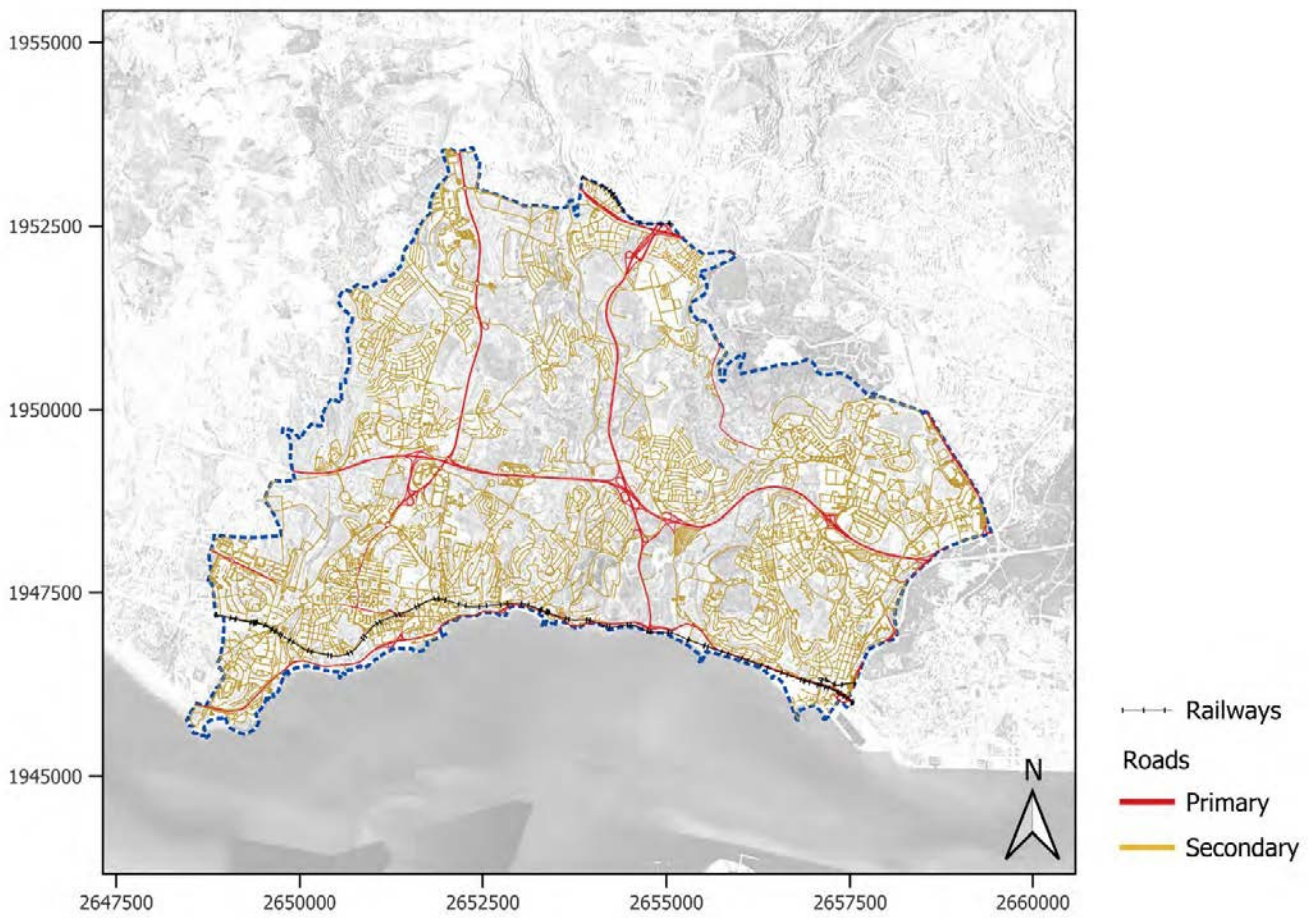




Figure A1.3-7: Map of roads and railways in the Piran CCLL.

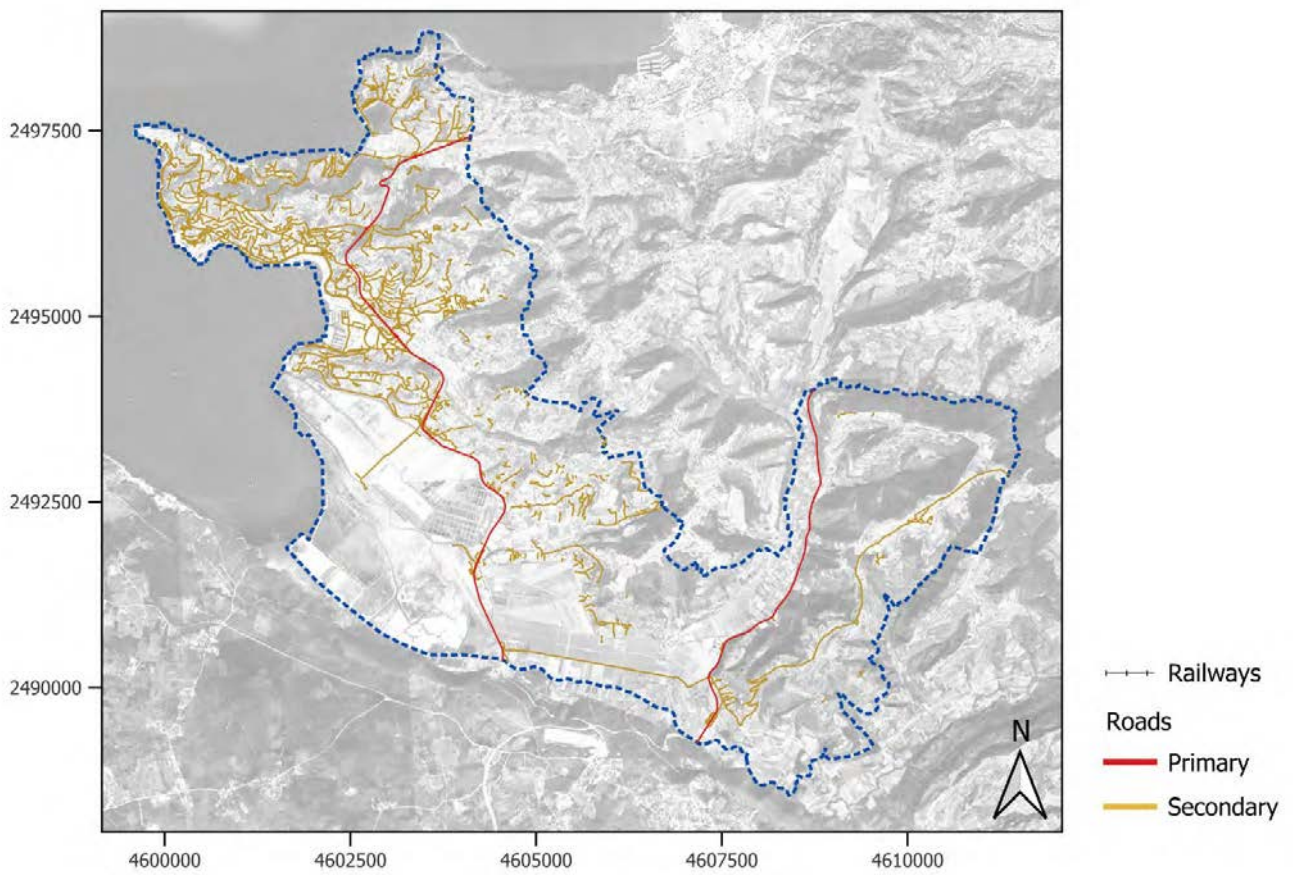




Figure A1.3-8: Map of roads and railways in the Samsun CCLL.

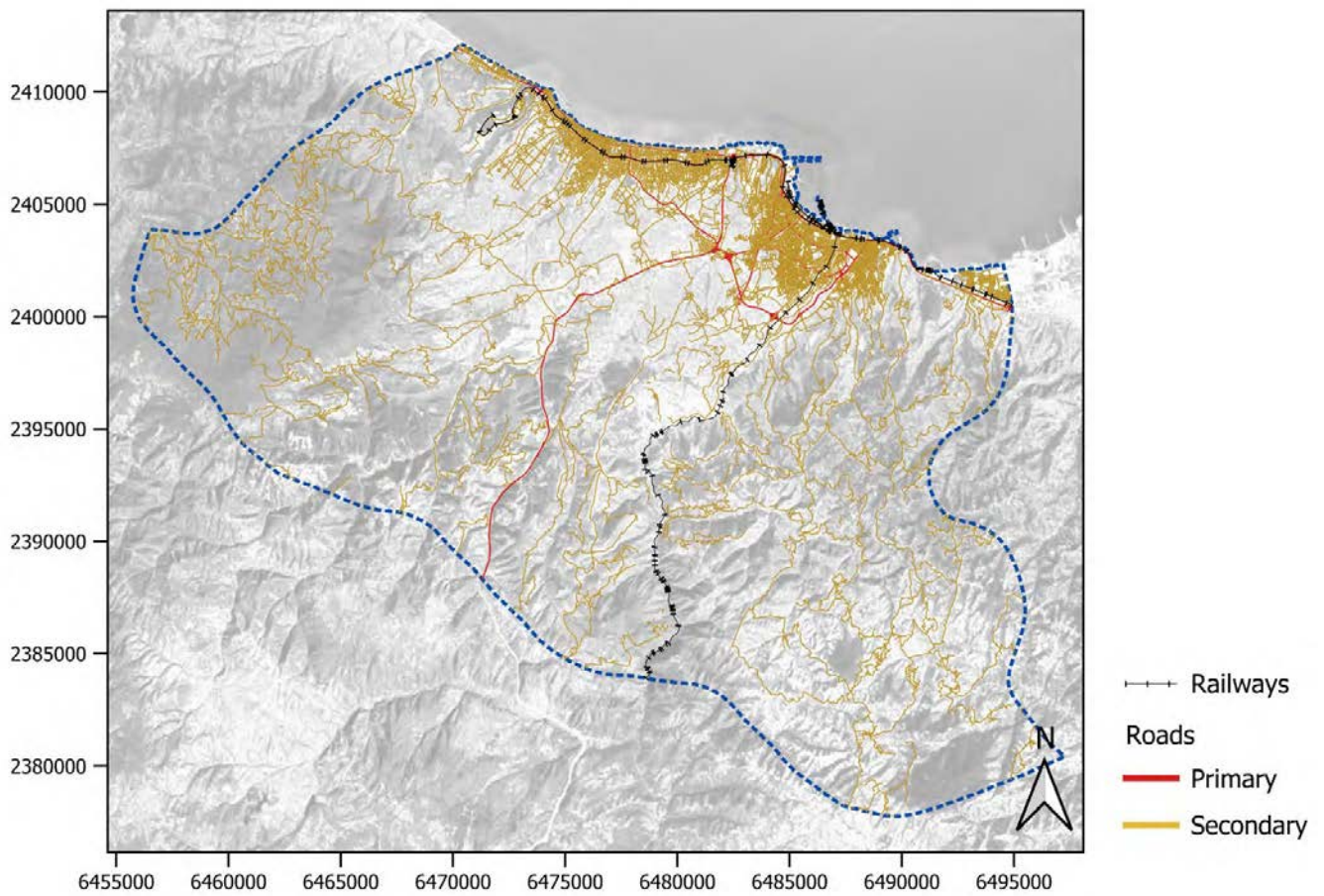




Figure A1.3-9: Map of roads and railways in the Sligo CCLL.

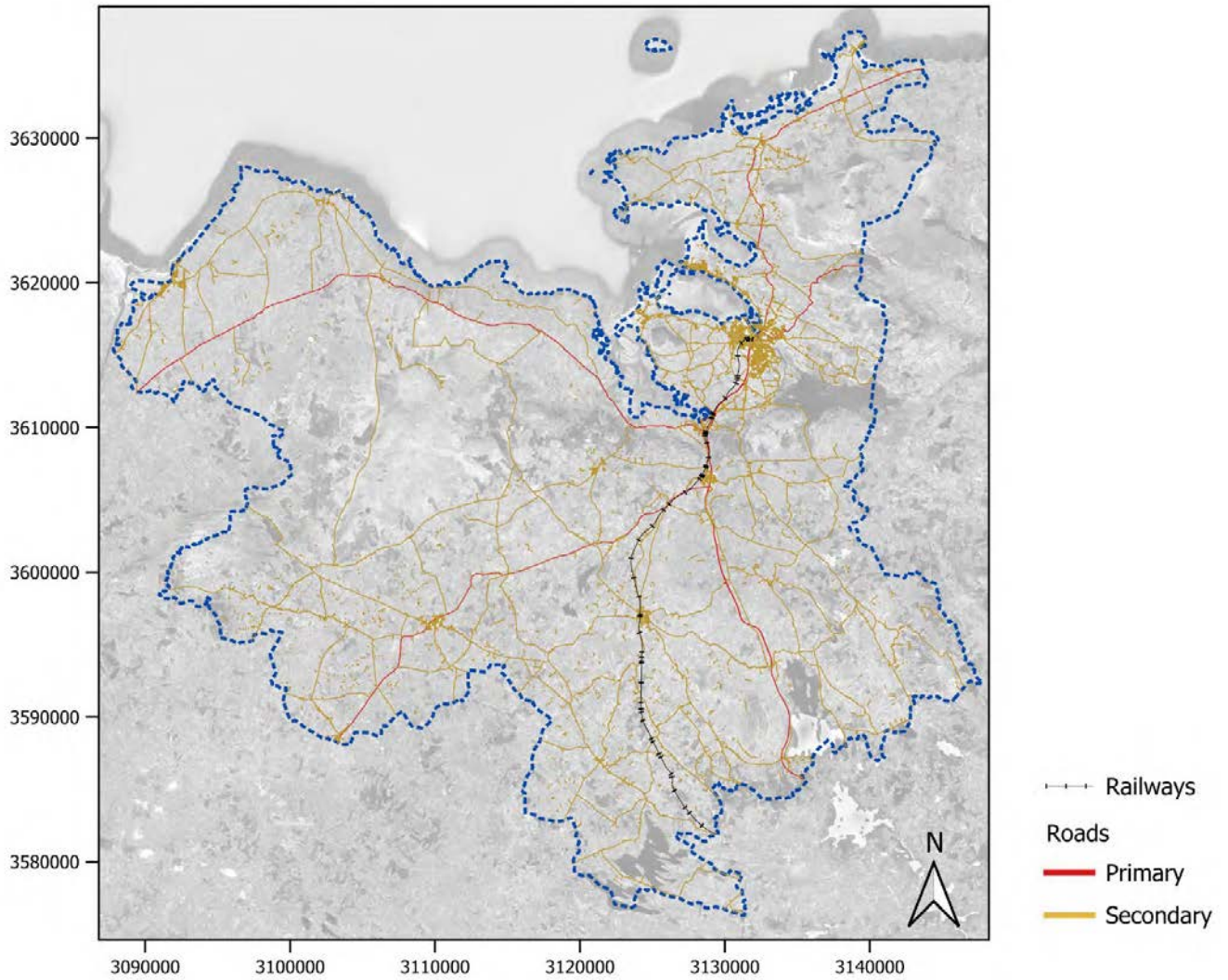
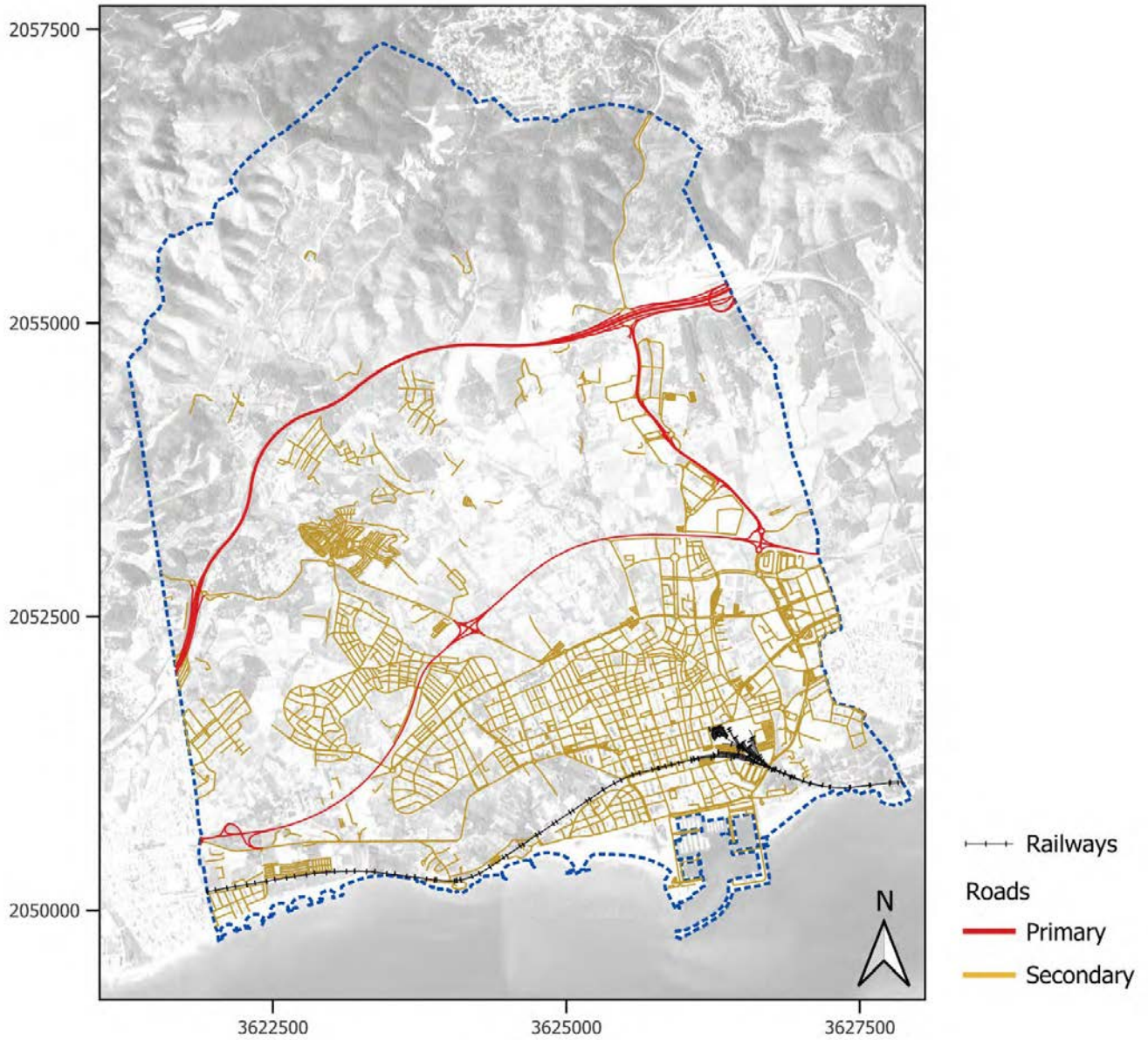




Figure A1.3-10: Map of roads and railways in the Vilanova i la Geltrú CCLL.





APPENDIX 2 – CCLL-SPECIFIC HAZARD MAPS

A2.1. Fluvial flooding

Source: JRC/EFAS

Figure A2.1-1: Fluvial flood hazard map (100-year return period) for the Dublin CCLL.

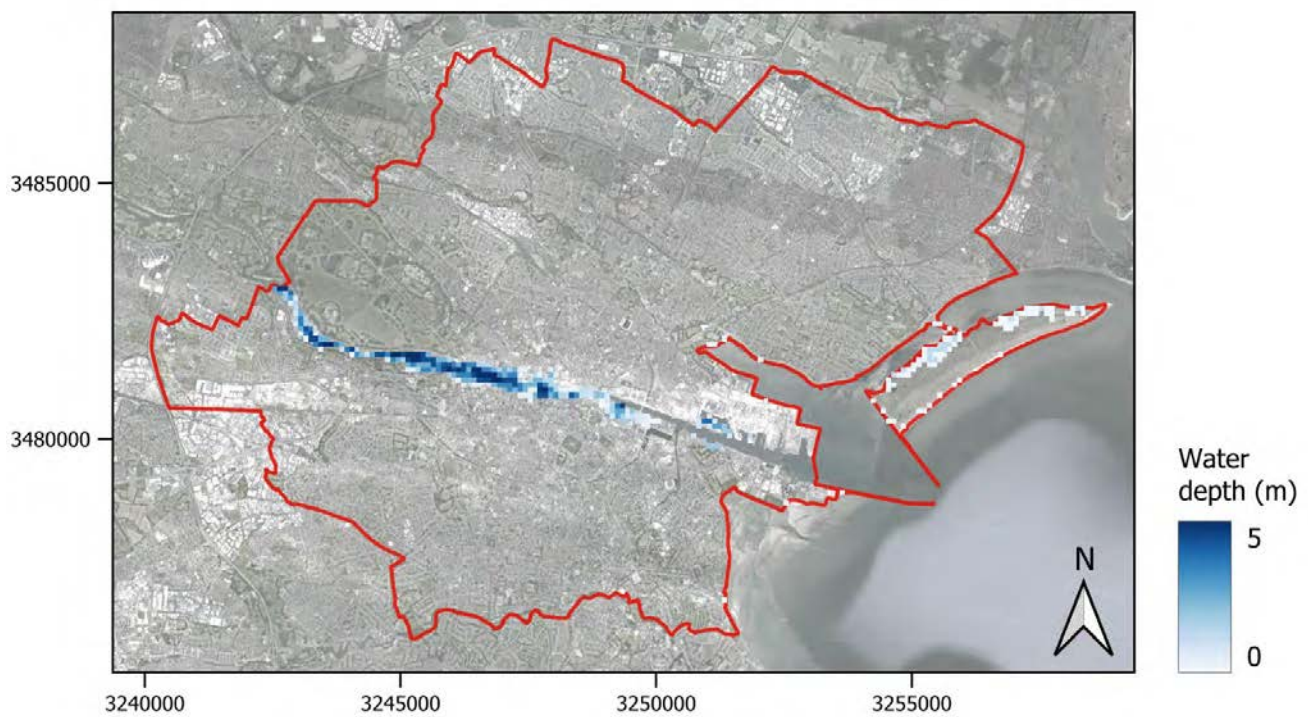




Figure A2.1-2: Fluvial flood hazard map (100-year return period) for the Gdańsk CCLL.

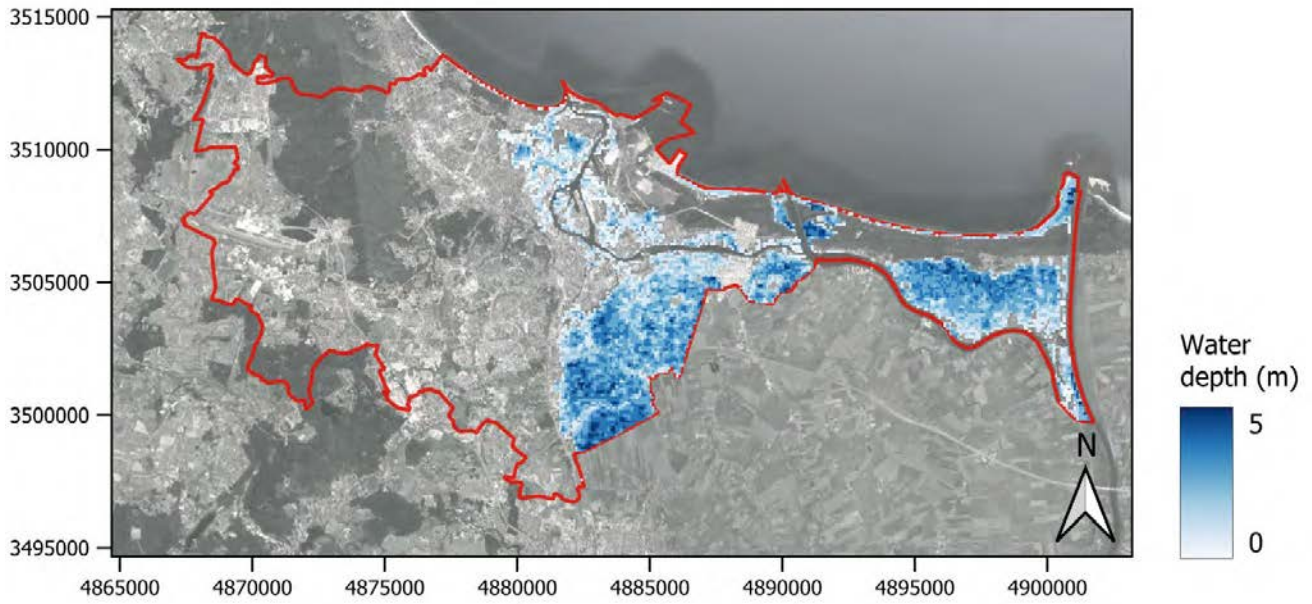


Figure A2.1-3: Fluvial flood hazard map (100-year return period) for the Samsun CCLL.

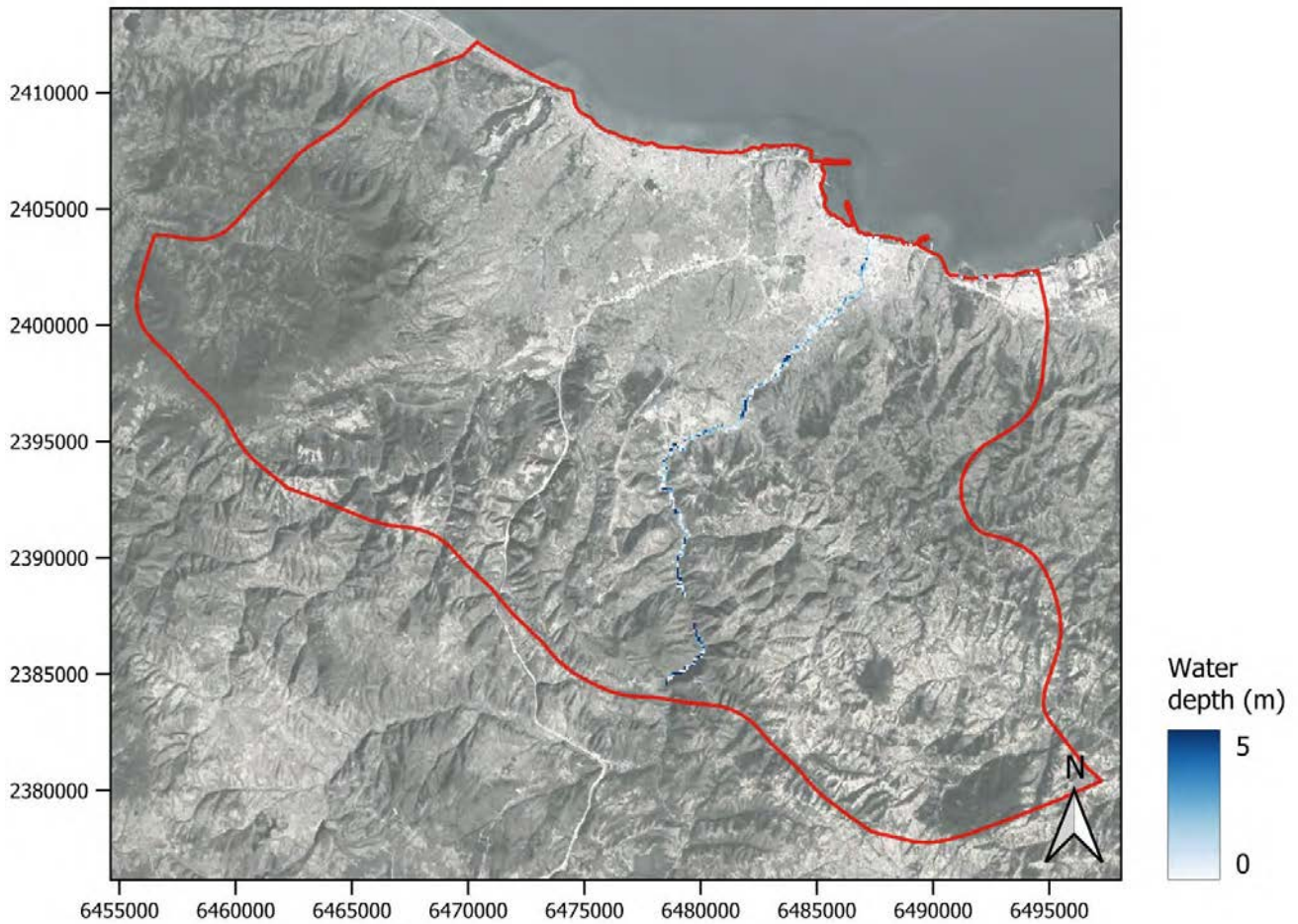
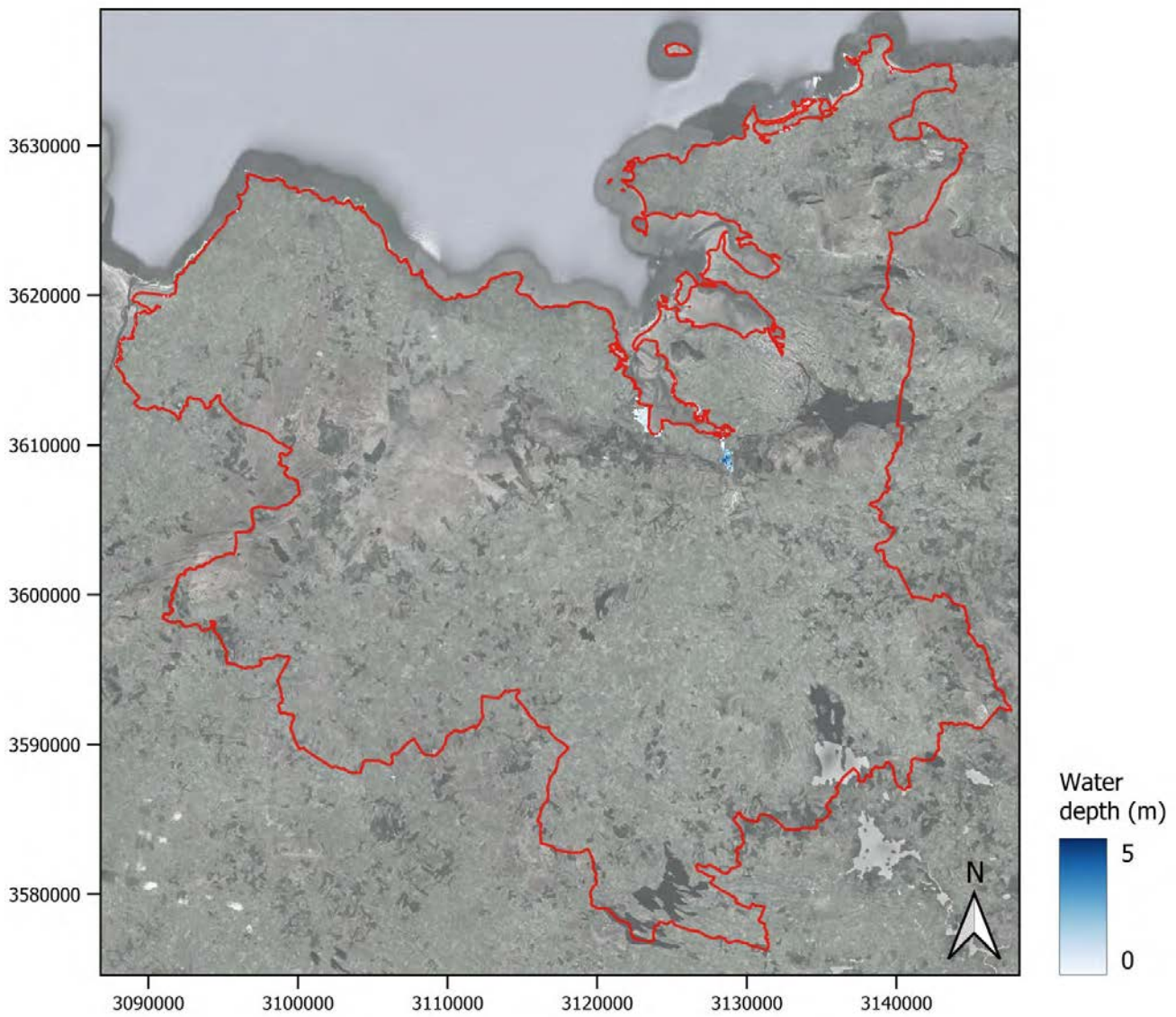




Figure A2.1-4: Fluvial flood hazard map (100-year return period) for the Sligo CCLL.





A2.2. Coastal flooding

Source: Aqueduct (downscaled)

Figure A2.2-1: Coastal flood hazard map (100-year return period) for the Dublin CCLL.

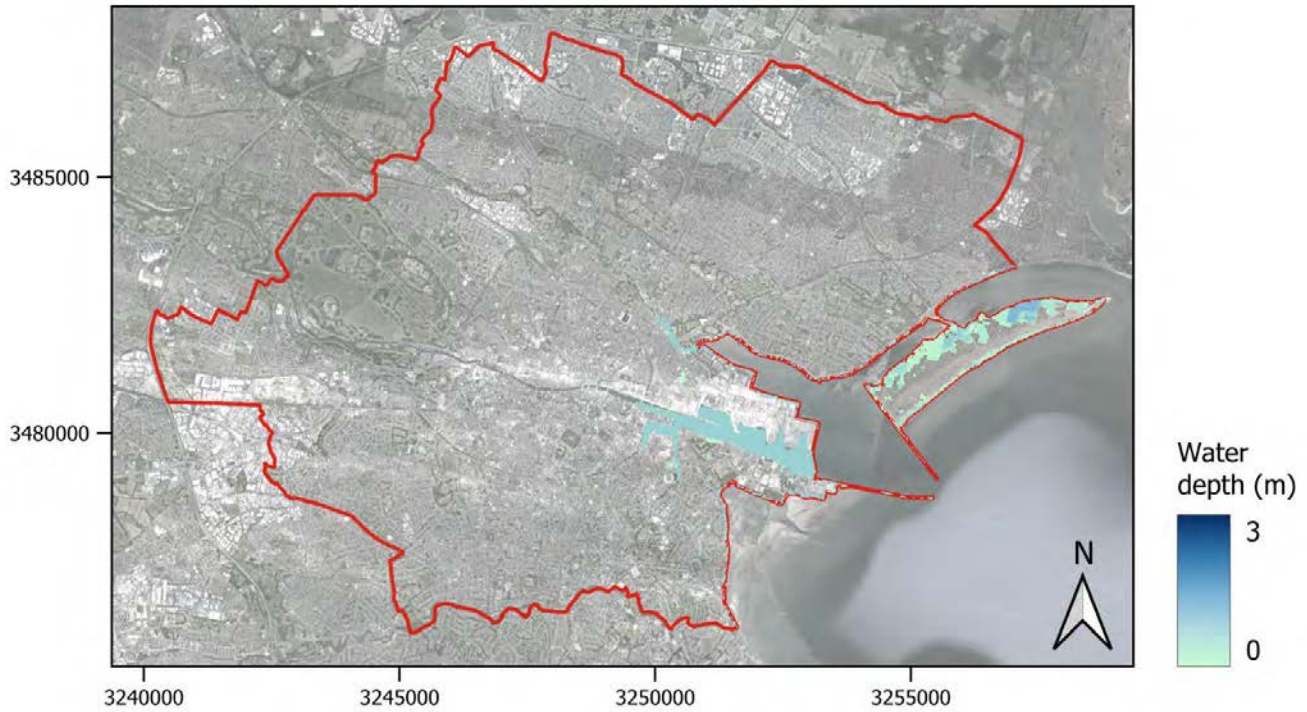


Figure A2.2-2: Coastal flood hazard map (100-year return period) for the Gdańsk CCLL.

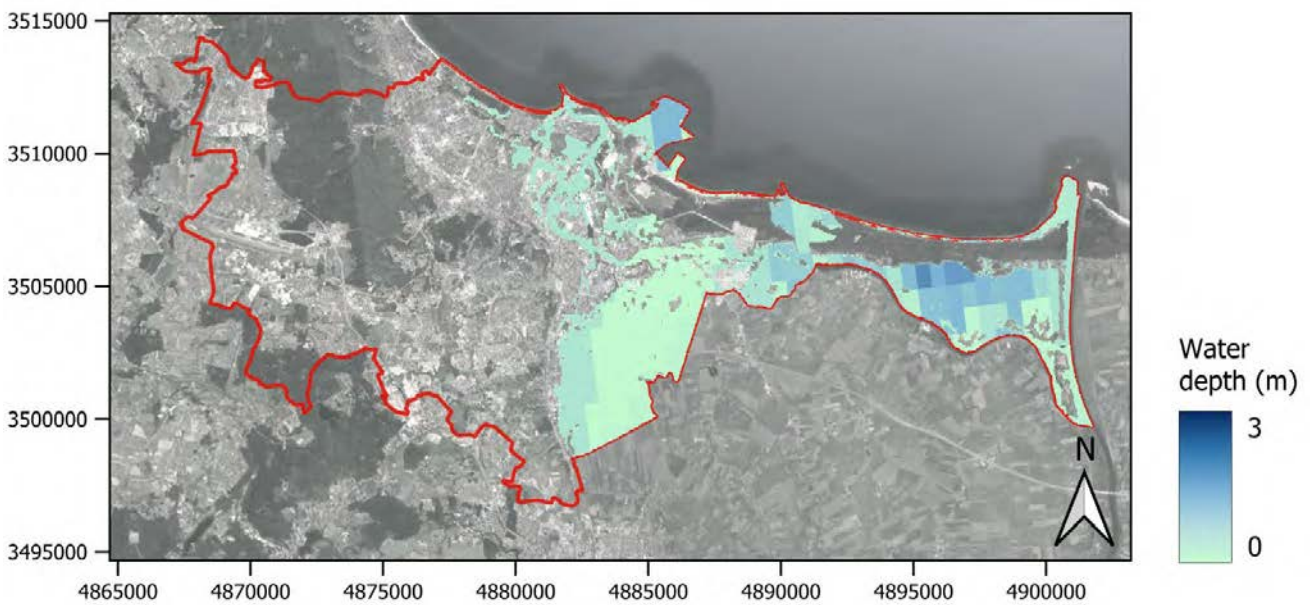




Figure A2.2-3: Coastal flood hazard map (100-year return period) for the Oarsoaldea CCLL.

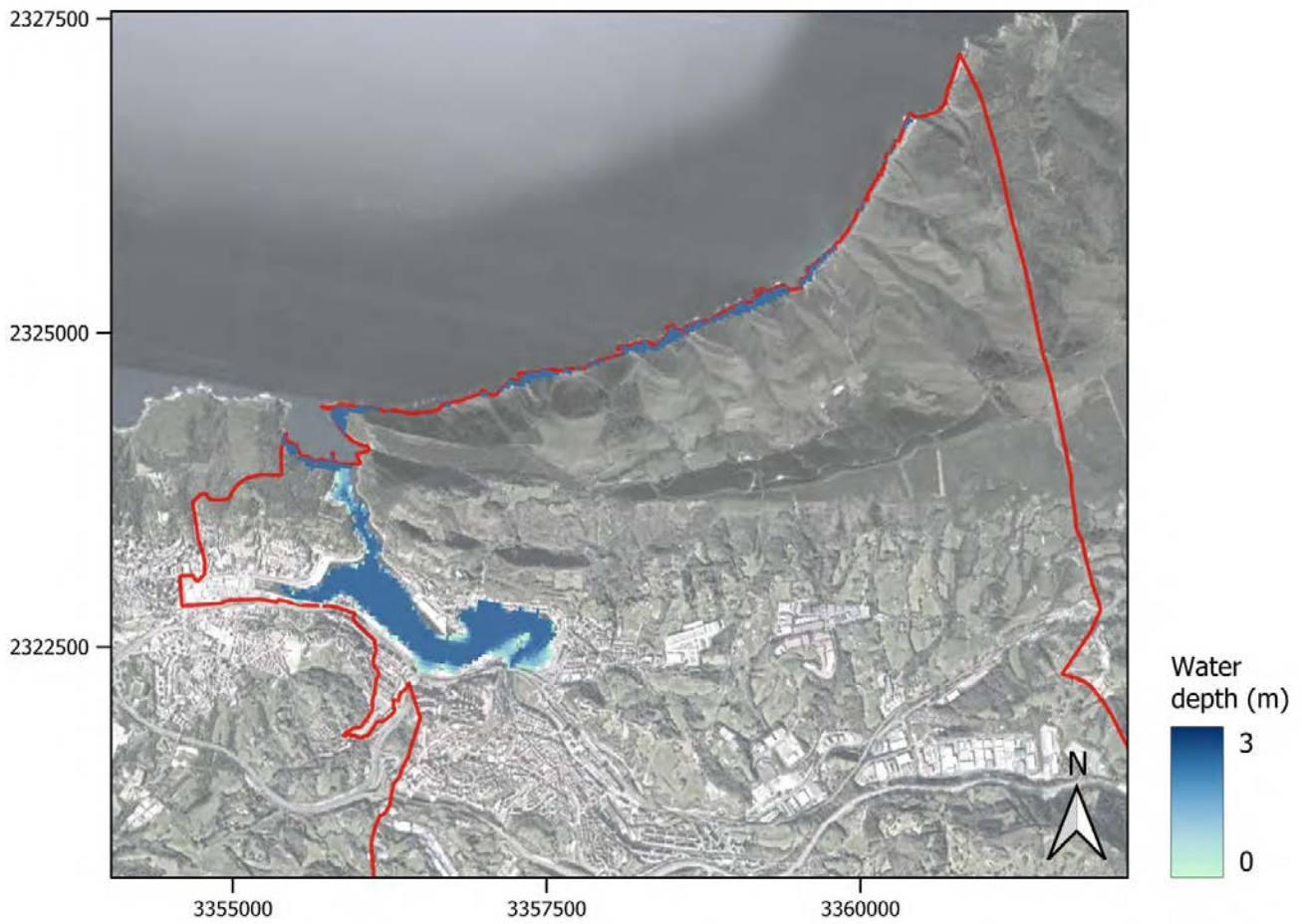




Figure A2.2-4: Coastal flood hazard map (100-year return period) for the Oeiras CCLL.

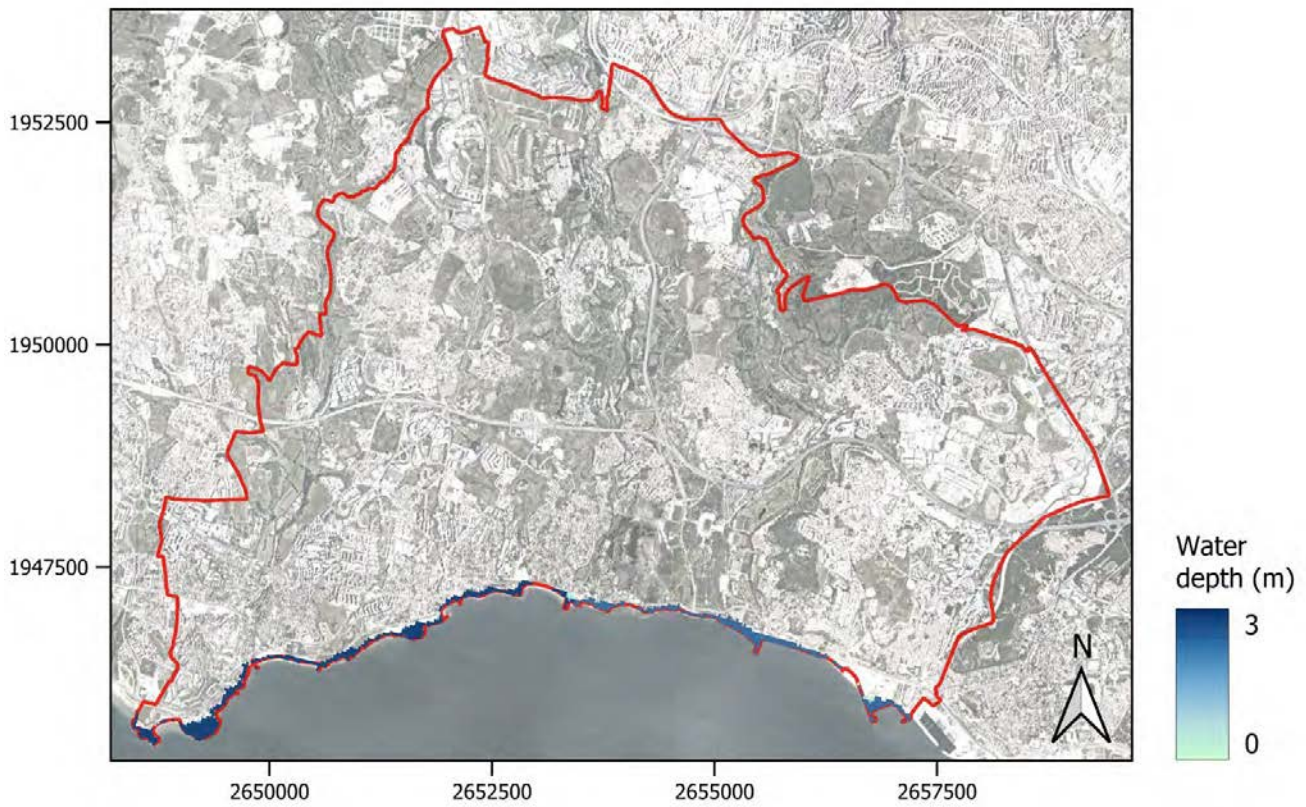




Figure A2.2-5: Coastal flood hazard map (100-year return period) for the Piran CCLL.

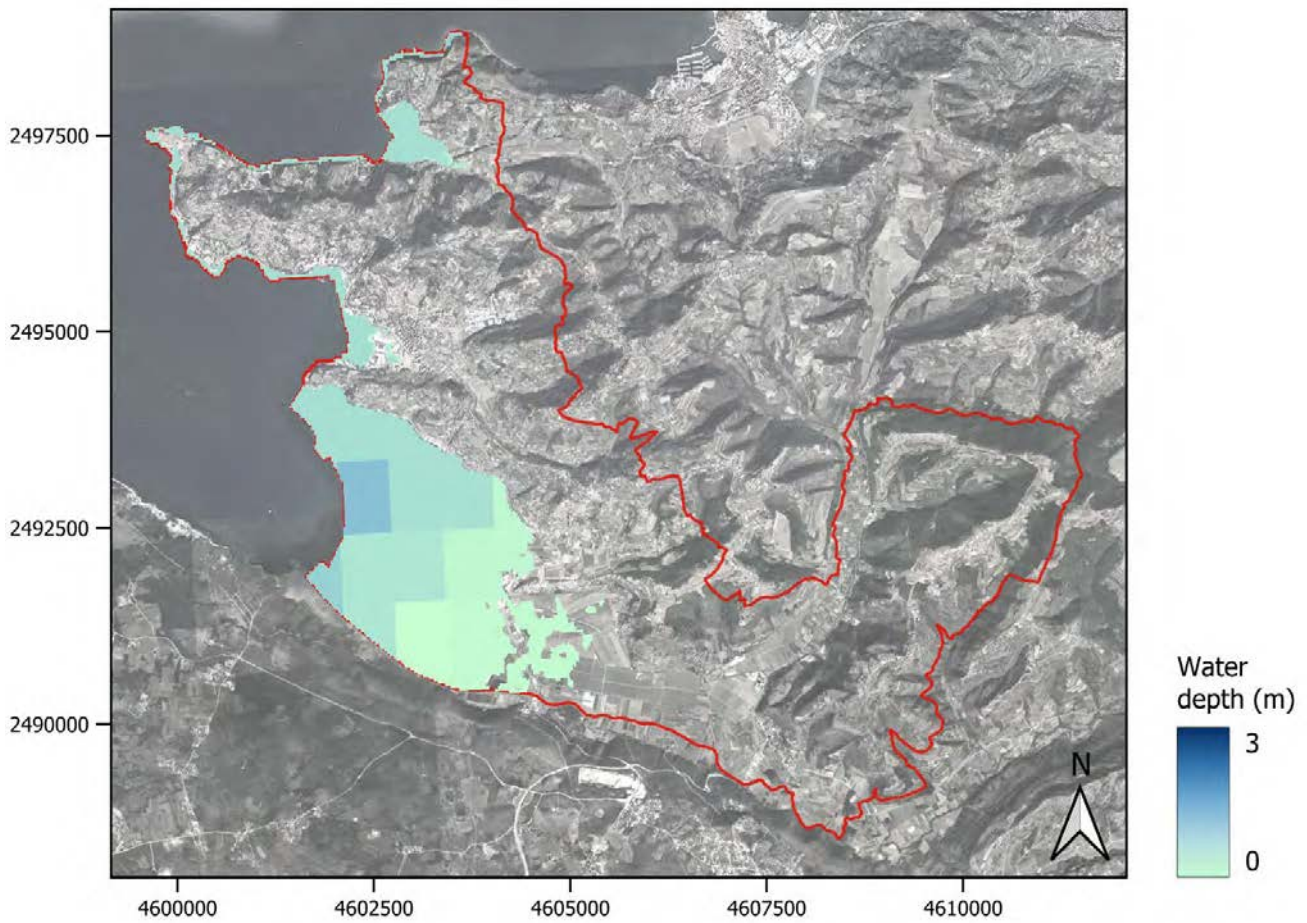
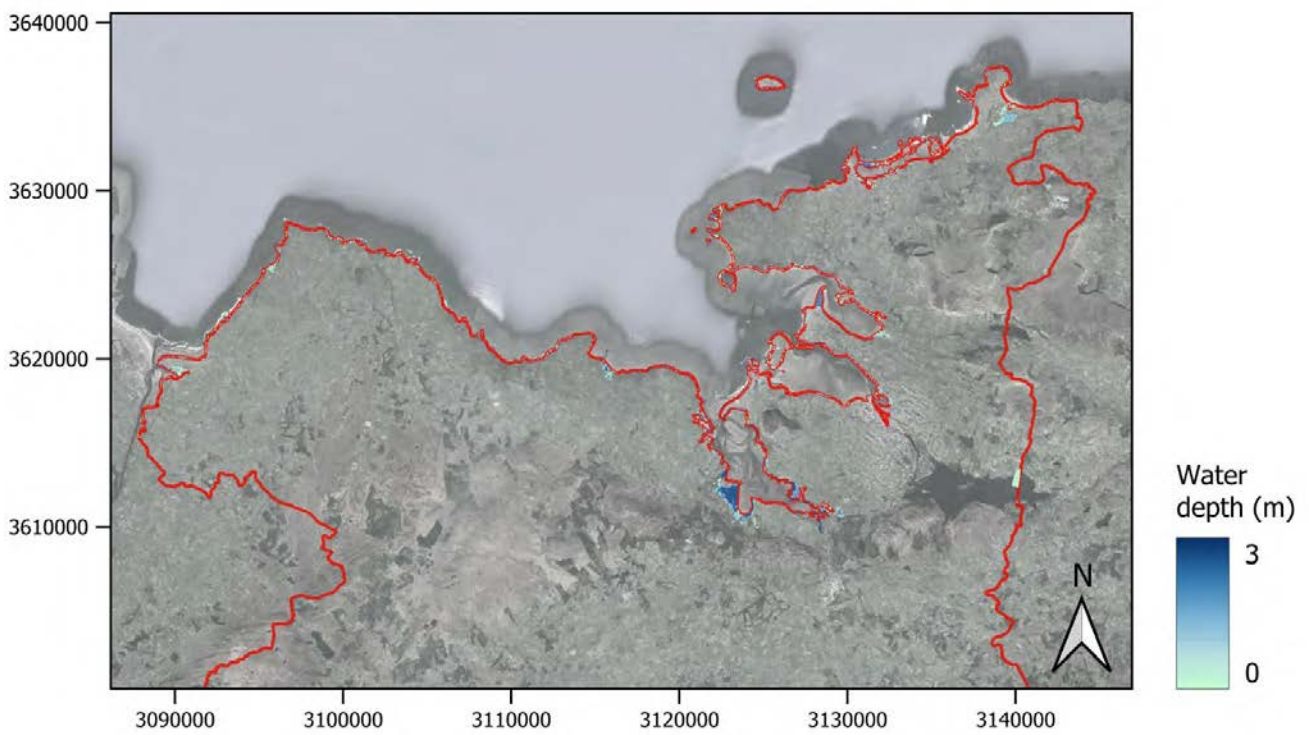




Figure A2.2-6: Coastal flood hazard map (100-year return period) for the Sligo CCLL.





A2.3. Landslide

Source: ELSUS / LHASA (for the Samsun CCLL)

Figure A2.3-1: Landslide susceptibility map for the Benidorm CCLL.

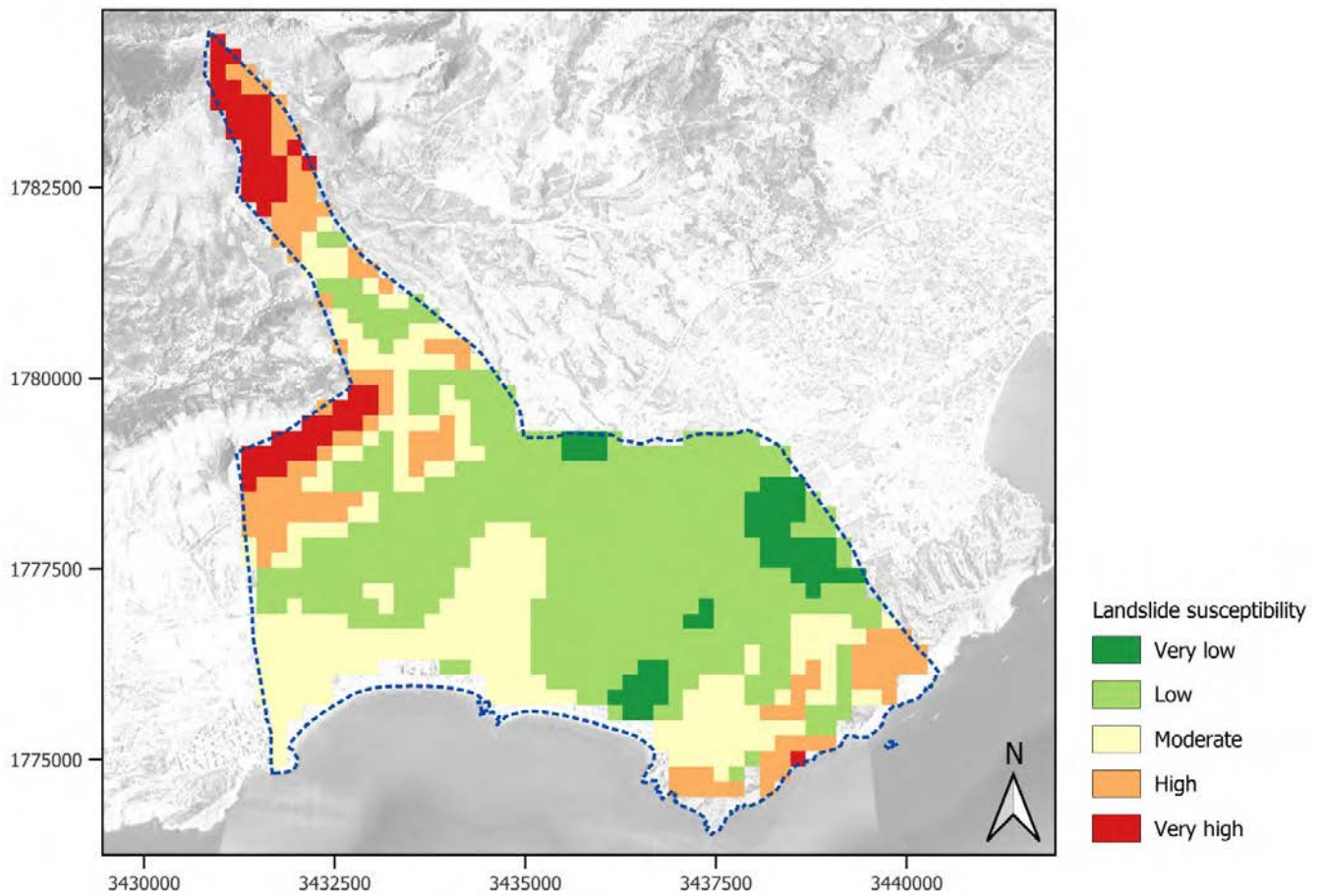




Figure A2.3-2: Landslide susceptibility map for the Dublin CCLL.

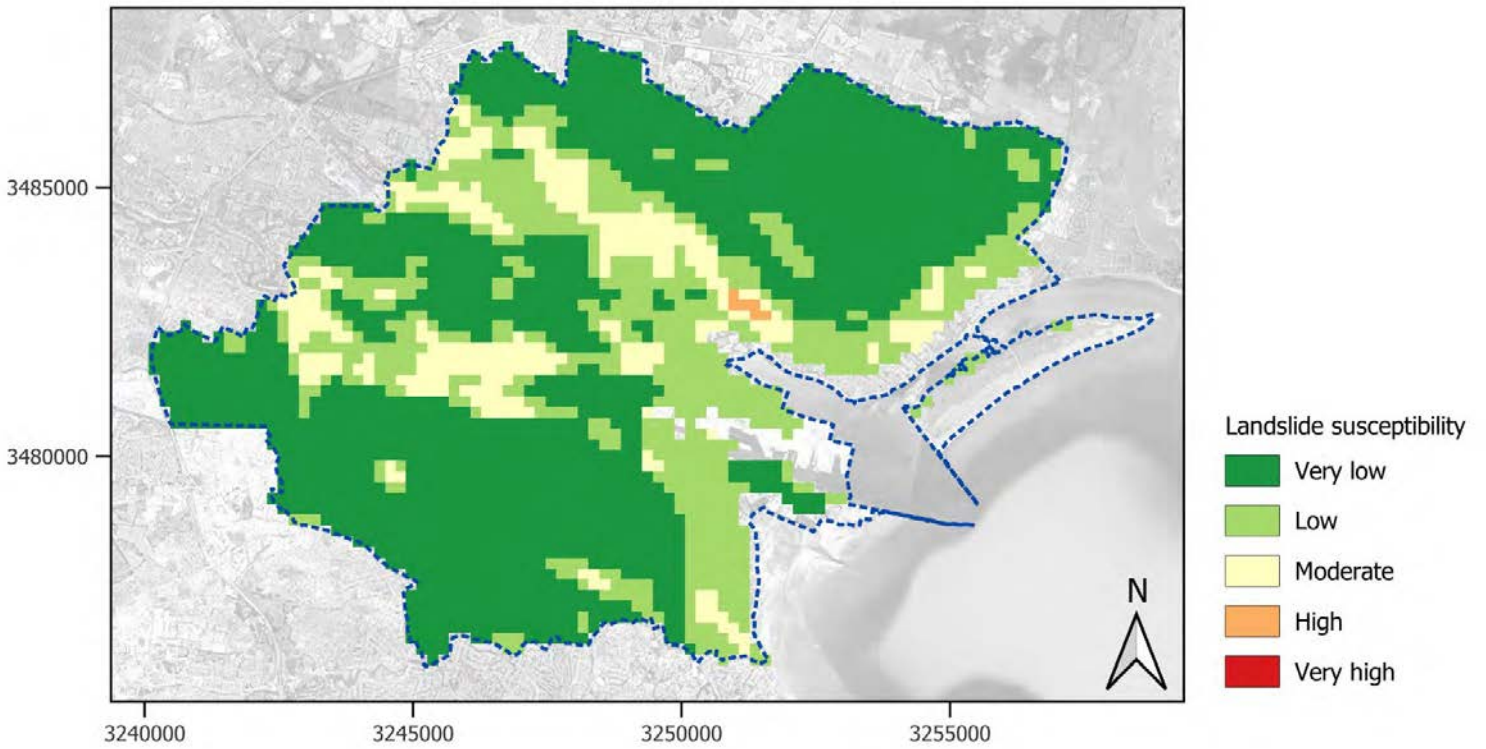


Figure A2.3-3: Landslide susceptibility map for the Gdańsk CCLL.

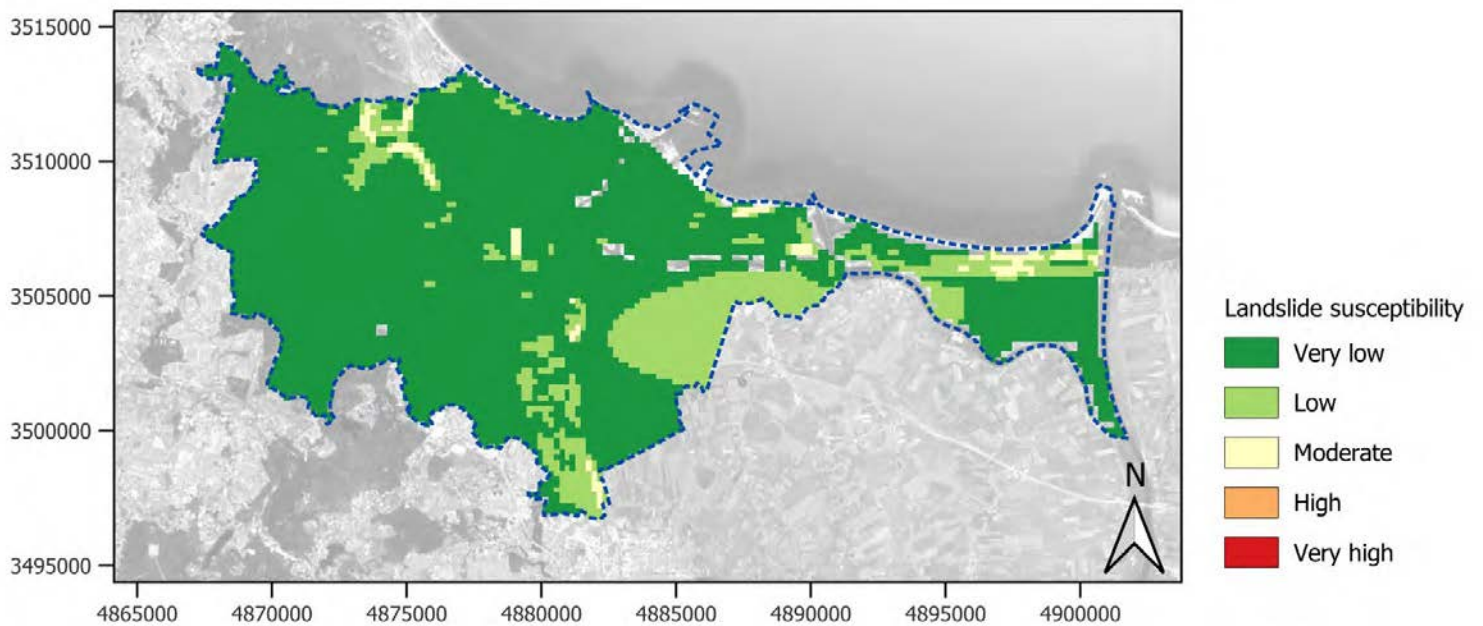




Figure A2.3-4: Landslide susceptibility map for the Massa CCLL.

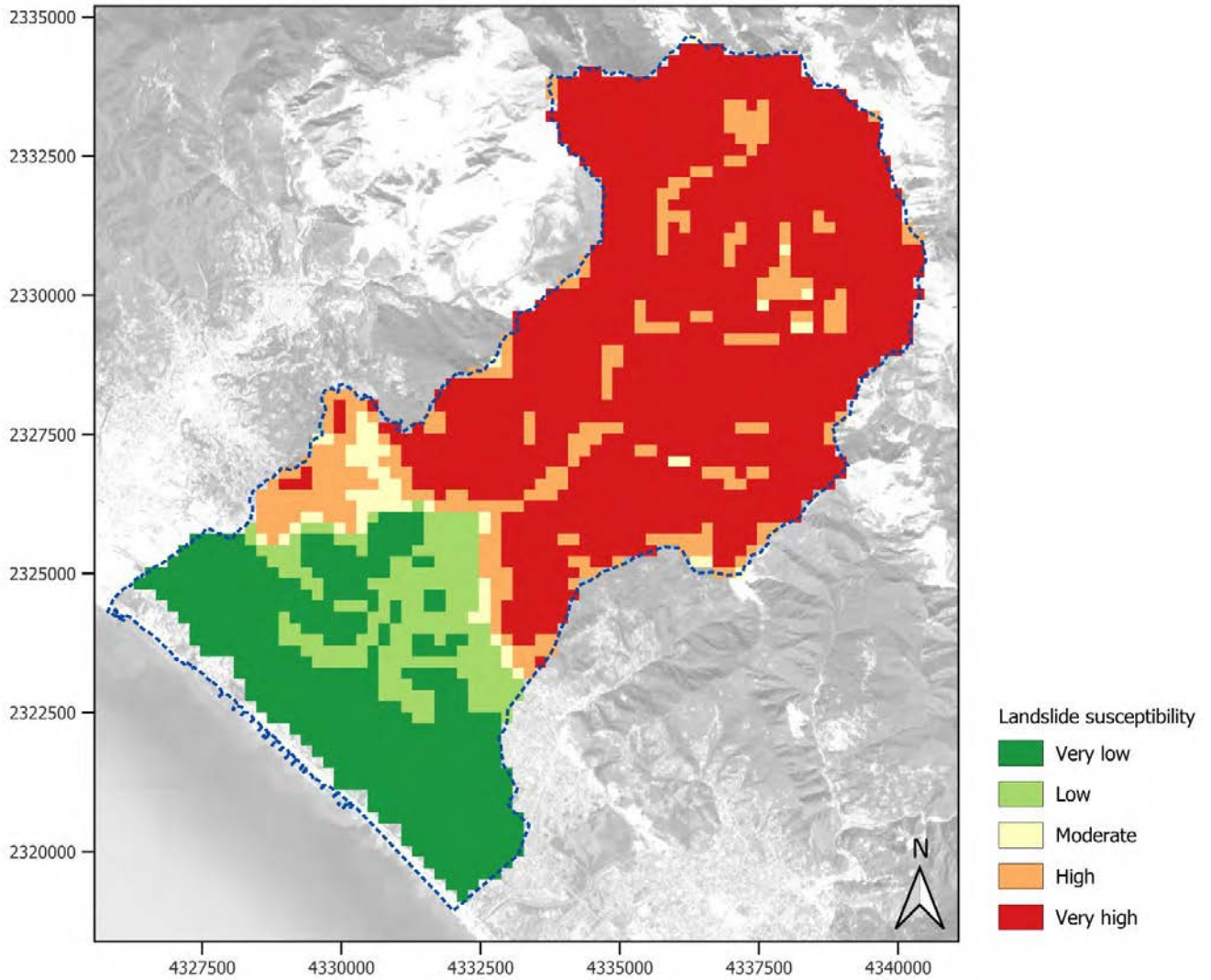




Figure A2.3-5: Landslide susceptibility map for the Oarsoaldea CCLL.

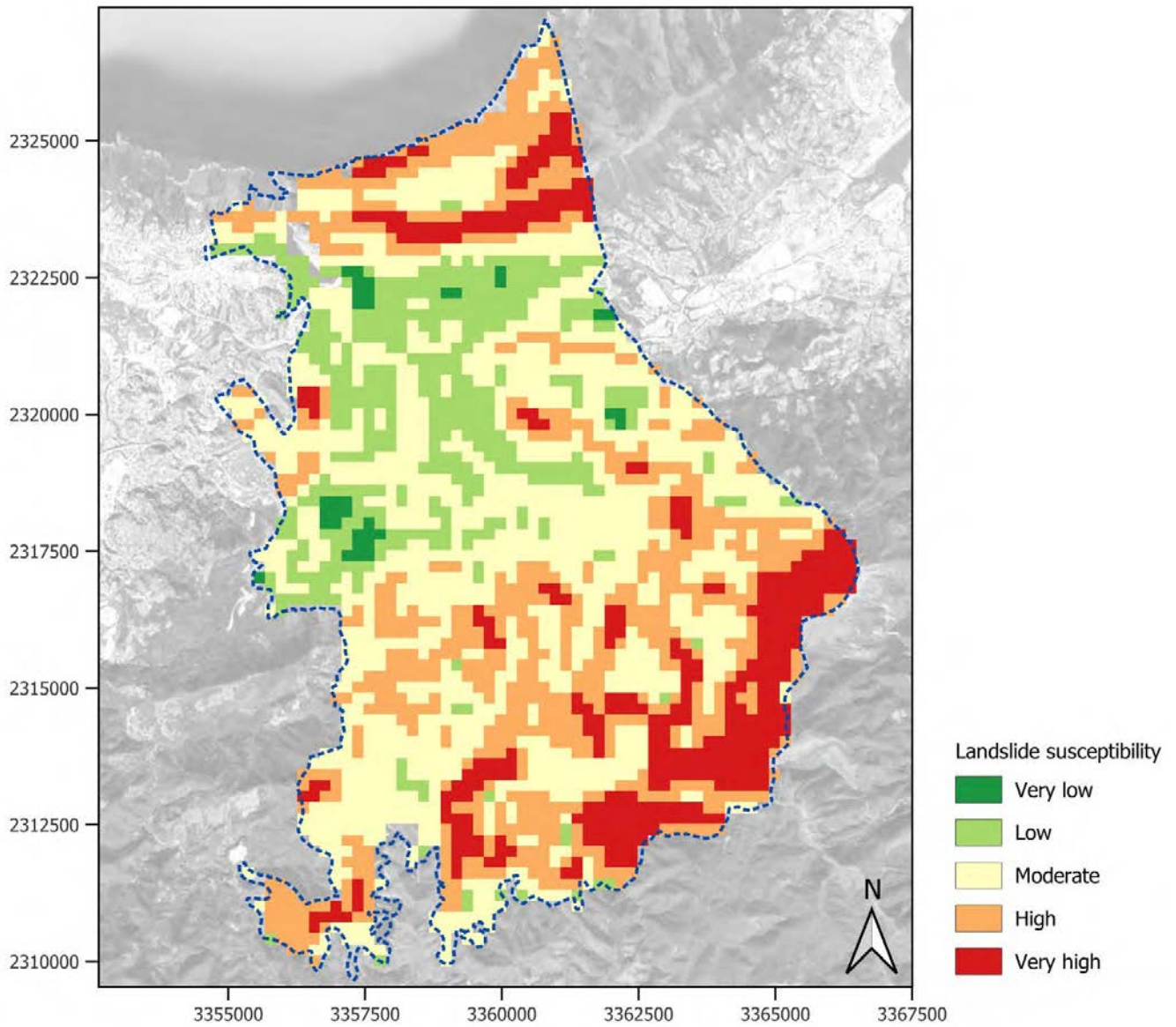




Figure A2.3-6: Landslide susceptibility map for the Oeiras CCLL.

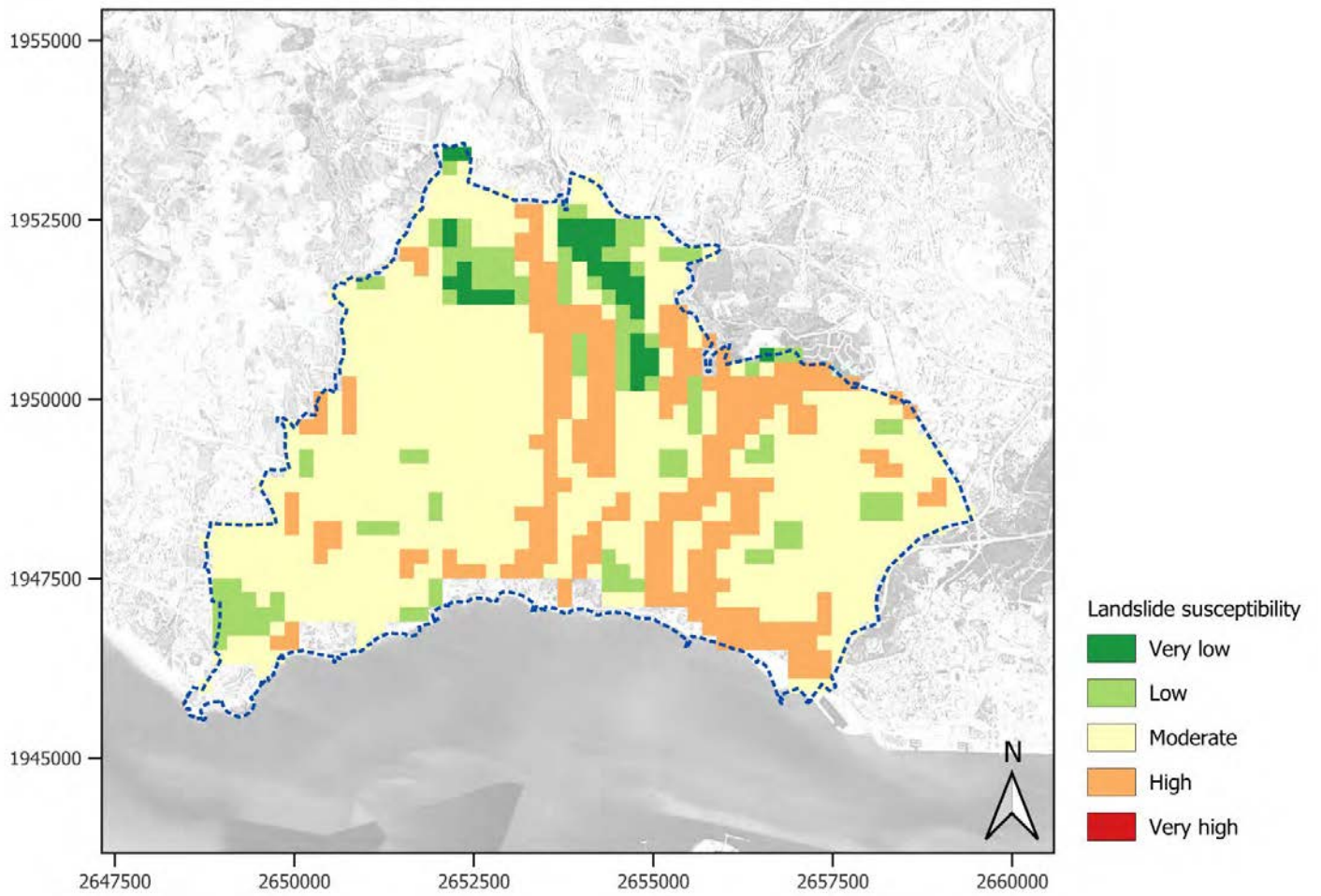




Figure A2.3-7: Landslide susceptibility map for the Piran CCLL.

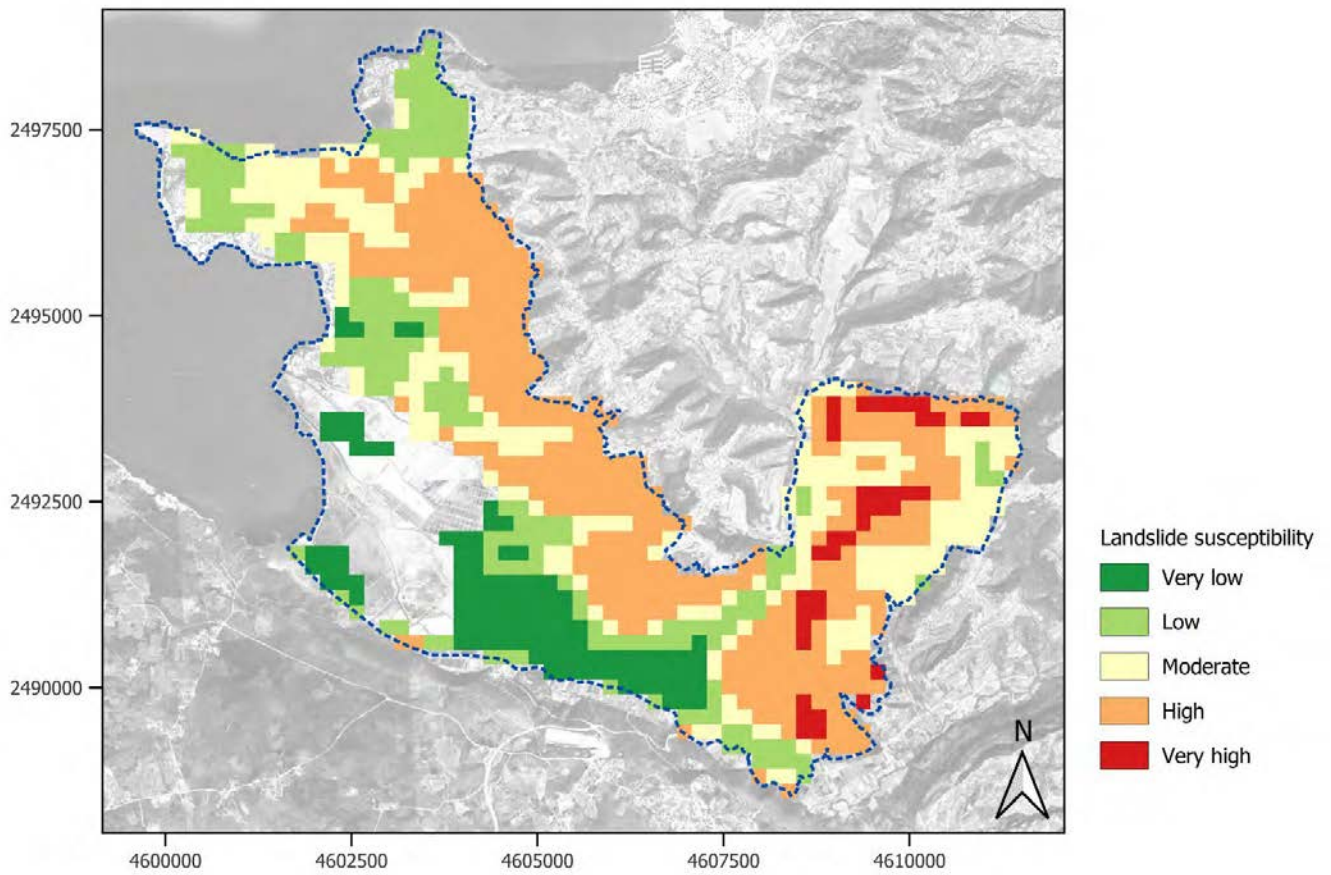




Figure A2.3-8: Landslide susceptibility map for the Samsun CCLL.

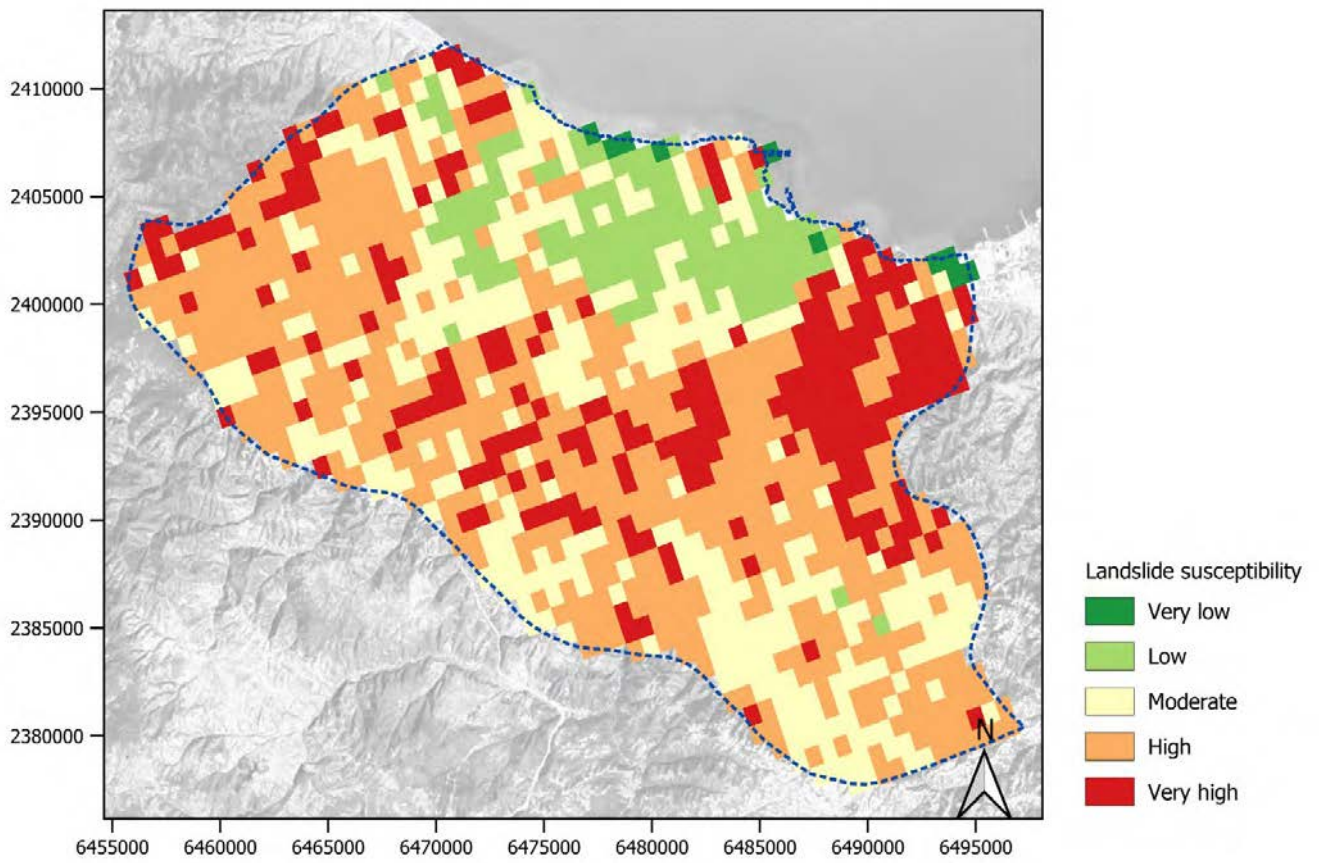




Figure A2.3-9: Landslide susceptibility map for the Sligo CCLL.

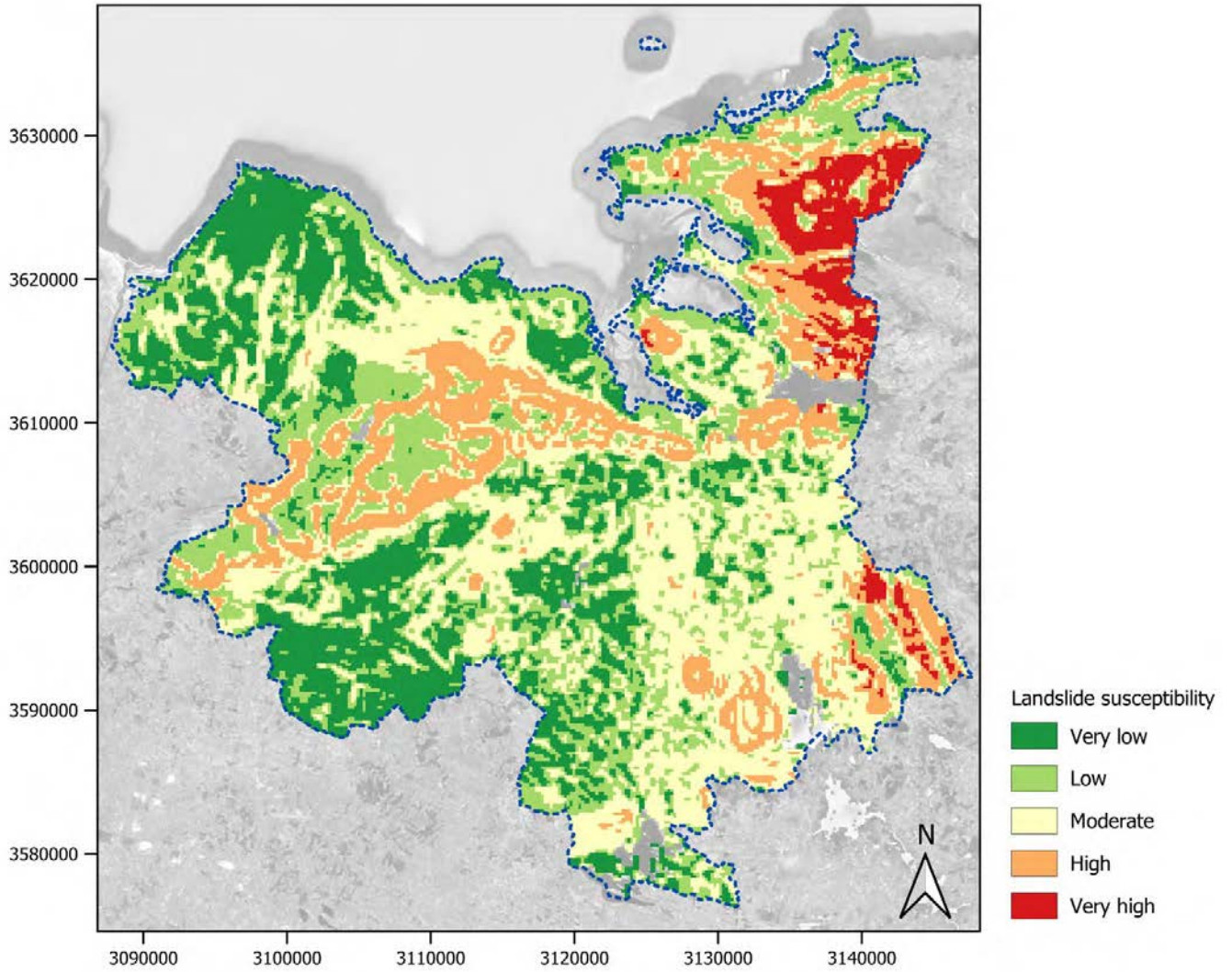
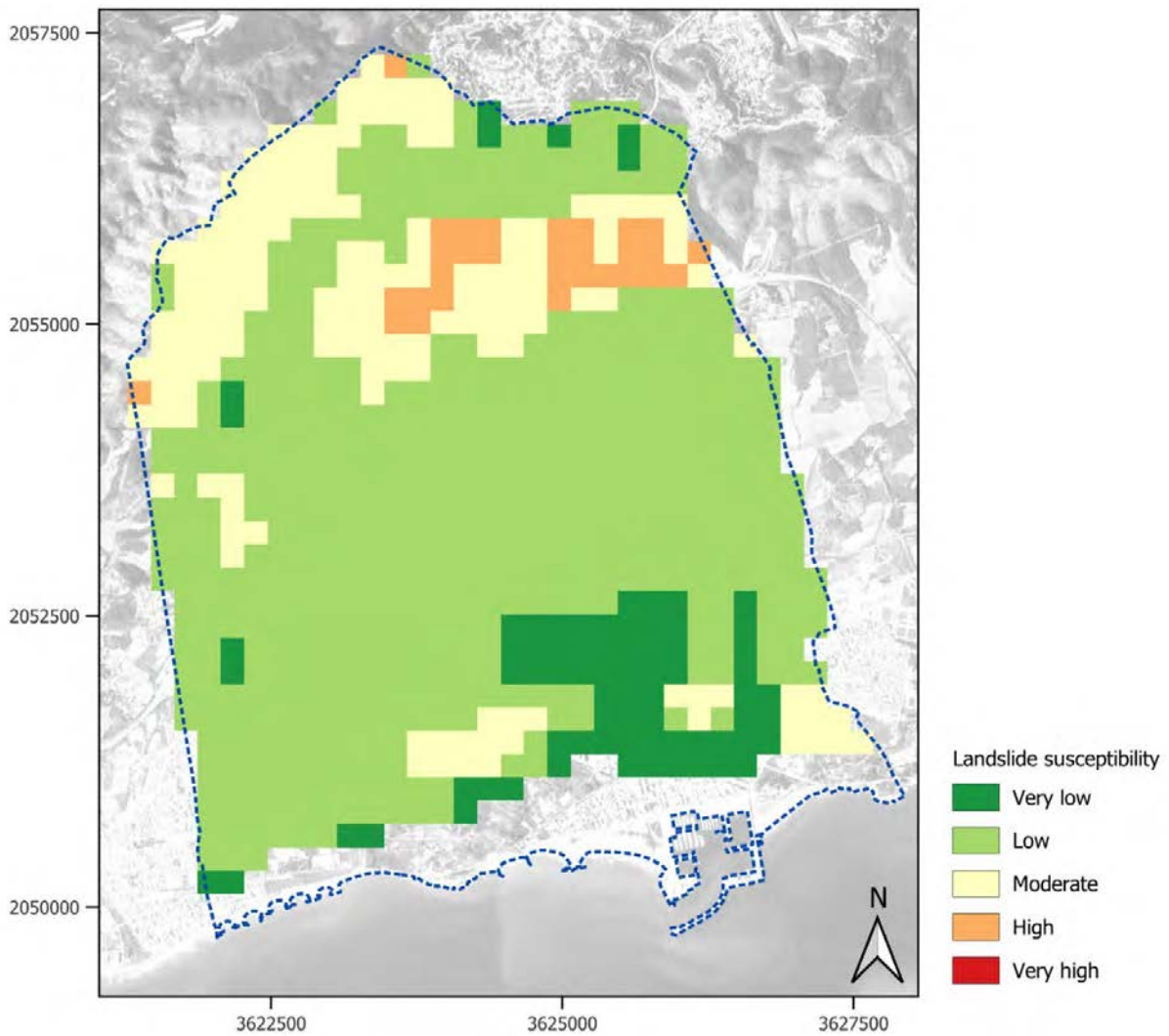




Figure A2.3-10: Landslide susceptibility map for the Vilanova i la Geltrú CCLL.





A2.4. Coastal erosion

Source: EUROSION

Figure A2.4-1: Evolutionary trend for coast segments in the Benidorm CCLL.

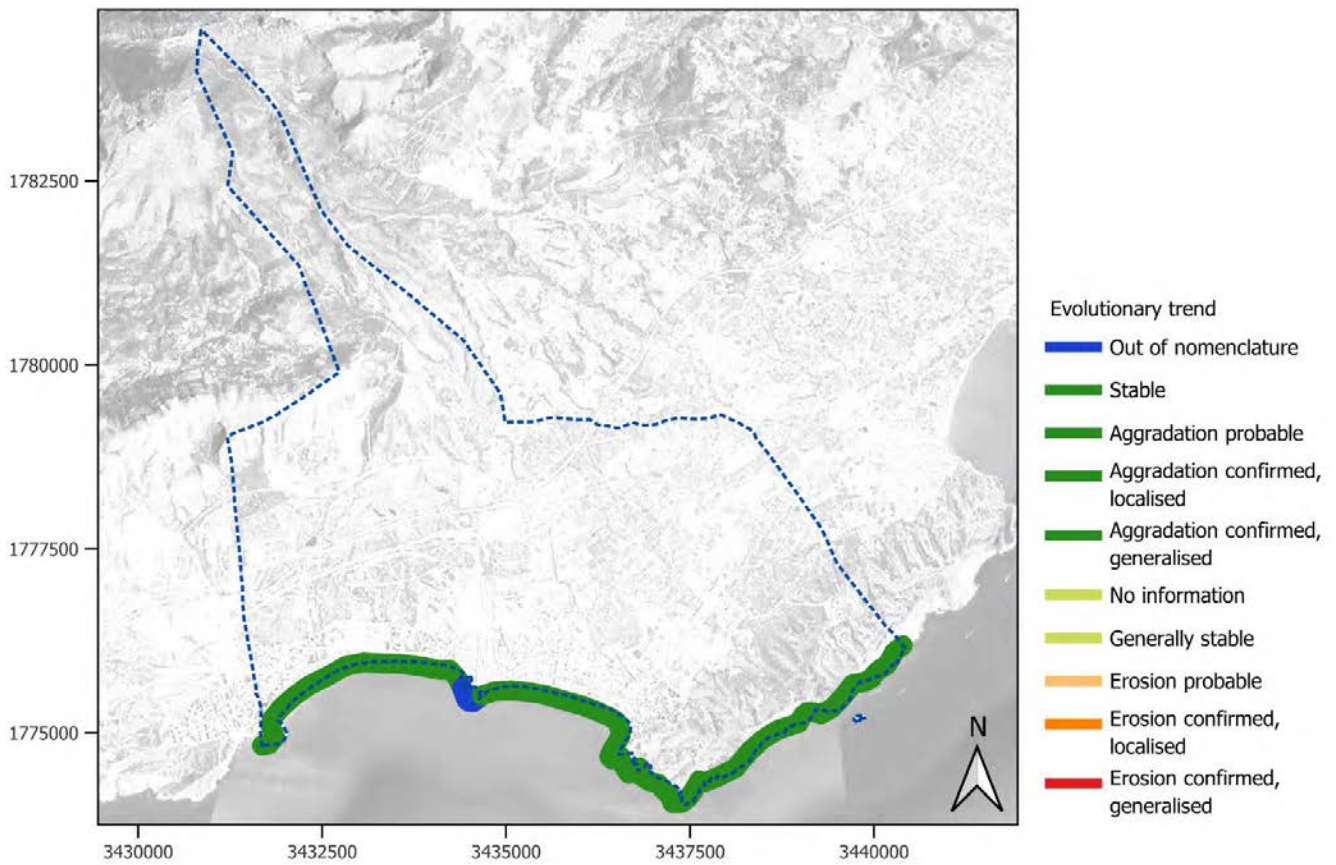




Figure A2.4-2: Evolutionary trend for coast segments in the Dublin CCLL.

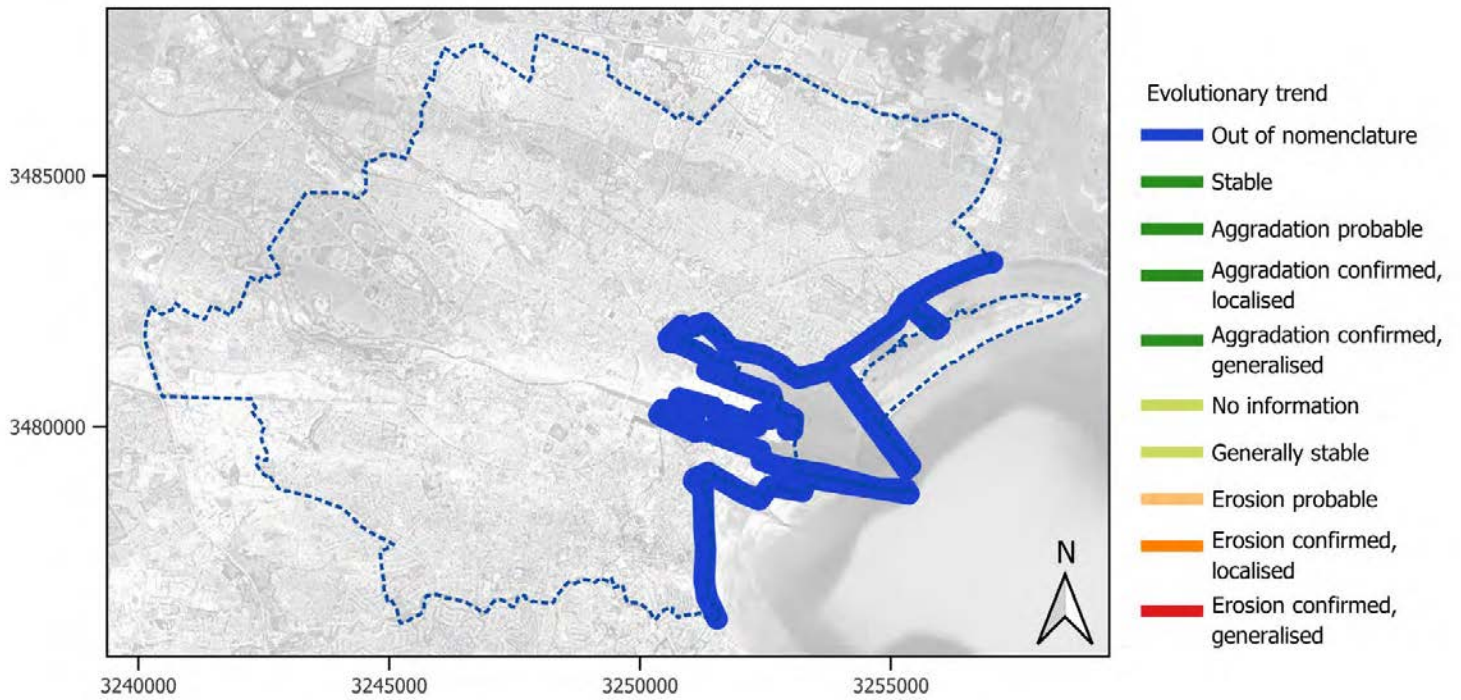


Figure A2.4-3: Evolutionary trend for coast segments in the Gdańsk CCLL.

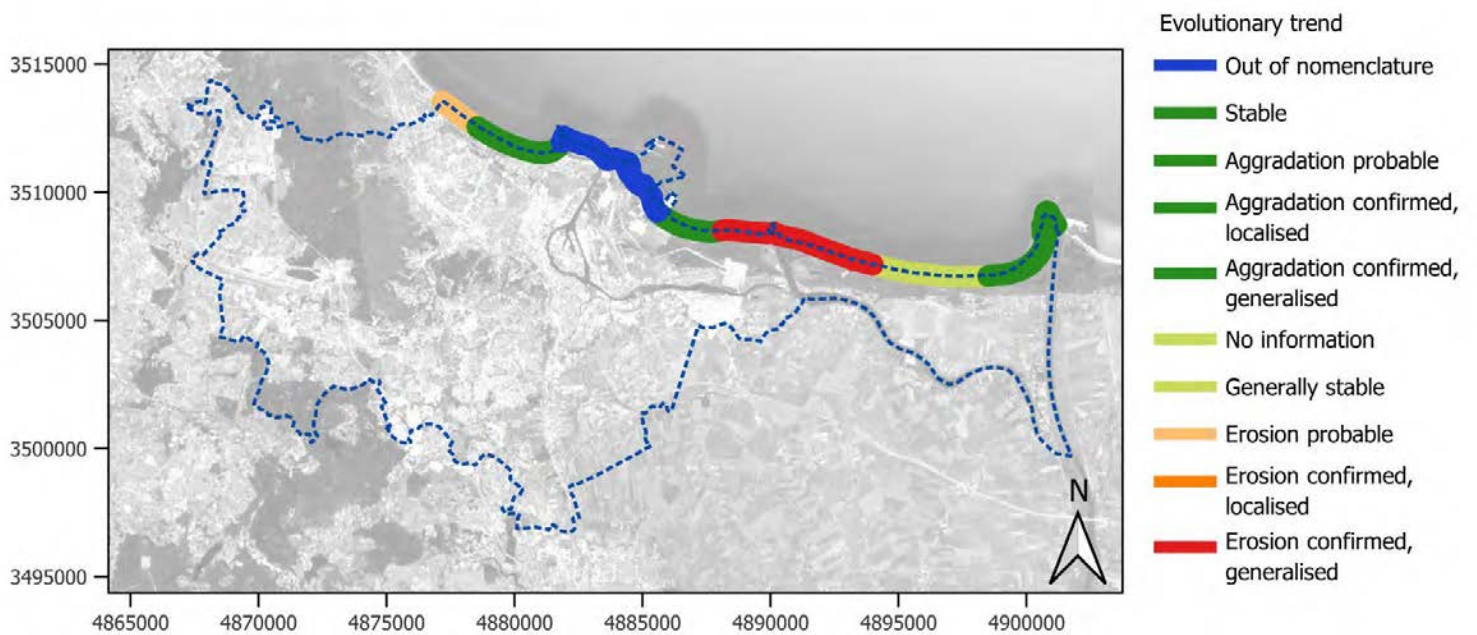




Figure A2.4-4: Evolutionary trend for coast segments in the Massa CCLL.

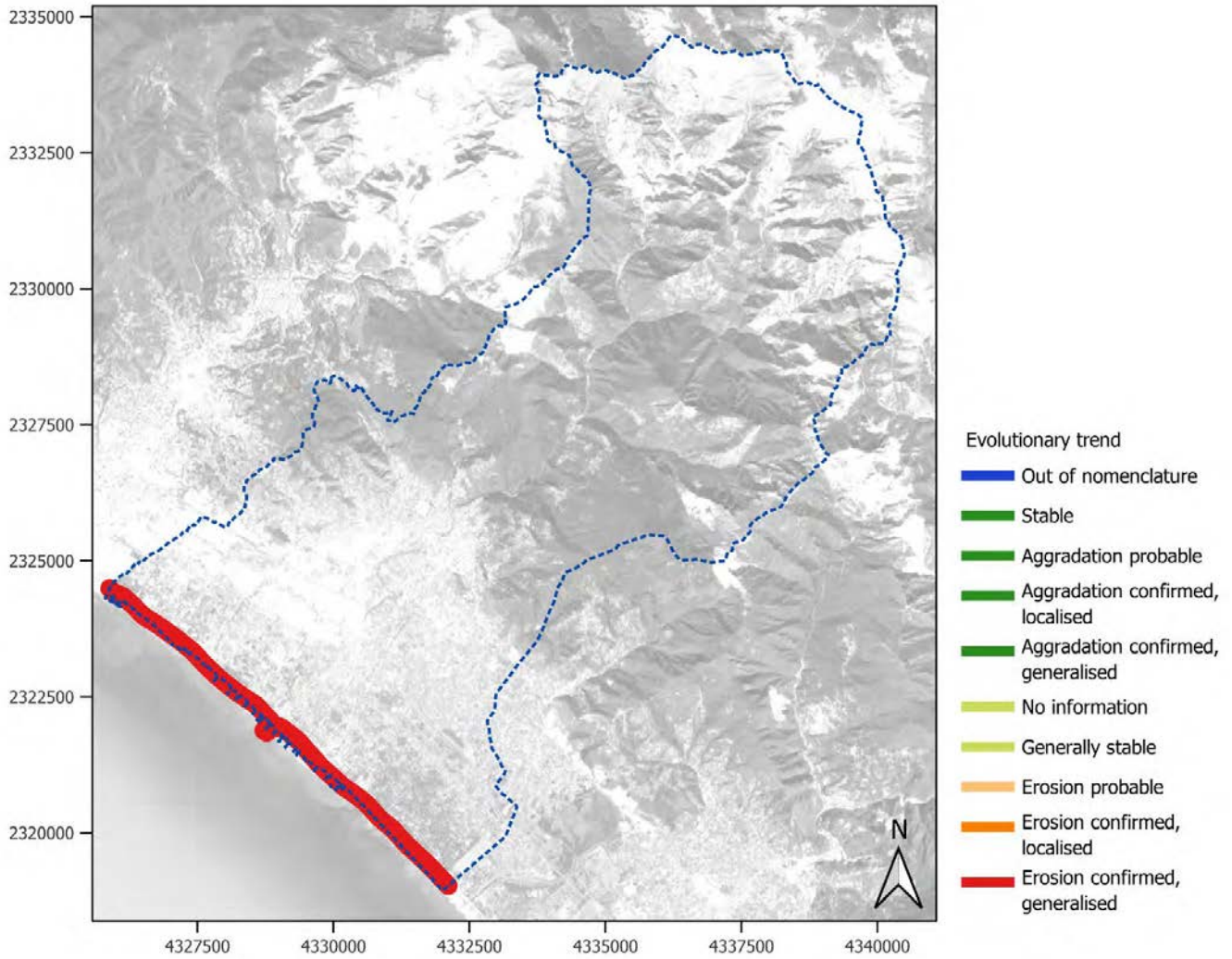




Figure A2.4-5: Evolutionary trend for coast segments in the Oarsoaldea CCLL.

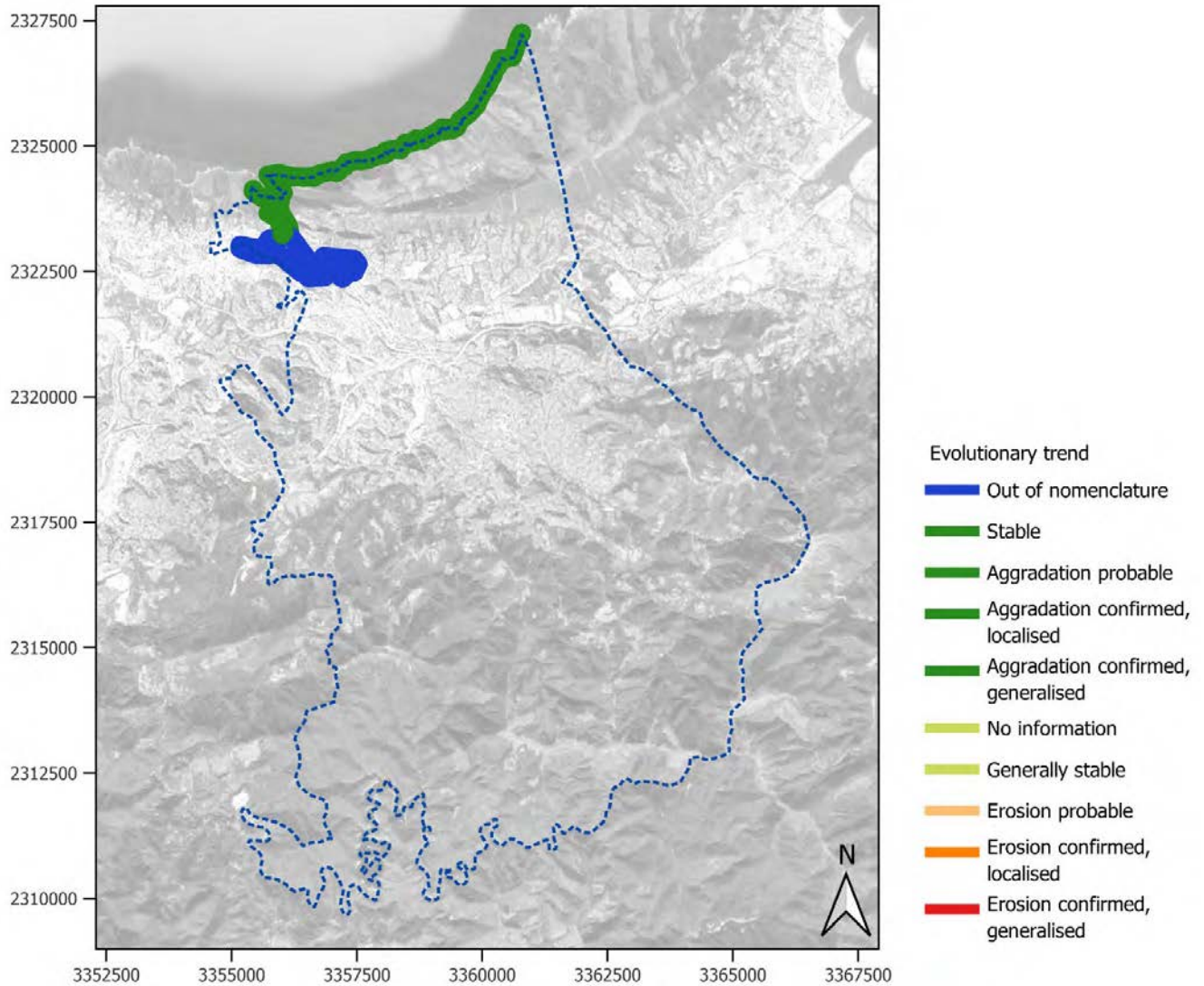




Figure A2.4-6: Evolutionary trend for coast segments in the Oeiras CCLL.

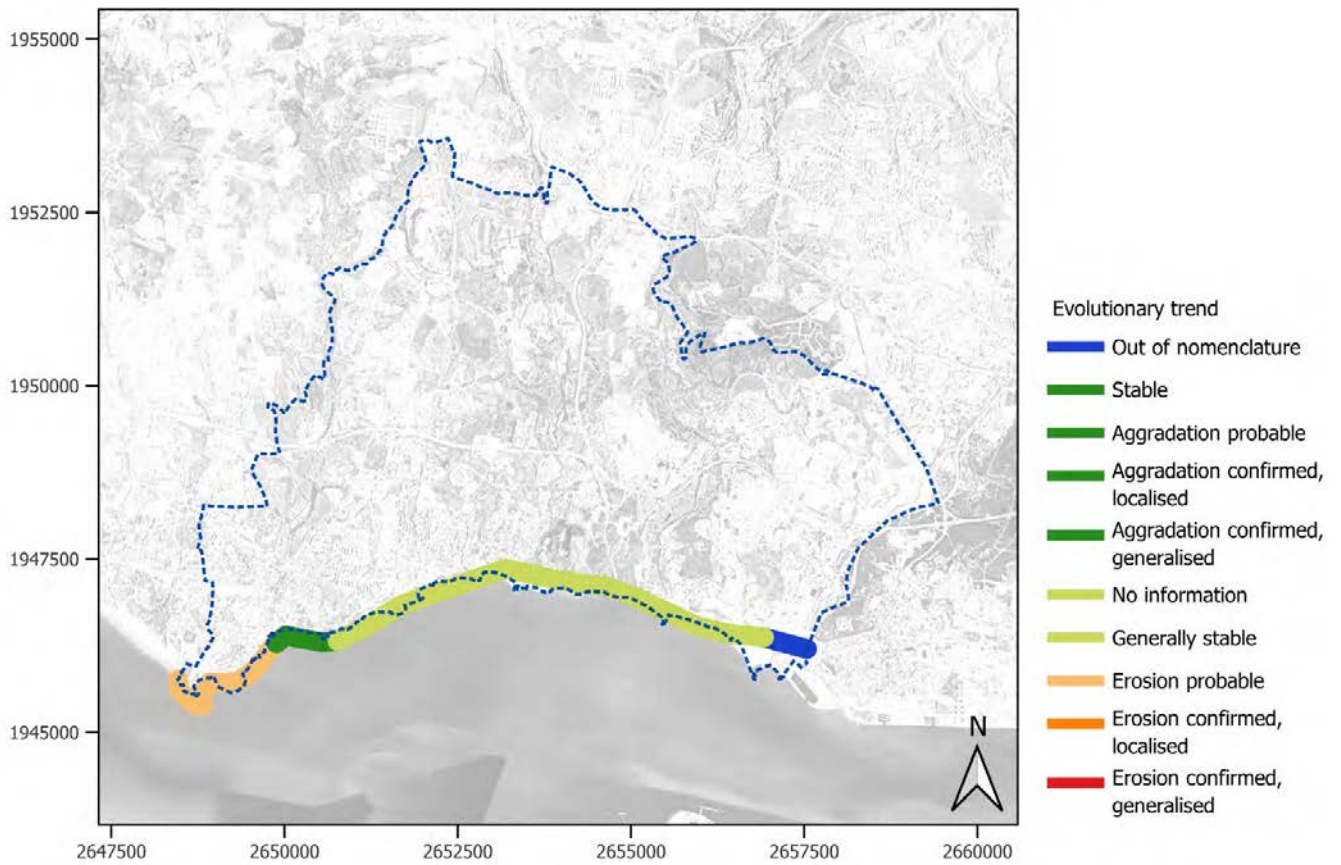




Figure A2.4-7: Evolutionary trend for coast segments in the Piran CCLL.

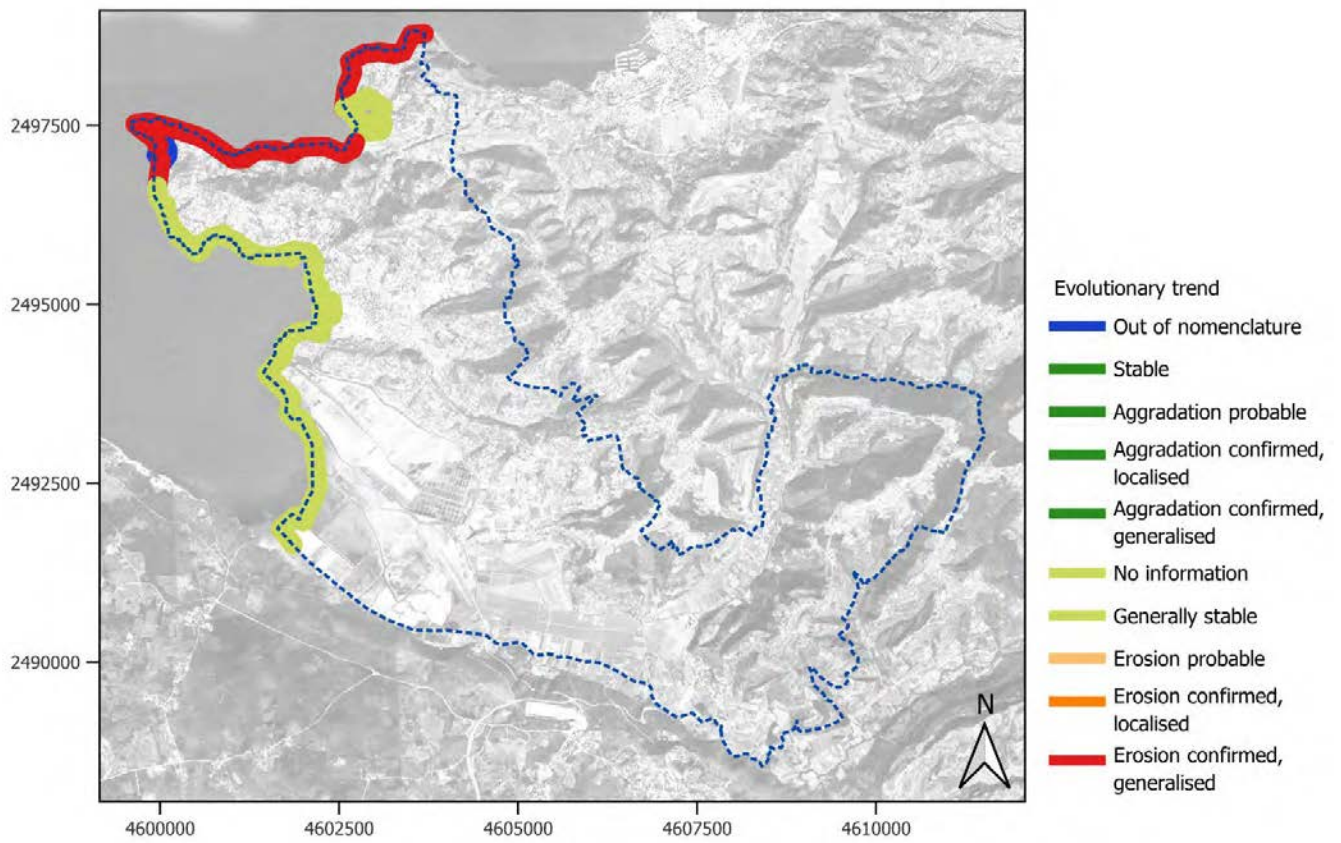




Figure A2.4-8: Evolutionary trend for coast segments in the Sligo CCLL.

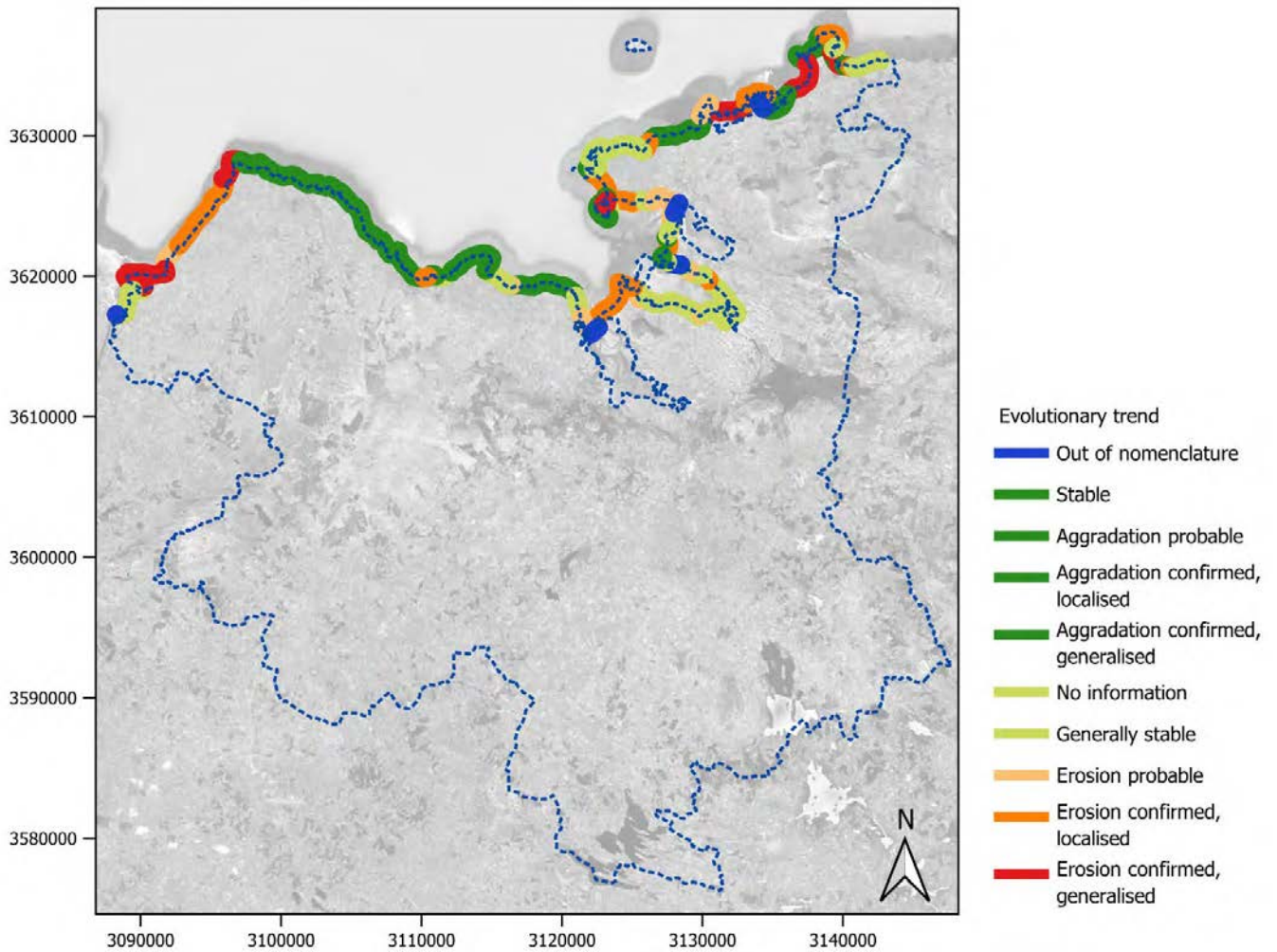




Figure A2.4-9: Evolutionary trend for coast segments in the Vilanova i la Geltrú CCLL.

